ISSN 1000-9620

# Marine Science Bulletin

Volume 7 • Number 2 2005

ISSN 1000-9620
02>
9 771000 962001

NATIONAL MARINE DATA AND
INFORMATION SERVICE OF CHINA

# MARINE SCIENCE BULLETIN

Vol.7 No.2 May, 2005

LIBRARY
JAN 31 2006
National Oceanic & Atmospheric Administration
U.S. Dept. of Commerce

## CONTENTS

The Crustal Structure Character of East China Sea ····· FANG Yinxia (方银霞) et al. ( 1 )

Study on Nutrient Limitation of Phytoplankton in the Field Experiment of the Yangtze River Estuary in Summer ····· ZHAO Weihong (赵卫红) et al. ( 13 )

Pollution Condition of Petroleum Hydrocarbon Pollutant and Estimation of Its Environmental Capacities in Summer in the Bohai Sea ····· WANG Xiulin (王修林) et al. ( 21 )

Species Diversity and Abundance Distribution of Pelagic Siphonophores in Nan Wan Bay of Taiwan, China, in Late Autumn and Early Winter ····· ZHANG Jinbiao (张金标) et al. ( 30 )

Distribution Pattern of Heavy Metals in the Surface Sediments of the Jiaozhou Bay ····· CHEN Zhengxin (陈正新) et al. ( 41 )

Study on Treating Halobios Pollution by Hydroxyl Radical ····· BAI Mindong (白敏冬) et al. ( 57 )

A New Way to Study Water-Vapor Absorption Coefficient ····· ZHOU Liangming (周良明) et al. ( 67 )

Biogeochemistry of Nutrient Elements in the Changjiang (Yangtze River) Estuary ····· WANG Baodong (王保栋) et al. ( 72 )

Red Tide Frequency Analysis Using the Extreme Value Theory ····· XIE Zhonghua (谢中华) et al. ( 80 )

Study on the Adsorption of Metal Ions by Immobilized Marine Algae with the Existence of Clay ····· ZHENG Shenghua (郑盛华) et al. ( 86 )

Toxic Effects of Phthalates on Ocean Algae ····· QIU Haiyuan (邱海源) et al. ( 91 )

LIBRARY
Pacific Islands Fisheries Science Center
NOAA Fisheries
Honolulu, Hawai'i

# The Crustal Structure Character of East China Sea

FANG Yinxia (方银霞), LIU Jianhua (刘建华)

1 *Key Lab of Submarine Geoscience, SOA, Hangzhou* 310012, *Zhejiang, China*

2 *The Second Institute of Oceanography, SOA, Hangzhou* 310012, *Zhejiang, China*

**Abstract** This paper presents actuality of investigation and study of the crustal structure characters of East China Sea at home and abroad. Based on lots of investigation and study achievements and the difference of the crustal velocity structure from west to east, the East China Sea is divided into three parts — East China Sea shelf zone, Okinawa Trough zone and Ryukyu arc-trench zone. The East China Sea shelf zone mostly has three velocity layers, *i.e.*, the sediment blanket layer (the velocity is 5.8-5.9 km/s), the basement layer (the velocity is 6.0-6.3 km/s), and the lower crustal layer (the velocity is 6.8-7.6 km/s). So the East China Sea shelf zone belongs to the typical continental crust. The Okinawa Trough zone is located at the transitional belt between the continental crust and the oceanic crust. It still has the structural characters of the continental crust, and no formation of the oceanic crust, but the crust of the central trough has become to thinning down. The Ryukyu arc-trench zone belongs to the transitional type crust as a whole, but the ocean side of the trench already belongs to the oceanic crust. And the northwest Philippine Basin to the east of the Ryukyu Trench absolutely belongs to the typical oceanic crust.

**Keywords** East China Sea, Okinawa Trough, Crustal Structure

## Introduction

The crustal structure of East China Sea is rather complex. Its continental shelf area is basically of the continental crust, but several arguments have existed about the crustal property and structure of Okinawa Trough all the while. The Chinese scientists have done lots of geologic and geophysical investigation and research in the East China Sea, and have accumulated abundant gravity, magnetic and seismic data and information since the 1970s. For instance, the Chinese Academy of Sciences conducted more than 20 sonobuoy seismic refraction and 7 OBS seismic refraction measurements in the East China Sea continental shelf and Okinawa Trough, and relatively comprehensive studies about the submarine structure and infrastructure of East China Sea in the period 1982—1984. A geological profile was obtained which extended about 900 km long from the mouth of Changjiang River to Ryukyu Trench by the Geologic Profile Committee of China. The continental margin's geological and geophysical characteristics and the crustal structure of East China Sea were investigated systematically for the first time. Based on lots of geological and geophysical investigation and research, and guided by the plate

Received on November 9, 2004

tectonic theory, Liu Guangding et al.[1-2] studied the geological structure's evolution history of East China and the adjacent seas. The results show that the west part of East China Sea is of the continental crust, and the east part is of oceanic crust with relatively simple structure. The high accuracy 3D seismic tomography imaging research in China Seas and the adjacent regions by Liu Futian [3] and Liu Jianhua[4] shows that the Sea of Japan and Philippine Sea which are located to the east of the Ryukyu Arc's west margin and the Korea Peninsula's west coast have the oceanic crust features of the young ocean basin, and the Bohai Sea, Yellow Sea and the middle-west part of East China Sea to the west of the boundary mentioned above belong to the continental crust. The crustal structure characters of Okinawa Trough indicate that it is the transitional area from the oceanic crust to the continental crust. Furthermore, Jin Xianglong, Xu Dongyu, Liu Xiqing, Li Naisheng, Liu Jianhua, Xu Weiling et al. have successively published a series of papers discussing the crustal structure and property of the East China Sea, especially Okinawa Trough [5]. The crustal structure research of the East China Sea by foreign scientists mostly fastened on the origin and the crustal property of Okinawa Trough. Many kinds of research on the crustal structure of Okinawa Trough have been carried out such as the seismic reflection, the gravity inversion, the telluric electric- magnetic sounding, the seismic tomography imaging, the ocean bottom seismograph (OBS), the isotopic element and elemental composition analysis of the basalt taken from Okinawa Trough. Based on lots of investigation and study data and achievements, and according to the difference of the crustal velocity structure from west to east, this paper divides the East China Sea into three zones, *i.e.*, the East China Sea shelf zone, Okinawa Trough zone and Ryukyu arc-trench zone, and then discusses the crustal structure and property of each zone.

## 1 The Crustal Structure of East China Sea Shelf Zone

The East China Sea shelf zone has a rather thick crust layer of sedimentary rock and graniticrock, but no whinstone layer. It belongs to the typical continental crust, and can be divided into three layers — upper, middle and lower crust layers[6]:

( 1 ) Upper crust layer: In addition to the Mesozoic and Cenozoic sediment strata, it also contains the Paleozoic weak metamorphic rock, granite and a slight amount of mesite-basite rock whose density is 2.67 g/cm$^3$ and velocity is 5.8-6.0 km/s. The thickness of upper crust layer varies between 12-15 km and its chemical composition is mostly acidite.

( 2 ) Middle crust layer: It is composed of magmatite and metamorphic rocks (including acidite, gneiss and graniton). Its chemical composition is mainly neutral rock whose density is 2.80 g/cm$^3$ and velocity is 6.4 km/s. This layer is about 7 km thick, and thins eastwards.

( 3 ) Lower crust layer: The lithology of lower crust is mainly granulite that belongs to basite. Its density is 2.90 g/cm$^3$ and velocity is 7.4 km/s. This layer is commonly 10 km thick, and becomes thinner eastwards.

Lots of sonobuoy seismic refraction and OBS measurement data got from the East China Sea, especially the profiles passing across the continent shelf of East China Sea, Okinawa Trough, Ryukyu

Arc, Ryukyu Trench and Philippine Sea are very important to study the crustal velocity structure of East China Sea (Fig.1). Measurement results show that the crustal velocity structure is different along both the cross direction and the vertical orientation. Along the cross direction there are three uplifts and three basins. The three uplifts are west uplift (the east part of Minzhe Uplift), Diaoyudao uplift and Ryukyu Arc uplift. The three basins are East China Sea shelf basin, Okinawa Trough basin and Philippine Sea basin. Along the vertical orientation, from top to the depth there are five velocity layers, with velocities of 1.8-2.2 km/s, 2.4-2.8 km/s, 3.0-3.6 km/s, 4.2-5.1 km/s and 5.75-6.0 km/s respectively. Hereinto, the velocity of upper crust layer is about 3.4 km/s, the velocity of middle crust layer is about 5.9-6.2 km/s, and the velocity of lower crust layer is about 7.1 km/s [9]。At present, there are about 70 wells in the East Tianwaitian-1 well shows that the velocity layers of 1.8-2.2 km/s and 2.4-2.8 km/s are the sediment of

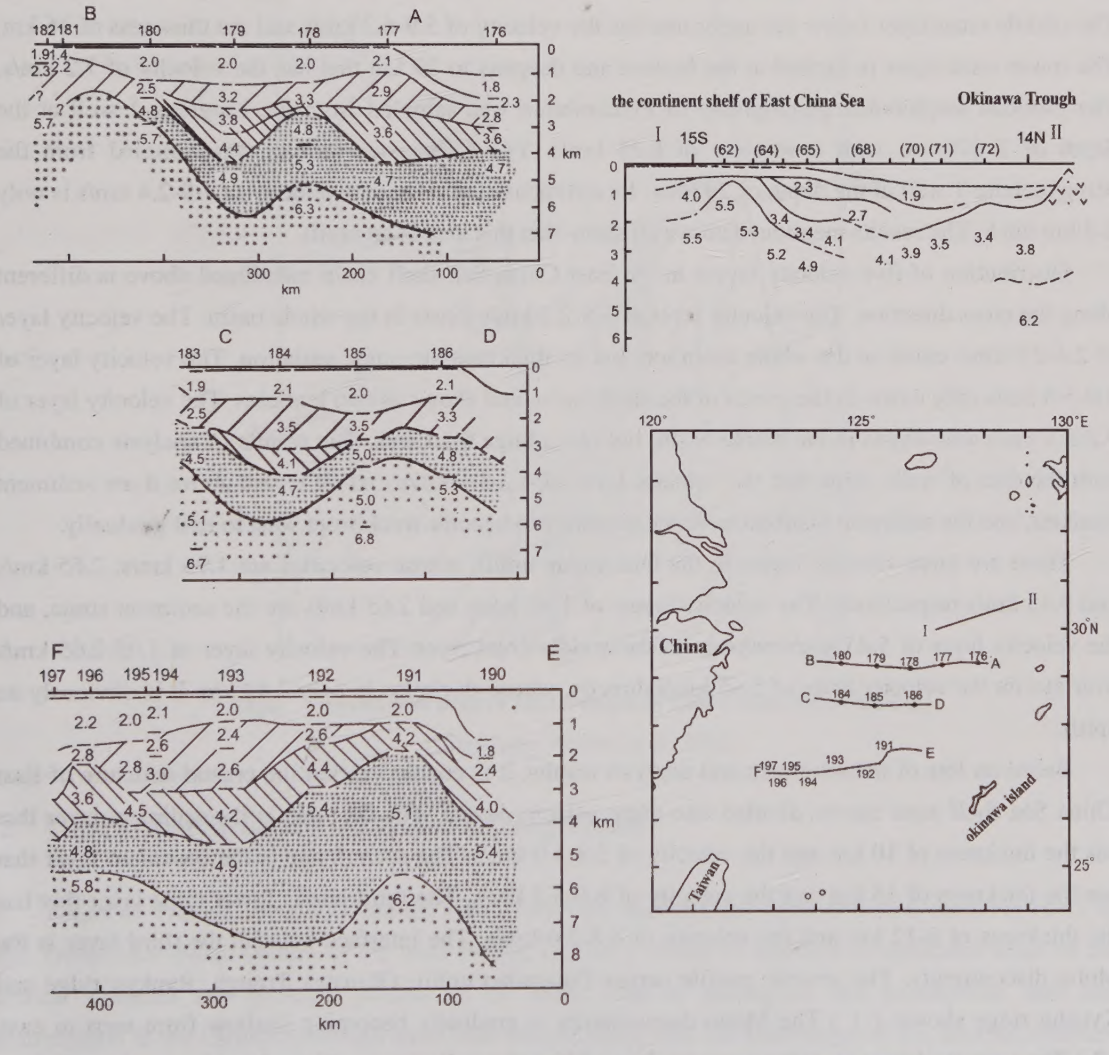


**Fig.1 The sonobuoy measurement profiles in the east continent shelf of East China Sea**

(After Ludwing et al., 1968; Leyden et al., 1973)[7-8]

China Sea shelf basin. The oldest stratum revealed by well is the orthogneiss of Wendong group. The Pliocene-Quaternary, the velocity layer of 3.0-3.6 km/s is the sediment of Oligocene-Miocene, the velocity layer of 4.2-5.1 km/s is the sediment of Eocene, the velocity layer of 5.75-6.0 km/s is presumed as the sediment of Jurassic-Paleocene, and the velocity layer of 6.0 km/s is presumed as a suit of weak metamorphic rocks of the upper Palaeozoic[6]. So as a whole, the continent shelf basin of East China Sea is a large size sedimentary basin of Mesozoic-Cenozoic, and its upper crust is composed of sediment blanket of Paleozoic, Mesozoic and Cenozoic, and its middle crust layer consists of the metamorphic basements or magmatic rocks.

In the east part of Minzhe Uplift, the results of the OBS measurements and the well drilling (Lingfeng-1 well and Mingyuefeng-1 well) both show that the stratum can be divided into three velocity layers. The upper part is the upper crust layer that has the velocity of 3.4 km/s and the thickness of 3 km. The middle crust layer below the upper one has the velocity of 5.9-6.2 km/s and the thickness of 16 km. The lower crust layer is located at the bottom and deepens to 29 km that has the velocity of 7.2 km/s. The biotitize amphibolite plagiogneiss of Precambrian was sampled from the Lingfeng-1 well at the depth of 2 370 m, with a velocity of 6.25 km/s. The Cretaceous granite was sampled from the Mingyuefeng-1 well at the depth of 2930m. Its sediment blanket with a velocity of 1.9-2.4 km/s is only 2-3 km thick. The results mentioned above all show that this area is an uplift.

Distribution of five velocity layers in the East China Sea shelf basin mentioned above is different along the cross direction. The velocity layer of 1.8-2.2 km/s exists in the whole basin. The velocity layer of 2.4-2.8 km/s exists in the whole basin too, but its thickness has some variation. The velocity layer of 3.0-3.6 km/s only exists in the center of the shelf basin, and shows as two lenticles. The velocity layer of 4.2-5.1 km/s also exists in the whole basin, but has a large thickness. The results of analysis combined with the data of wells show that the velocity layer of 4.2-5.1 km/s and all layers above it are sediment blankets, and the sediment blankets have the tendency to become thick from west to east gradually.

There are three velocity layers in the Diaoyudao uplift, whose velocities are 1.95 km/s, 2.65 km/s and 5.45 km/s respectively. The velocity layers of 1.95 km/s and 2.65 km/s are the sediment strata, and the velocity layer of 5.45 km/s belongs to the middle crust layer. The velocity layer of 1.95-2.65 km/s overlays on the velocity layer of 5.45 km/s directly, whose thickness is only 2.44 km. It is obviously an uplift.

Based on lots of measurement and analysis results, it is concluded that the crustal structure of East China Sea shelf zone can be divided into three velocity layers. The first one is the sediment layer that has the thickness of 10 km and the velocity of 5.8-5.9 km/s. The second one is the basement layer that has the thickness of 15 km and the velocity of 6.0-6.3 km/s. The third one is lower crust layer that has the thickness of 8-12 km and the velocity of 6.8-7.6 km/s. The interface beneath the third layer is the Moho discontinuity. The seismic profile across Daoyudao uplift, Okinawa Trough, Ryukyu ridge and Kyushu ridge shows: ( 1 ) The Moho discontinuity is gradually becoming shallow from west to east. ( 2 ) The velocity layers in different zones have different implications, although each zone has all three layers. The velocity layer of 6.0-6.3 km/s distributed along the coast is absent in the Kyushu ridge.

( 3 ) The crust becomes thin from west to east, but the thinned layers are the first and second layers, not the third one.

The crustal thickness along the coastal area of Zhejiang and Fujian provinces is about 33-35 km. The Moho discontinuity rises up from the continent of East China to Ryukyu Arc uniformly. The Moho depth does not have any big changes of gradient, although it has some local and small range fluctuation. But the crustal thickness becomes thin sharply at the eastern margin of the shelf basin; its thickness thins from 26 km to 18 km sharply. The isoline of the thickness expands in the NE–NNE direction and appears as the gradient zone of the Moho isoline. It is revealed that this changed area of the Moho isoline belongs to the transitional crust (Fig.2).

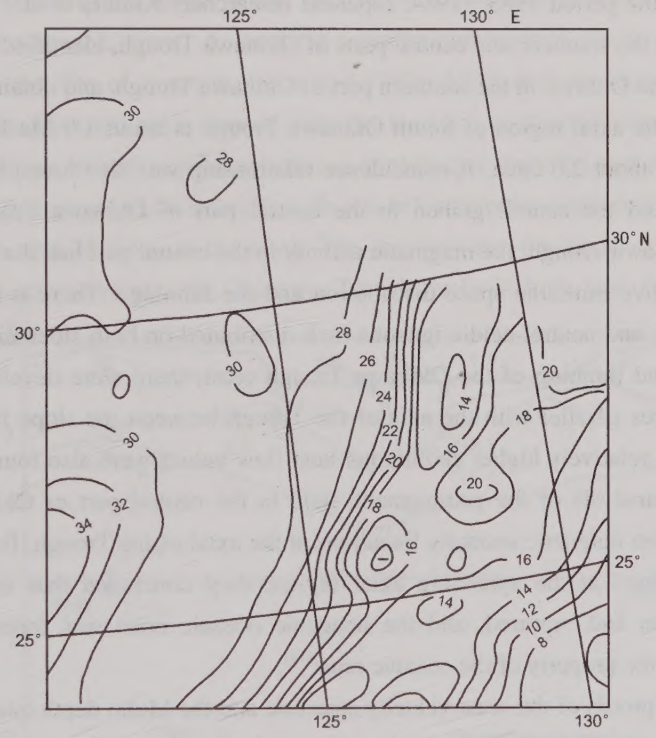


**Fig.2 Distributive map of Moho depth of East China Sea (unit:km)**

(After Jiang Weiwei et al., 2002)

## 2 The Crustal Structure of Okinawa Trough Zone

Okinawa Trough, lying between the East China Sea shelf and the Ryukyu Arc, is the component of the Trench-Arc-Basin system of the west Pacific Ocean. It is one of the most complicated areas of the crustal structure and geologic process in the earth. Lots of geological and geophysical data and information in the Okinawa Trough have been accumulated. But the knowledge of the internal structure of Okinawa Trough is still inadequate. Many researchers have conducted substantial research work from various aspects on the genesis and the crustal property of Okinawa Trough and some different opinions

have been reached. To the present, there are three main different opinions: ( 1 ) Okinawa Trough is a back-arc basin generated by the collision of the oceanic plate and the continent plate, and it is a marginal basin generated after the Ryukyu Arc separated from the Asian continent. There are a series of graben-type normal faults parallel with the axial direction in the center of Okinawa Trough, so Okinawa Trough has the property of the oceanic crust. ( 2 ) Okinawa Trough still doesn't reach the stage of the oceanic crust greatly, and as a whole it still belongs to the continent crust. ( 3 ) Okinawa Trough is located in the transitional zone between the continent crust and the oceanic crust, and it has the property of the transitional crust.

The submarine geologic survey was carried out in the Okinawa Trough and the adjacent regions by the Japanese side in the period 1983—1984. Japanese researchers Kimura et al.[10] found the magnetic anomaly lineations in the southern and central parts of Okinawa Trough, identified the polarity events of Brunhes、Jaramillo and Olduvai in the southern part of Okinawa Trough, and obtained that the spreading time of the crust in the axial region of South Okinawa Trough is about 1.9 Ma B. P., and the average spreading velocity is about 2.0 cm/a. A coincidence relationship was also found between the magnetic anomaly lineations and the central graben in the central part of Okinawa Trough. Along with the spreading of the Okinawa Trough, the magmatic activity in the central part had the obvious zonation and asymmetry of the active time, the space distribution and the lithology. There is mainly basic igneous rock in the axial part, and neutral-acidic igneous rock distributed on both sides discontinuously. Along with the spreading and thinning of the Okinawa Trough crust, there were developed a mass of NEE direction fault fractures parallel with the axis of the Trough between the slope fracture and the slope base fracture [11]. The relatively higher geothermal heat flow values were also found in that area [12]. At home, based on the analysis of the geomagnetic field in the central part of Okinawa Trough, Liang Ruicai et al. tracked the magnetic anomaly lineations at the axial of the Trough. In the light of the fresh tholeiitic basalt obtained at the spreading axial region, they concluded that the lithosphere of the spreading axial region had ruptured, and the neogenic oceanic crust was formed, and the crust of Okinawa Trough had the property of the oceanic crust[13].

But the obtained proofs of the crust velocity structure and the Moho depth queried the viewpoint of the oceanic crust after further investigation. The data of the sonobuoy seismic refraction measurement showed that the crustal velocity structure of Okinawa Trough was different along both the cross direction and the vertical orientation. As a whole, there are six velocity layers along the vertical orientation, which are1.8-2.11 km/s，2.4-2.8 km/s，3.4-3.6 km/s，4.0-5.3 km/s，5.96-6.0 km/s and over 7.0 km/s from top to bottom. This distribution of the velocity structure illustrates that there were developed three suits of sediment layers above the acoustic basement layer at the Okinawa Trough. It is known that the crust of Okinawa Trough would be very young if it began to develop the oceanic crust and to spread. The current central tensional fracture graben is the center of the upwelling and the formation of the neogenic oceanic crust; and it is also the center of the spreading. So the sediment layer on the central tensional fracture graben should be very thin, or even there was not any sediment. In fact, there are thick sediments developed in the central tensional fracture graben in the Okinawa Trough,

especially the sediments of Holocene and Pleistocene become thick from the slope to the center of the Trough, and the biggest thickness at the central tensional fracture graben is more than 3 000 m. Furthermore, the information of the seafloor dredge investigations up to 1994 shows that there are some scattered basalt rocks in the southern part and the central tensional fracture graben of Okinawa Trough. But it can't be confirmed that the large-scale striped large-scale basalt is developed in the spreading center, and the oceanic tholeiitic basalt crust is developed in the spreading center of the Trough even more. Additionally, the granite rock layer (the velocity is 6.0 km/s and the thickness is 4-5 km) was detected by OBS refraction seismic measurements in the DELP-1984 and DELP-1988 cruises. The measurement data also showed that the crust thickness at the thinnest part is still more than 18km[14] (Fig.3). So until the present time, there is still lack of the exact proof that the Okinawa Trough has already developed the oceanic crust. A Japanese scientist summarized the investigation and study achievements around the Sea of Japan in the period 1982—1992, and was inclined to think that the Okinawa Trough is the back-arc basin formed after the back-arc continental crust of Ryukyu Arc was pulled apart. The back-arc spreading process becomes more active from the east part to the west part of the trough. The crustal structure of Okinawa Trough still belongs to the continental crust; its thickness is 27-30km in the north, and 23-24km in the south. The thickness has the tendency to thin from north to south. Based on the characteristics of Okinawa Trough such as high heat flow values, intensive

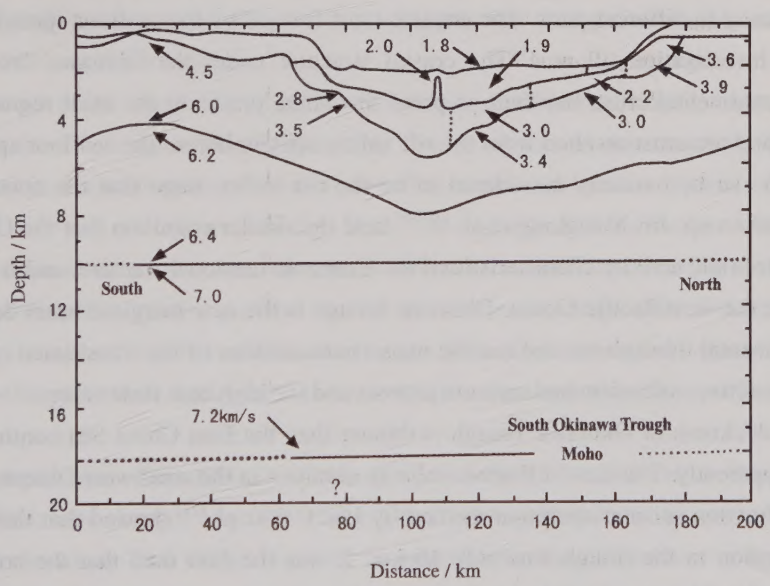


**Fig.3 The 2D velocity pattern on the basis of seismic profile from the DELP cruise in the south Okinawa Trough (The number in the figure is the velocity value of P wave)**

(After Hirata et al., 1991)[14]

earthquake and volcanic activities, extension faults and rapid sedimentation, many researchers at home consider that the evolution of Okinawa Trough has already reached the transitional stage between the highest stage of continental tension rifting and the stage of back-arc seafloor spreading. But it still hasn't

reached the stage of the seafloor spreading and the formation of oceanic crust. The Okinawa Trough crust still has the structure characteristics of continental crust, but the crustal thickness of the trough has already become thinned [15].

Along with further investigation and research, more and more researchers found that it was not enough to describe the complex crustal structure of Okinawa Trough using the simple subdivision of the continent crust or the oceanic crust. Then the viewpoint of the transitional crust has come forth. Based on the element-isotopic geochemical characteristics study of the basalt obtained from the Okinawa Trough, Honma H et al. [16] considered there had developed the underplating process under the lower crust of Okinawa Trough. This indicates that although the crust of Okinawa Trough belongs to the continent crust, the upwelling of the mantle magma has already occurred. Using the seismic tomography imaging method of P and S waves, the subducting plate of the west Pacific Ocean was studied by Zhou Huawei and Clayton W et al.[17]. They found that Okinawa Trough had the characteristic of the zonation along the east-west direction. The velocity of P wave is high in the East China Sea shelf zone, and lower in the Okinawa Trough zone, and the region with lower velocity extends in the NE direction. The lower velocity anomaly is more distinct in the Okinawa Trough and inside the Ryukyu Trench. The high velocity belt outside the Ryukyu Trench is discontinuous in the Okinawa Trough. This indicates that the subsection character of Okinawa Trough crust is the reflection on the earth surface of the physical property discrepancy in different parts. The oceanic crust formed by the seafloor spreading hasn't been found in much investigation till now. The crustal structure under the Okinawa Trough shows the property of the continental crust, but there is proof that some places in the axial region of the trough belong to the island arc crust resulted from the rift valley activity before the seafloor spreading. So the Okinawa Trough can be basically considered to be the rift valley stage that the continent begins to spread and be broken up. Jin Xianglong et al. [18-20] held the similar cognition that the Okinawa Trough has the obvious tectonic activity characteristic of the Cenozoic tensional fracture, and it is the youngest back-arc basin in the west Pacific Ocean. Okinawa Trough is the new marginal basin developed on the basis of the continental lithosphere, and has the main characteristics of the transitional crust such as the thinned crust, the active volcanism and tectonic process and the high heat flow values.

The crustal thickness of Okinawa Trough is thinner than the East China Sea continental shelf and Ryukyu Island apparently. The data of P wave velocity obtained in the southwest Okinawa Trough using the two boats refraction seismic operation method by Lee C S et al. [21] showed that the Moho depth at the shallowest region in the trough was only 16 km. It was the first time that the conception of the thinned crust in the Okinawa Trough had been established. The results computed from the newest gravity data indicate that the crustal thickness is about 26-30 km in the East China Sea shelf zone, about 19-22 km in the Okinawa Trough zone, and about 24-28 km in the Ryukyu Island arc zone [22]. So the Moho discontinuity in the Okinawa Trough has uplifted higher than the East China Sea shelf zone and the Ryukyu Island arc zone in varying degrees. The Moho in the Okinawa Trough appears as an uplifted zonal area, and the strike direction of the isobath is in the northeast. The thickness of Moho is about 17-18 km in the south part and about 18-20 km in the north part of the Okinawa Trough. Therefore the

cognition is obtained that the crustal structure of Okinawa Trough belongs to the thinned continental crust.

## 3 The Crustal Structure of Ryukyu Arc-trench Zone

Ryukyu Arc may be divided into the inner arc and the outer arc. The inner arc is mainly composed of the Quarternary volcanic rock which is known as the Tokara volcanic chain. The outer arc is mainly composed of the granite or the sedimentary rock formed in different times and intruded by the diabase. The biggest crustal thickness of Ryukyu Arc is about 31 km, and has a good coincidence relation with the lowest gravity anomaly of 30 mGal. Here the gravity anomaly is about 140 mGal less than the highest value of Okinawa Trough, but the crustal thickness increases 10 km approximately. The sediment is comparatively thin at the top and the west slope of the outer arc, and the maximal free-air anomaly can reach 95 mGal. The second layer whose seismic velocity is 6.0 km/s has become thinned apparently from the continent slope to the Ryukyu Ridge. This phenomenon shows that the crustal structure has changed intensively. The computational results show that the crustal thickness is thinning drastically with a gradient of 2 km per 10 km towards the trench. This feature indicates that the crust of Ryukyu arc-trench zone is the typical transitional crust between the continental crust and the oceanic crust. And here may be the region where the crustal structure changed most drastically in the west marginal area of the west Pacific Ocean.

The water depth of the slender Ryukyu Trench adjoining the Ryukyu Ridge is more than 6 500 m in the most part of the axial region. The depth of the Trench center can even reach up to 7 500 m. The width of the Ryukyu Trench bottom is about 10 km. The crustal thickness is thinner than both the East China Sea shelf zone and the Okinawa Trough zone. The upper mantle has become rising rapidly from the continental slope to the trench, and the crustal thickness at the base of trench is commonly 6 km. Correspondingly, there is a gravity gradient zone at the continental slope side of the trench, where the gravity anomaly increases from 270 mGal at the slope to 380 mGal at the axial region of the trench. The gradient is 20 mGal per 10 km. All of these indicate that the crust under the Ryukyu Trench is obviously of the oceanic property.

The Moho depth varies from 12 km to 20 km in the trench and from 20 km to 30 km in the arc. The isobath of the Moho here changes very drastically. Thus, the most distinct Moho gradient zone is located at this region in the whole East China Sea area. In general, the crustal structure of Ryukyu arc-trench zone belongs to the transitional crust, but the crustal structures of the arc and the trench are not alike incompletely, and they have their own characteristics. Four velocity layers were obtained at the two measurement points (C18, C19) on the ocean side of the trench using the two boat seismic refraction method in the south and the middle part of Ryukyu Trench which are located to the south of the Tokara Strait. The P wave velocity of the first layer is respectively 2.0 km/s and 2.8 km/s, and the thickness is respectively 0.06 km and 2.9 km. The P wave velocity of the second layer is 4.4 km/s, and the thickness is respectively 2.3 km and 0.7 km. The P wave velocity of the third layer is respectively 6.5 km/s and

6.3 km/s, and the thickness is respectively 2.85 km and 1.5 km. The velocity of the upper mantle is 8.1 km/s. The velocity structure indicates that the ocean side of the south and the middle parts of Ryukyu Trench belong to the oceanic crust. But the seismic refraction profile on the continental slope side shows that there exists a thick layer (probably thicker than 6 km) with a velocity of 5.0 km/s which underlays a layer whose thickness is 3 km and the velocity is 3.0 km/s, and there is another sediment layer (the thickness is less than 1 km) whose velocity is 2.0 km/s above the latter layer. In addition, the free-air anomaly on the continental slope side of the trench is about 100mGal higher than the axial region. This phenomenon indicates that the crust is composed of the high-density rock, and it is possibly part of the continental crust similar to the crust of Ryukyu Arc[23]. The seismic research in the north part of Ryukyu Trench shows that the crust on the continent side of the trench has transited to the oceanic crust[7].

The Moho depth of the northwest Philippine Sea basin located to the east of Ryukyu Trench is deeper in the north part than in the south part. Except the ocean ridge regions, the Moho depth varies between 14-11 km, so the crust belongs to the typical oceanic type. The Moho depth of Philippine Sea at the shallowest place is less than 10 km, and the minimum depth value may reach 4 km. The sediment in the Philippine Sea is very thin too. The sediment covers the whinstone layer directly. And there is no granitics layer. Therefore the crust of Philippine Sea belongs to the typical oceanic crust, its crustal structure is relatively simple, and each layer basically distributes in a horizontal style.

## 4 Conclusions

Based on lots of investigation and study achievements, this paper analyses and discusses the crustal structure and the crustal property synthetically. According to the differences in the crustal velocity structure from west to east, the East China Sea is divided into three zones, *i.e.*, East China Sea shelf zone, Okinawa Trough zone and Ryukyu arc-trench zone. The East China Sea shelf zone mostly has three velocity layers — the sediment blanket layer (the velocity is 5.8-5.9 km/s), the basement layer (the velocity is 6.0-6.3 km/s), and the lower crust layer (the velocity is 6.8-7.6 km/s). The crust of East China Sea shelf zone belongs to the typical continental crust. The Okinawa Trough zone is located at the transitional belt between the continental crust and the oceanic crust. It still has the structural characters of the continental crust, without any formation of the oceanic crust, but the crust of the central trough has begun to thin down. The crust of the Ryukyu arc-trench zone belongs to the transitional type crust as a whole, but the ocean side of the trench already belongs to the oceanic crust. And the northwest Philippine Basin to the east of the Ryukyu Trench absolutely belongs to the typical oceanic crust.

## Acknowledgments

The project is funded by the National Basic Research Program of China (No.G20000467).

## References


[1] Liu Guangding. *Map Series of Geology and Geophysics of China Seas and Adjacent Regions.* Beijing: Geological Publishing House, 1992 (in Chinese).

[2] Liu Ganging. *Geological and Geophysical Features of China Seas and Adjacent Regions*. Science Press, Beijing, 1992, 55-65 (in Chinese).

[3] Liu Futian, Li Qiang, Liu Jianhua et al. *The Seismic tomography Imaging of Japan Sea and Adjacent Regions.In:The Geophysics Progress in 1980s*. Scientific Books and Periodicals Press, Beijing, 1989, 260-274 (in Chinese).

[4] Liu Jianhua, Wu Hua, Liu Futian. Features of 3D Velocity Distribution and Lithosphere Structure in South China and its contiguous Sea Area. *Chinese Journal of Geophysics*, 1996, 39(4): 483-492 (in Chinese).

[5] Jiang Weiwei, Liu Shaohua, Zhu Dongying. Actuality of Investigation and Study of Geology and Geophysics of East China Sea and Okinawa Trough. *Progress in Geophysics*. 2001, 16(4): 71-84 (in Chinese).

[6] Xu Weiling, Huang Zhaoxiong, Le Junying. The Geologic Profile of the Mouth Of Changjiang Rive-Ryukyu Trench. In: *Geological and Geophysical Features of China Seas and Adjacent Regions*. Science Press, Beijing, 1992, 289-301 (in Chinese).

[7] Ludwing W J, Murauchi S, Den N et al. Structural of East China Sea-Western Philippine Sea margin off southern Kuyshu. *Japan. JGR*, 1968, 78(14): 2 526-2 536.

[8] Leyden R, Ewing M, Murauchi S. Sonobuoy Refraction measurements in East China Sea. *Am. Assoc. Pet. Geol. Bull.*, 1973, 57: 2 396-2 403.

[9] Luan Xiwu, Gao Dezhang, Yu Puzhi et al. The Crustal Velocity Structure of a Profile in the Area of East China Sea and its Vicinity. *Progress in Geophysics*, 2001, 16(2): 28-35 (in Chinese).

[10] Kimura M. Back-arc rifting in the Okinawa Trough. *Marine and Petroleum Geol.,* 1985, 2(3): 222-240.

[11] Kimura M, Frukawa M, Izawa E et al. Report on DELP 1984 Cruise in the Okinawa Trough, Part7, Geologic Investigation of the Central Rift in the Middle to Southern Okinawa Trough. *Bull. Eri. Univ. Tokyo,* 1991, 66(1): 179-210.

[12] Kimura M, Uyeda S, Kato Y et al. Active Hydrothermal Mounds in the Okinawa Trough Back-arc Basin. *Japan, Tectorlophysics*, 1988, 22: 135-147.

[13] Liang Ruicai, Wang Shugong, Wu Jinlong. Preliminary Study on Geophysical Field and the New Oceanic Crust in the Middle Region of the 0kinawa Trough. *Marine Geology & Quaternary Geology,* 2001, 21(1): 51-55 (in Chinese).

[14] Hirata N, Kinoshita H, Katao H et al. Report on DELP 1988 Cruise in the Okinawa Trough, Part3, Crustal Structure of the Southern Okinawa Trough. *Bull. Earthq. Res. Inst.,* 1991, 66: 37-70.

[15] Zhou Zuyi, Liao Zongting, Jin Xingchun et al. Okinawa Trough:The Hightest Stage of Continental Tension Rifting in Back-arc Setting. *Marine Geology & Quaternary Geology*, 2001, 21(1): 57-64 (in Chinese).

[16] Honma H, Kusakabe M, Kagami H et al. Major and Trace Element Chemistry and D/H, $^{18}O/^{16}O$, $^{87}Sr/^{86}Sr$ and $^{143}Nd/^{144}Nd$ Rations of Rocks from the Spreading Center of the Okinawa Trough, a Marginal Back-arc

Basin. *Geo. Journal (Japan),* 1991, 25(2): 121-136.

[17] Zhou H, Clayton R W. P and S Wave Travel Time Inversions for Subducting Slab under the Island Arcs of Northwest Pacific. *J. Geophys .Res.*, 1990, 95: 6 829-6 851.

[18] Jin Xianglong, Yu Puzhi, Lin Meihua et al. Preliminary Study of the Crustal Structure Property in Okinawa Trough. *Oceanologia et Limnologia Sinica,* 1983, 14(2): 105-116 (in Chinese).

[19] Jin Xianglong, Zhuang Jiezao, Tang Baojue et al. The Structural Features of Seismic Reflection of Okinawa Trough. *Oceanologia et Limnologia Sinica,* 1985, 16(6): 481-487 (in Chinese).

[20] Jin Xianglong, YU Puzhi. The Structural Features and the Evolution of Okinawa Trough. *Science in China (B)*, 1987, 2: 196-203 (in Chinese).

[21] Lee C S, Shor G G, Bibee L D, Lu R S et al. Okinawa Trough: Origin of a Back-arc. *Marine Geology,* 1980, 35: 219-241.

[22] Jiang Weiwei, Liu Shaohua, Hao Tianyao et al. Imputation of Crustal Thickness of East China Sea and Okinawa Trough Using Gravity Data. *Progress in Geophysics*, 2002, 17(1): 35-41 (in Chinese).

[23] Shi Yizhong. *The Moho and the Crustal Structure.In: Geologic Geophysical Features of China Seas and Adjacent Regions*. Science Press, Beijing, 1992, 71-79 (in Chinese).

# Study on Nutrient Limitation of Phytoplankton in the Field Experiment of the Yangtze River Estuary in Summer

ZHAO Weihong (赵卫红)[1], LI Jintao (李金涛)[1,2] , WANG Jiangtao (王江涛)[2]

1 *Key Laboratory of Marine Ecology and Environmental Sciences, Institute of Oceanology, Chinese Academy of Sciences, Qingdao* 266071, *Shandong, China*

2 *College of Chemistry and Chemical Engineering, Ocean University of China, Qingdao* 266003, *Shandong, China*

**Abstract** From July 23rd to August 15th, 2001, a field cultivation experiment was carried out to determine the limitation factors of phytoplankton in the Yangtze River estuary and the adjacent areas. The results indicated that the potential limiting nutrient was phosphorus in the Yangtze River diluted water area, nitrogen in the offshore of the Yangtze River estuary and the conversion of phosphorus to nitrogen in the middle area. Iron and silicon were not the potential limiting factors. If there were some kinds of limiting factors in the water, the growth of phytoplankton would be limited obviously. In case of disappearance of the limiting factor, the phytoplankton would grow fast. When the *Noctiluca scintiuans* bloom occurred, the phytoplankton biomass level was very low in a short time due to the grazing pressure. When the grazing pressure disappeared, the phytoplankton would grow quickly in abundant nutrients condition.

**Keywords** the Yangtze River estuary; phytoplankton; nutrient limitation

## Introduction

The growth of phytoplankton, which is the main primary producer in the ocean, is always limited by some nutrients such as nitrogen and phosphorus. This limitation has spacial variation, and even in the same area, the nitrogen and phosphorus limitation has seasonal alternation [1]. There are many ways to determine the nutrient limitation of phytoplankton growth. Among them, the enrichment bioassay is the closest to the natural condition and is accepted by many scholars [2-7].

In recent years, abundant nutrients have been imported into the estuary area through the Yangtze River [8, 9], which makes the environment of the Yangtze River estuary and the adjacent areas more complicated and diverse. Harrison et al. (1990) [10] studied the proportion of nutrients in the Yangtze River estuary area and found that phytoplankton growth was limited by phosphorus in the extension areas of the Yangtze River estuary due to the overhigh ratio of nitrogen to phosphorus; limited by nitrogen in the area of 500 km far offshore of the estuary; in the near mouth area, because of the high concentration of suspended particulate materials, primary productivity was mainly limited by

Received on April 8, 2005

illumination. Shen Zhiliang (1993) [11] used the same method and found that in the Yangtze River estuary, primary productivity was mainly limited by diaphaneity, while the nutrients hadn't obvious limiting effect. Pu Xinming et al. (2000, 2001) [4, 5] used an enrichment bioassay and nutrients investigation to study the demand of phytoplankton for the nutrients in autumn and spring, and considered that the estuary area could be divided into several parts based on the distance from the estuary in autumn: the illumination limitation near estuary area; the illumination and phosphorus limitation in the middle area; nitrogen limitation in the area offshore estuary. The borderline of the conversion from phosphorus to nitrogen limitation locates along the approximately 31 isohaline. In spring, this sea area could be divided into the near estuary area; the Yangtze River diluted area; Taiwan warm current influence area and the Yellow Sea coast-wise current area. In order to further understand the limitation factors of phytoplankton growth in the Yangtze River estuary, a field experiment of nutriental addition cultivation were carried out during a summer cruise. Among the three experimental stations, the algal blooms were observed in the two stations in which one was the *Skeletonema costatum* bloom and the other was the *Noctiluca scintiuans* bloom.

## 1 Materials and Methods

### 1.1 The stations of the field culture experiment

Three typical stations such as C105 (32° N, 123° E), C205 (31° N, 123° 30′ E), C304 (29° 40′ N, 123° 18′ E) were chosen to do the field culture experiments. C105 represented the bayou area of the near coast, C205 represented the transitional area, and C304 represented the offshore estuary area [4, 12]. The culture experiment stations are shown in Figure 1.

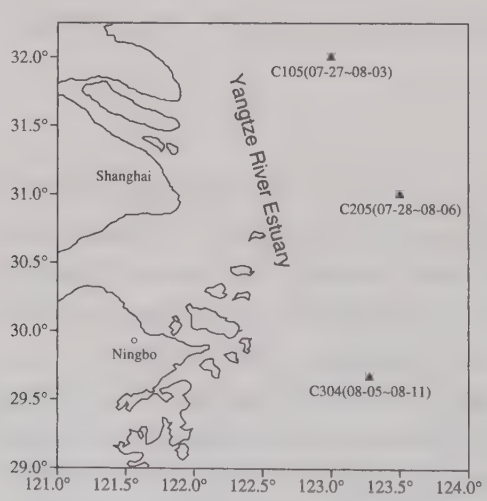


**Fig. 1 The stations of field culture experiments**

### 1.2 Method of field culture experiment

After R/V "Jinxing No.2" arrived at the preconcerted station, collect the surface seawater, filtrate

the seawater with 200 μm mesh cleaned by hydrochloric acid to get rid of macro-zooplankton and macro suspended particulate material, then put the filtrate into six five-liter transparent plastic bottles which were cleaned by hydrochloric acid respectively, number them from one to six. Add the nitrate, phosphate, silicate, iron and vitamins stock solutions into the bottles with the adjustable mechanical pipette, and the added nutrients' concentrations are showed in Table 1. Cover the bottles and put the bottles into culture trunk on the board in which the bathing water is circulated and the temperature is similar to the surface seawater's. The illumination is natural sunlight. Shake bottles three or four times every day to keep the quantity of deliquescent air in the culture medium and prevent organisms from conglomeration.

**Tab. 1 Added nutrients' concentrations in field enrichment experiments / mol • $L^{-1}$**

| Series | No.1 | No.2 | No.3 | No.4 | No.5 | No.6 |
|---|---|---|---|---|---|---|
| | control | all-N | all-P | all-Si | all-Fe | all added |
| $NaNO_3$ | 0 | 0 | 30 | 30 | 30 | 30 |
| $NaH_2PO_4$ | 0 | 5 | 0 | 5 | 5 | 5 |
| $Na_4SiO_4$ | 0 | 20 | 20 | 0 | 20 | 20 |
| Fe | 0 | 0.4 | 0.4 | 0.4 | 0 | 0.4 |
| Vitamins | no | add | add | add | add | add |

Note: Vitamine=100 μg/L $V_{B1}$+0.5 μg/L $V_{B12}$; all-N, all-P, all-Si, all-Fe represent all the nutrients added except nitrogen, phosphorus, silicon and iron; All the added represents all nutrients added.

When the field culture experiment of C205 station has continued for six days, add the nitrate into the all-N series, phosphate into the all-P series and both nitrate and phosphate into the all added series respectively at the $7^{th}$ day. The concentration of added nitrate and phosphate was 15 μmol/L and 2 μmol/L respectively. The methods of culture and sampling were the same as those adopted at the beginning of experiment.

### 1.3 Methods of sampling and preservation

Remove 250 mL culture water every day from the beginning of adding nutrients, filtrate with 0.45 μm cellulose acetate membrane, seal the filtrated membrane into a bag and freeze it in the dark which is used to measure chlorophyll-a. Put the filtrate into plastic bottles, add chloroform, then preserve the bottle with the filtrate in -20 ℃ which is used to measure nutrients.

### 1.4 Determination of nutrients and chlorophyll-a

Nutrients are determined by ChemLab autoanalyzer of nutrients. The determination of ammonia is by Berthelot reaction, nitrite by diazotizing colour, nitrate by the copper-cadmium reduction method. Dissolved inorganic nitrogen (DIN) is the total concentration including ammonia, nitrate and nitrite. Phosphate is determined by the reduced molybdophosphoric acid method. Silicate is determined by the

reduced molybdosilicic acid method.

Chlorophyll-a is determined by spectrophotometer [13]. Extract the membrane sample by 10 mL 90 % acetone solution under 4 ℃ in the dark for 24 h, then separate the extracting solution by centrifuge, aspirate the above limpid solution to determine the absorbency at 750 nm, 664 nm, 647 nm, 630 nm respectively by 721 photometer.

## 2 Results and Discussion

### 2.1 Initial concentrations of nutrients and chlorophyll-a in the field experiment

The initial concentrations of chlorophyll-a at C105, C205 and C304 stations were 45.30, 0.55 and 2.78 μg/L. The chlorophyll-a concentration of C105 was higher than that of other two stations. The seawater of C105 station appeared brown due to the *Skeletonema costotam* bloom occurring. The Yangtze River diluted water turns to northeast from the river mouth in summer and can reach the C105 station [14]. The salinity of surface seawater at the C105 station was 18.32, and its nutrients' concentrations were higher than those of other two stations. DIN concentration was 20 μmol/L, phosphate concentration was about 1 μmol/L, silicate concentration was about 10 μmol/L. Salinities of surface seawater at C205 and C304 stations were 26.34 and 31.05 respectively, which indicated that both stations were influenced less by the Yangtze River diluted water, and the nutrients were lower than that of C105. The culture temperature depended on the temperature of the circulating water that came from the surface water with the ship running. So t he culture temperature ranged from 28 ℃ to 29.5 ℃.

### 2.2 Nutrient and chlorophyll-a changes during the culture process

Figure 2 and Figure 3 showed the curves of nutrients and chlorophyll-a changes with time in each culture experiment at C105, C205 and C304 stations. During the C105 station seawater culture, the concentration of chlorophyll-a was high at the beginning, up to 40 μg/L. Figure 2 showed that the

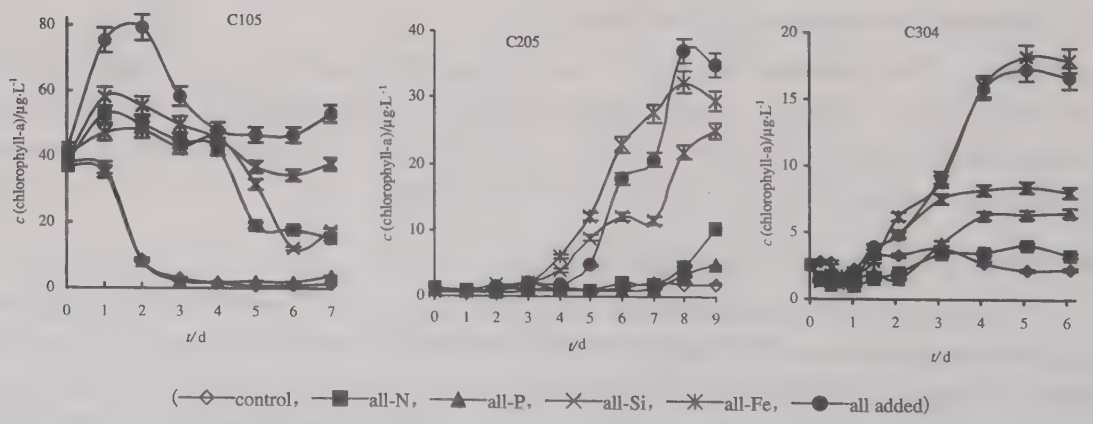


**Fig. 2 The curves of chlorophyll-a in each culture experiment**

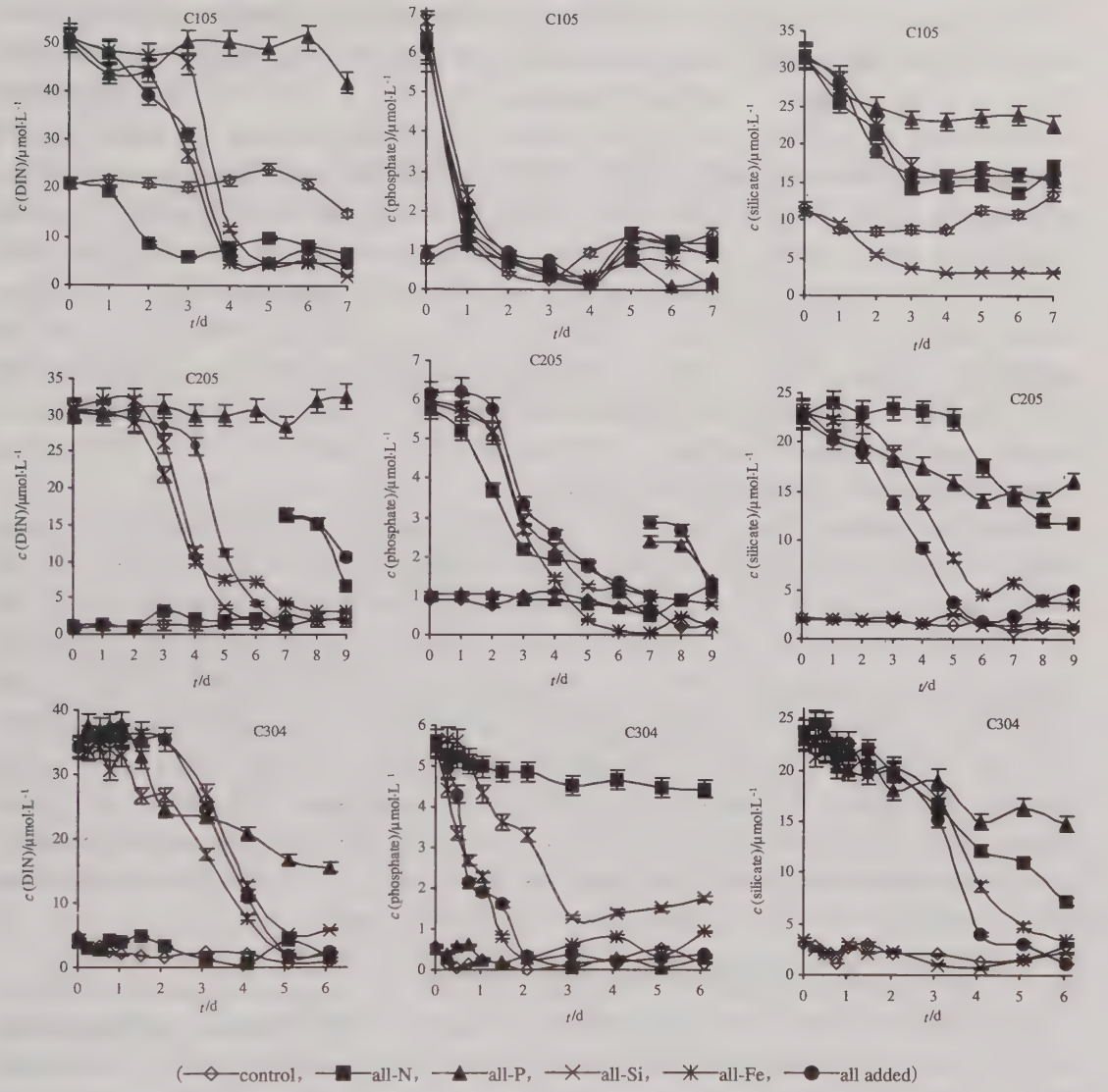


**Fig. 3 The curves of nutrients in each culture experiment**

chlorophyll-a in control and all-P series declined quickly from the 1st day and kept at the 1 to 2 μg/L level at later period .The chlorophyll-a in other series rose to a peak on the 1st or 2nd day. The peak value in all added series was up to 80 μg/L, in all-N, all-Fe and all-Si series up to 50-60 μg/L. Since then, the concentration of chlorophyll-a began to decline, and at the end of the culture, the concentration in all-N and all-Si series declined to 20 μg/L, in all-Fe and all added series to 40-50 μg/L. During the cultivation, the concentration change of DIN, phosphate and silicate appeared an opposite trend to that of chlorophyll-a (Figure 3), viz, the nutrient concentrations declined with chlorophyll-a elevation. The phytoplankton adsorbed less nutrients in control and all-P series due to the limitation by nutrient. However, in all-N, all-Si, all-Fe and all added series, the nutrients were correspondingly enough, the phytoplankton was not limited by the nutrients and their adsorption to nutrients was obvious.

The curves of chlorophyll-a at the C205 station showed that the concentration of chlorophyll-a in all-Si, all-Fe and all added series began to elevate obviously from the 4th day, which suggested that the response of phytoplankton to nutrients enrichment was obvious. However, the chlorophyll-a concentrations in all-N, all-P and control series had less changes with time. After the second enriching nitrate at the 7th day, the phytoplankton in all-N series grew rapidly and chlorophyll-a reached 10 μg/L at the end of the culture. In all-P series, the chlorophyll-a also had an elevation trend after enriching phosphate, but the elevation was not very acute which perhaps was due to the less culture time. In all added series, the chlorophyll-a elevated suddenly after the second enriching nutrient. The nutrients declined rapidly in all-Fe, all-Si and all added series and almost depleted on the 7th day, the DIN concentration declined from 31 μmol/L to 3 μmol/L, phosphate from 6 μmol/L to 0.3 μmol/L, silicate from 23 μmol/L to 3-4 μmol/L. The nutrients in all-N, all-P and control series changed little. In all-N and all-P series, the phytoplankton began to grow after the limiting factors were removed by the second enriching nutrient, and the nutrient declined quickly.

The chlorophyll-a concentrations in the control series at the C304 station had not obvious change during the cultivation and kept at about 2.5 μg/L. The chlorophyll-a concentrations in other series rose slowly in initial 1.5 days. Except all-N series, the chlorophyll-a concentrations in other enriched series rose rapidly from the 2nd day and came into a steady stage till the end of culture. The chlorophyll-a concentrations in all-Fe and all added series reached 8 μg/L. The phytoplankton in all-N series grew very slowly all the time and the highest chlorophyll-a concentration was 5 μg/L. Except the control series, the nutrients in other series had an opposite change trend to the chlorophyll-a. The various nutrients in the control series had little change, but the decreasing extents of the DIN in all-N series, phosphate in all-P series and silicate in all-Si series were less. The DIN, phosphate and silicate in all-Si, all-Fe and all added series declined considerably, the DIN from 32 μmol/L to 2-5 μmol/L, phosphate from 5.5 μmol/L to 0.3-0.5 μmol/L, silicate from 24 μmol/L to 2-5 μmol/L.

### 2.3 The potential nutrient limiting index of phytoplankton

Enrichment Bioassays method is an efficient way to detect nutrient limitation of phytoplankton. AGP (algae growth potential) denotes the maximum biomass of phytoplankton growth in the water. The AGP in the all added series denotes the maximum phytoplankton biomass in the abundant nutrients condition. If one kind of nutrients isn't added, the AGP denotes the maximum biomass that was supported by this no added nutrient. If the ratio of the AGP supported by the no added nutrient to that by the all added nutrients is less than 50%, this nutrient is the limitation nutrient [15]. Because this method ignores the influences of hydrologic factors, such as sunlight, temperature, water movement et al., and predation, the nutrient limiting intensity determined by this method is the potential limitation.

Nutrient potential limiting index is defined as

$$L(X)=\frac{AGP_{(All)}}{AGP_{(All-X)}}\times\frac{1}{2}$$

if $L(X)$ is higher than 1, the element $X$ is a limiting factor. The higher the value is, the more intense the limiting effect is.

Table 2 showed the nutrient potential limiting index at each station. At the C105 station, the

phosphorus potential limiting index was higher than 1, but those of silicon, nitrogen and iron were all lower than 1. So phosphorus was a potential limiting factor at this station, but silicon, nitrogen and iron were not.

**Tab. 2 The nutrient potential limiting index at each station**

| Station | N | P | Si | Fe |
|---|---|---|---|---|
| C105 | 0.75 | 1.13 | 0.82 | 0.71 |
| C205* | 5.21 | 8.18 | 0.85 | 0.37 |
| C304 | 2.13 | 1.36 | 1.03 | 0.47 |

*: The nutrient potential limiting index was calculated based on the maximum biomass before the secondly enrichment.

At C205, the phosphorus potential limiting index was the highest, 8.18; the nitrogen's was next, 5.21. The potential limiting factors at this station were phosphorus and nitrogen, but not iron and silicon. The chlorophyll-a curves in Figure 2 showed that the growth of phytoplankton were limiting obviously in all-N, all-P and control series, but in the other series, the phytoplankton grew quickly from the third day. When nitrate or phosphate was secondly added into all-N, all-P and all added series on the $7^{th}$ day, the phytoplankton grew fast from then on.

The *Noctiluca scintiuans* bloom occurred at the C304 station. The potential limiting index indicated that the potential limiting factor was nitrogen, and then was phosphorus. Due to the intensive phytoplankton action in summer, the nutrient level was very low, and the relative higher salinity at C304 suggested that the Yangtze River diluted water influenced little the water of this station, which made the nutrients structure appear a low N/P, less than 15 in this cruise. So, this station belonged to the nitrogen limiting area. In the control series, due to the lower nutrients level, the phytoplankton biomass changed at a very low level. Zooplankton in ocean may prey on about 0 %-70 % phytoplankton [16], so zooplankton forms a grazing pressure on phytoplankton and primary productivity. Because of the *Noctiluca scintiuans* grazing pressure, the phytoplankton biomass was at a low level in a short time. When the grazing pressure disappeared, the phytoplankton would grow quickly in the abundant nutrients condition.

## 3 Conclusions

(1) The results of the enrichment bioassays experiments indicated that the potential limiting nutrient was phosphorus in the inshore area of the Yangtze River estuary; nitrogen in the offshore area of the Yangtze River estuary and the conversion of phosphorus to nitrogen in the middle area. Iron and silicon were not the potential limiting factors.

(2) If there were some kinds of limiting factors in the water, the growth of phytoplankton would be limited obviously. In case of disappearance of the limiting factors, the phytoplankton would grow fast.

(3) When the *Noctiluca scintiuans* bloom occurred, the phytoplankton biomass was at a low level in short time due to the grazing pressure. When the grazing pressure disappeared, the phytoplankton would grow quickly in the abundant nutrients condition.

## Acknowledgements

This work is jointly supported by KZCX2-207 from CAS and the National Basic Research Program of China (2001CB409703).

## References

[1] Fisher T R, Peele E R, Ammerman J W et al. Nutrient limitation of in Chesapeak Bay. *Mar Ecol Prog Ser*, 1992, 82: 51-63.

[2] Wang Yong, Jiao Nian-zhi. Response of phytoplankton to nutrient addition in Jiaozhou Bay. *Marine Sciences*, 2002, 26(4): 8-12, (in Chinese).

[3] Zhou Li, Zhang Jing. Experimental study on the nutrient limitation in the spring of Bohai Sea. *Oceanologia Et Limnologia Sinica*, 2001, 32(6):673-678, (in Chinese).

[4] Pu Xin Ming, Wu Yulin, Zhang Yongshan. Nutrient limitation of phytoplankton in the Changjiang Estuary I: condition of nutrient limitation in autumn. *Acta Oceanologa Sinica*, 2000, 22(4): 60-66, (in Chinese).

[5] Pu Xin Ming, Wu Yulin, Zhang Yongshan. Nutrient limitation of phytoplankton in the Changjiang Estuary II: condition of nutrient limitation in Spring. *Acta Oceanologa Sinica*, 2001, 23(3): 57-65, (in Chinese).

[6] Bernhard A E, Peele E R. Nitrogen limitation of phytoplankton in a shallow embayment in northern Puget Sound. *Estuaries*, 1997, 20(4): 759-769.

[7] Hutchins D A, Bruland K W. Iron-limited diatom growth and Si:N uptake ratios in a costal upwelling regime. *Nature*, 1998, 393(6685): 561-564.

[8] Wang Baodong. Study on the extension and transportation of the Changjiang River diluted water. *Journal of Oceanography of Huanghai & Baihai Sea*, 1998, 16(2): 41-47, (in Chinese).

[9] Lu Saiying, Ge Renfeng, Liu Lihui. The seasonal variation and physical transportation of nutrients in continental shelf area of the East China Sea. *Acta Oceanologa Sinica*, 1 996, 18(5): 41-51, (in Chinese).

[10] Harrison P J, Hu M H, Yang Y P et al. Phosphate limitation in estuarine and coastal waters of China. *J Exp Biol Ecol*, 1990, 140: 79-87, (in Chinese).

[11] Shen Zhiliang, The effects of physic-chemical environment on the primary productivity in the Yangtze River Estuary. *Transactions of Oceanology and limnology*, 1993, 1:47-51, (in Chinese).

[12] Ye Xianshen, Zhang Yong, Xiang Youtang. Characteristic of nitrate distribution in the Changjiang River estuary and its cause of formation. *Marine Science Bulletin*, 2000, 19(1): 89-92, (in Chinese).

[13] Parson T R, Maita Y and Lalli C M. A manual of chemical and biological methods for seawater analysis. Pergamon Press, New York, 1984, p173.

[14] Liao Qiyu, Guo Binghuo, Liu Zanpei. Analysis of direction change mechanism of the Changjiang River Diluted water in summer. *Journal of Oceanography of Huanghai & Baihai Sea*, 2001, 19(3): 19-25, (in Chinese).

[15] Maestrini S Y, Breret M, Berland B R et al. Nutrients limiting the algal growth potential (AGP) in the Po River Plume and an adjacent area, Northweat Adriatic Sea: Enrichment bioassays with the test algae *Nitzschia closterium* and *Thalassiosira pseudonana*. *Estuaries*, 1997, 20(2): 416-429.

[16] Zhang Wuchang, Wang Rong. Grazing pressure of micro-zooplankton on phytoplankton and primary productivity in marine ecosystem. *Acta Ecologica Sinica*, 2001,21(8):1 360-1 368 (in Chinese).

# Pollution Condition of Petroleum Hydrocarbon Pollutant and Estimation of Its Environmental Capacities in Summer in the Bohai Sea

WANG Xiulin (王修林)[1], LI Keqiang (李克强)[1], SHI Xiaoyong (石晓勇)[1], ZHU Chenjian (祝陈坚)[1], HAN Xiurong (韩秀荣)[1], DENG Ningning (邓宁宁)[1], CHEN Hu (陈 虎)[2]

1 *College of Chemistry and Chemical Engineering, Ocean University of China, Qingdao* 266003, *Shandong, China*

2 *Qingdao Land of Statepower Environment Engineering CO.LTD, Qingdao* 266071, *Shandong, China*

**Abstract** The pollution condition of petroleum hydrocarbon (PH) was summarized in the Bohai Sea in this paper. The results showed that the mean concentration of PH was (25.7±13.6) mg/m$^3$, varying from 4.4 to 64.8 mg/m$^3$ in the survey sea area. Laizhou Bay and Bohai Bay have been contaminated badly inshore. The dynamic model for distribution of marine PH among multiphase environments in the Bohai Sea has been established. The environmental capacities ($EC_O$) and surplus environmental capacities ($SEC_O$) of PH have been estimated in the Bohai Sea according to the dynamic model. The results showed that the $EC_o$ separately were about 29 169 t/a, 177 306 t/a and 298 446 t/a under the first, second and third, fourth class seawater quality standards requirement. And the $EC_O$ of Bohai Bay, Liaodong Bay, Laizhou Bay and Central Bohai Sea were about 5 255 t/a, 8 869 t/a, 4889 t/a and 10 156 t/a respectively under the first and second class seawater quality standards requirement.

**Keywords** Bohai Sea; petroleum hydrocarbon; environmental capacity; dynamic model

The zones around the Bohai Sea are the most developed area in north China [1]. With the development of economy and increasing of population, the marine environment quality has become worse and worse in Bohai Sea, especially in the coastal regions of Bohai Bay, Liaodong Bay and Laizhou Bay [1]. As reported, the petroleum hydrocarbon (PH) contamination in the Bohai Sea was mainly due to the discharge of oily wastewater from inland [1]. There were about 8 734 392.3 $10^4$ t water input in the Bohai Sea annually, which included about 4 500 491.7 $10^4$ t water from rivers such as Yellow River, Haihe River, Liaohe River and Luanhe River, about 32 967.5 $10^4$ t water from the straight discharge outlet, 125 456.9 $10^4$ t water from the mixing discharge outlet, about 22 581.8 $10^4$ t water from sewer and about 4 052 894.4 $10^4$ t mariculture wastewater [2]. It has been reported that the area not up to first and second national seawater class quality standards expanded from 24.6 % in 2001 to 41.3 % in 2002 in the Bohai Sea, and the petroleum hydrocarbon contaminated seriously in local regions[3]. Marine

Received on January 12, 2005

environmental quality has become worse and worse in the Bohai Sea, with a definite impact on the coastal ecosystem, such as decline of primary productivity and biodiversity [4,5]. Petroleum hydrocarbon pollutants have become one of the most serious environmental concerns in the Bohai Sea coastal area, but there are few reports about the pollution condition and distribution in the whole Bohai Sea, which greatly blocks the knowing of marine environment of Bohai Sea. To assess the influences of petroleum hydrocarbon pollutant on the marine ecosystem and to protect the environment, it is necessary to know its marine environmental capacity. But there has been no published report on the environmental capacity of petroleum hydrocarbon in the Bohai Sea till now. Therefore, survey of petroleum hydrocarbon was carried out in the Bohai Sea in August in 2002. Based on the survey, the environmental capacity of petroleum hydrocarbon of Bohai Sea and the important areas such as Bohai Bay, Liaodong Bay and Laizhou Bay were estimated with modelling.

## 1 Material and Method

### 1.1 Survey locations

An integrated survey was carried out in the Bohai Sea (37° 11′ -40° 48′ N, 117° 43′ -122° 09′ E) from 10 to 29 in August in 2002, and the petroleum hydrocarbon concentration was determined. Sixty-two locations were surveyed (Fig. 1) in the Bohai Sea, which was divided into 4 regions. There were 7 locations in the Bohai Bay, 16 in the Liaodong Bay, 11 in the Laizhou Bay, 23 in the Bohai Center and 5 in the Bohai Strait.

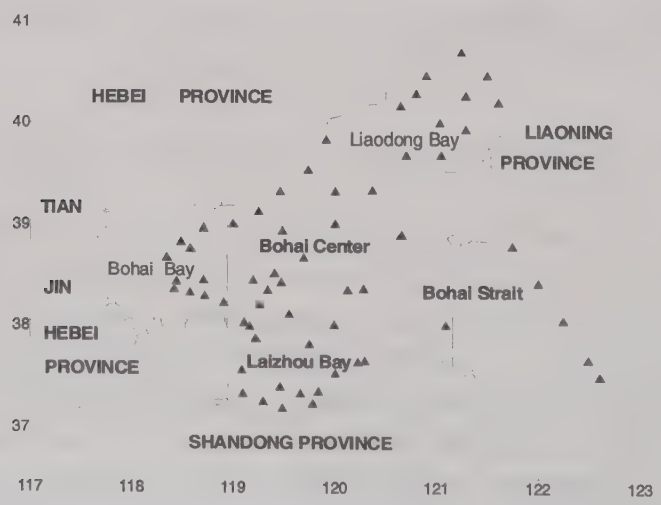


**Fig. 1 Survey locations and regions of Bohai Sea, "▲"represents a survey location**

### 1.2 Survey method

Surface water was sampled to analyze petroleum hydrocarbon by non-oil glass water sampler, and

immediately adjusted to weak acid (pH ≈ 4) using 1:3 $H_2SO_4$, and then extracted two times using 0.01 $m^3$ hexane, and the extraction was sealed up and stored in the dark at (5±2) ℃. PH concentration analysis was carried out by UV method [7] in lab, and the precision was about 98.3 %

## 2 Results and Discussion

### 2.1 Petroleum hydrocarbon pollution condition and distribution

Based on the analysis of samples in August (Tab. 1), 2002, it is indicated that the average concentration of PH was (25.7±13.6) mg/$m^3$ in the surface layer in the survey area of Bohai Sea, varying from 4.4 to 64.8 mg/$m^3$, and the average pollution index was 0.51±0.27, varying from 0.09 to 1.30, and the ratio of exceeding the set standard was 6 % under the first and second class national seawater quality standards requirement, and the detection ratio was 100 %. Further, the average concentrations of PH in the Bohai Bay, Liaodong Bay, Laizhou Bay and Bohai Center met the first and second national seawater class quality standards requirement, and the pollution index was less than 1, which indicated that the water quality in most areas of Bohai Sea was good.

**Tab. 1 Assessment of petroleum hydrocarbon in the areas of Bohai Sea**

| Marine regions | Concentration / mg • $m^{-3}$ | | Pollution index (Pi*) | | Exceeding-the-standard ratio / % |
|---|---|---|---|---|---|
| | Range | Average | Range | Average | |
| Bohai Bay | 19.4-36.6 | 26.8 | 0.39-0.73 | 0.54 | 0 |
| Liaodong Bay | 4.4-64.8 | 23.5 | 0.09-1.30 | 0.47 | 6 |
| Laizhou Bay | 27.8-59.6 | 42.0 | 0.56-1.19 | 0.84 | 30 |
| Bohai Center | 4.6-40.0 | 20.2 | 0.09-0.80 | 0.40 | 0 |
| Bohai Sea | 4.4-64.8 | 25.7 | 0.09-1.30 | 0.51 | 6 |

*: First and second class national seawater quality standards [9]

Figure 2 represents the distribution of PH concentration in the surface layer in the Bohai Sea, and the results indicated that PH concentration was high inshore and low offshore, and high in the Laizhou Bay and Bohai Bay, low in the Liaodong Bay and Baohai Center. Further, the PH concentration decreased from the internal Bay to the outer Bay in the Laizhou Bay and Bohai Bay, and the highest was more than 50 mg/$m^3$ in the Laizhou Bay, which exceeded the first and second class seawater quality standards (Fig. 2). Anyhow, PH contamination in the Bohai Sea was not serious as a whole, but the PH concentration in the coastal Laizhou Bay, Bohai Bay and Liaodong Bay exceeded first and second class seawater quality standards (Fig. 2). Compared with 2001, PH contamination became worse in the Laizhou Bay, and better in the Liaodong Bay, and changed little in other regions[10-17]. And compared

with the 1990s, PH contamination became better[1,4,17].

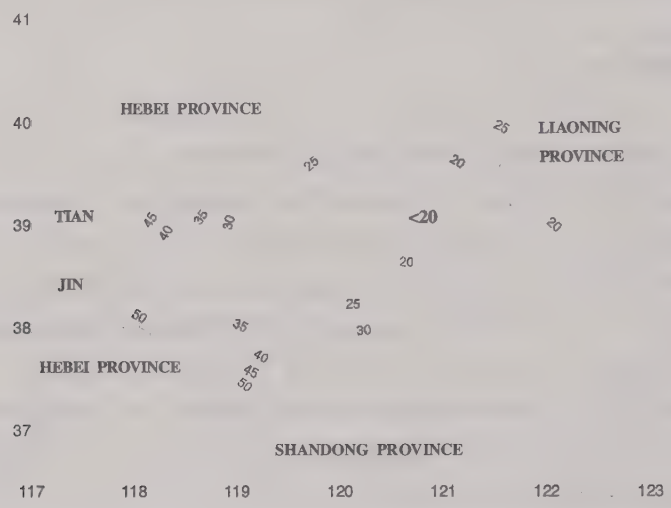


**Fig. 2 Distribution of petroleum hydrocarbon concentration (unit: mg/m$^3$)**

## 2.2 Estimation of environmental capacity of petroleum hydrocarbon

### 2.2.1 Dynamic model of petroleum hydrocarbon distributing in the marine environment of Bohai Sea

It can be indicated from the research in the Jiaozhou Bay that marine environmental capacity, which is subjected to the self-purification processes in the coastal area, such as physical processes, volatilization processes, biological processes, and geo-chemical processes, can be estimated according to the dynamic model for distribution of PH pollutant among multiphase environments [18,19]. Petroleum hydrocarbon dynamic model in the Bohai Sea was constructed based on the PH dynamic model in the Jiaozhou Bay, according to the basic principle [20-22] of dynamic model for distribution of marine contamination among multiphase environments. This model was a box model (Fig.3), which included such compartments as PH input, phytoplankton bioconcentration [24,25], suspended sediment adsorption[24], microorganism biodegradation[24], atmosphere volatilization[24,26,27] and transport to the outer sea by water exchange[27,28], and PH concentration ($C_{PH}$) was state function, water temperature[27] (T), phytoplankton biomass[29] (PPT), suspended sediment concentration (SS), etc, were force functions. The model was implemented on the platform of software Modelmaker 4.0 (FamilyGenetix LTD.). The equations were solved by a standard Runge-Kutta method, and the integration time step is typically one day. Initial value for state variable was prescribed as average of PH concentration from observations in the survey, and when the model ran stably, PH concentration of simulation in January was used as the initial value. The environmental capacity and surplus environmental capacity can be calculated according to the definition of marine environmental capacity, the discharged amount of PH in a period of time, when PH concentration in seawater reaches a certain quality standard (such as the

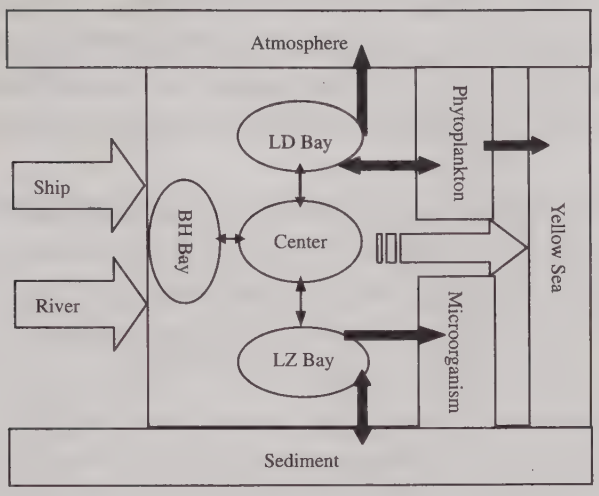


**Fig. 3 Dynamic conception model for distribution of petroleum hydrocarbon in the Bohai Sea**

national seawater quality standard) without any marine ecological disaster [19], after the self-purification capacity of PH has been calculated first, including hydrodynamic transport self-purification; suspended sediment adsorption self-purification; biological self-purification (such as bioconcentration, biomagnification and biodegradation), and atmosphere volatilization self-purification.

$$EC_O = EC_{O_V} + EC_{O_B} + EC_{O_PPT} + EC_{O_SS} + EC_{O_OUT} + M \quad (1)$$

Where:

$$\frac{dEC_{O_V}}{dt} = K_{atm}^0 \times e^{(\frac{\Delta H}{R \bullet T})} \times Q \times C_{PH} \quad (2)$$

$$\frac{dEC_{O_B}}{dt} = K_{bd} \times Q \times C_{PH} \quad (3)$$

$$\frac{dEC_{O_PPT}}{dt} = [K_{up} \times PPT \times C_{PH} - (K_{el} + K_m) \times PPT \times C_{PH_PPT}] \times Q \quad (4)$$

$$\frac{dEC_{O_SS}}{dt} = [K_{ad} \times SS \times C_{PH} - (K_{de} + K_s) \times SS \times C_{PH_SS}] \times Q \quad (5)$$

$$\frac{dEC_{O_OUT}}{dt} = K_{out} \times Q \times (C_{PH} - C_{PH_OUT}) \quad (6)$$

$$M = Q \times (C_S - C_I) \quad (7)$$

Where: $EC_O$—environmental capacity, $EC_{O_V}$—atmosphere volatilization self-purification capacity, $EC_{O_B}$ — microorganism biodegradation self-purification capacity, $EC_{O_PPT}$ — phytoplankton bioconcentration self-purification capacity, $EC_{O_SS}$—suspended sediment adsorption self-purification capacity, $EC_{O_OUT}$—hydrodynamic transport self-purification capacity, $M$—PH capacity in research

region for the national seawater quality standard, $T$—temperature, $t$—Time, $Q$—volume, $C_{PH}$—PH concentration, $PPT$—phytoplankton biomass, $SS$—suspended sediment concentration, $C_{PH_PPT}$—PH concentration in phytoplankton, $C_{PH_SS}$—PH concentration in suspended sediment, $C_{PH_OUT}$—PH concentration in Yellow Sea, $C_S$—PH concentration for the national seawater quality standard, $C_I$—PH background value.

Thus, on the assumption that the self-purification process and regulating principle were similar to the Jiaozhou Bay, the parameters from Jiaozhou Bay experiments can be used as the initial values of the parameters such as phytoplankton bioconcentration parameters ($K_{up}$, $K_{el}$, $K_m$), suspended sediment adsorption parameters ($K_{ad}$, $K_{de}$, $K_s$), microorganism biodegradation parameters ($K_{bd}$) and atmosphere volatilization parameter ($K^0_{atm}$). And the literature value[27,28] was used as the initial value of the hydrodynamic transport parameters ($K_{out_bhc}$, $K_{out_bhb}$, $K_{out_lzb}$, $K_{out_ppt}$) (Tab. 2). The input flux of PH from inland was 13 000 t/a [30], which was estimated according to the PH concentration and the wastewater discharge flux from rivers such as Yellow River, Haihe River, Liaohe River and Luanhe River, straight discharge outlet, mixing discharge outlet and sewage outlet. Based on the assumption that the seasonal

**Tab. 2 Model parameters**

| Symbol | Units | Initial value | Range | Parameters | Referance |
|---|---|---|---|---|---|
| $H$ | kJ/mol | 30 | — | Vaporization heat of PH | [24] |
| $K^0_{atm}$ | 1/day | 0.04 | 0.035-0.045 | Rate constant for volatilization of PH | [22] |
| $R$ | kJ/mol·K | 8.314 | — | Thermodynamic constant | - |
| $K_{bd}$ | 1/day | 0.032 | 0.028-0.036 | Biodegration rate constant for PH | [22] |
| $K_{up}$ | 1/day | 18357 | 16812-19902 | Uptake rate constant for bioaccumulation of PH by phytoplankton | [22,23] |
| $K_{el}$ | 1/day | 1.48 | 1.28-1.68 | Elimination rate constant for bioaccumulation of PH by phytoplankton | [22,23] |
| $K_m$ | 1/day | 0.18 | 0.17-0.19 | Rate constant for mortality of phytoplankton | [22] |
| $K_{ad}$ | 1/day | 28.32 | 27.90-28.74 | Adsorption rate constant for sorption of PH by suspended sediment | [21,22] |
| $K_{de}$ | 1/day | 1.22 | 1.14-1.30 | Desorption rate constant for sorption of PH by suspended sediment | [21,22] |
| $K_s$ | 1/day | 0.0225 | 0.0224-0.0226 | Sedimentation rate constant for suspended particles | [22] |
| $K_{out_bhc}$ | 1/day | 0.00138 | 0.00138 | Rate constant for PH hydrodynamical exchange in Bohai Center | [26] |
| $K_{out_bhb}$ | I/day | 0.00228 | 0.00228 | Rate constant for PH hydrodynamical exchange in Bohai Bay | [26] |
| $K_{out_lzb}$ | 1/day | 0.00369 | 0.00369 | Rate constant for PH hydrodynamical exchange in Laizhou Bay | [26] |
| $K_{out_ldb}$ | 1/day | 0.00084 | 0.00084 | Rate constant for PH hydrodynamical exchange in Liaodong Bay | [26] |
| $K_{out_ppt}$ | 1/day | 0.00138 | 0.00138 | Rate constant for phytoplankton transport to the Yellow Sea | [26] |

variation of PH average concentration in the Bohai Sea was similar to that in Jiaozhou Bay, the parameters could be adjusted in some sort according to the survey value in the Bohai Sea in 2002 (Tab. 1).The result in Table 2 indicated that the varying range had little contrast with the initial values given, which illustrates the rationality of the model parameters from the experiments in the Jiaozhou Bay and the literature.

2.2.2 Estimation of environmental capacity of petroleum hydrocarbon

Based on the model, environmental capacity such as $EC_O^{I,II}$, $EC_O^{III}$ and $EC_O^{IV}$ and surplus environmental capacity ($SEC_O$) of PH in Bohai Sea were estimated under the condition of first, second and third, fourth class national seawater quality standards[9] requirement. The result indicates that $EC_O^{I,II}$ was about 29 169 t/a, $EC_O^{III}$ was about 177 306 t/a, and $EC_O^{IV}$ was about 298 446 t/a. The surplus environmental capacity ($SEC_O$) of PH under the condition of first and second class seawater quality standards requriement in the Bohai Sea was about 13 000 t/a, higher than zero, which indicates that the seawater quality met the first and second class standards requirement, according with the survey. Based on the model, the environmental capacity ($EC_O^{I,II}$) of PH in the regions of Bohai Sea was estimated under the condition of first and second class national seawater quality standards requirement. The result indicates that $EC_O^{I,II}$ in the Bohai Bay was about 5 255 t/a, $EC_O^{I,II}$ in the Liaodong Bay was about 8 869 t/a , $EC_O^{I,II}$ in the Bohai Bay was about 4 889 t/a and in the Bohai Center was about 10 156 t/a. $EC_O$ in the Laizhou Bay was the least in the four regions, and then came the Bohai Bay, which indicated that the capacity of accepting PH pollutant was lower in the two bays, so the seawater quality was worse; $EC_O$ in the Bohai Center was the most, so the seawater quality was better. Therefore, the model was rational and the simulation matched the survey value reasonably well. Thus we can conclude that the first and second class seawater quality standards could be satisfied and more PH pollutants could be accepted in the Bohai Sea. It should be pointed out, however, that the results were estimated regarding the Bohai Sea as a whole. Seawater quality in some area might exceed the first and second class seawater quality standards. Because of less data, estimation of $EC_O$ of PH in the Bohai Sea was done in this paper, more calculation about $EC_O$ (such as calculation according to the marine functional zoning of Bohai Sea[31]) will be done based on further survey in the Bohai Sea in the future.

## 3 Conclusions

The pollution condition of petroleum hydrocarbon pollutant in the Bohai Sea was summarized in this paper. The results showed that, the mean concentration of PH was (25.7±13.6) mg/m$^3$, varying from 4.4 to 64.8 mg/m$^3$ in the survey sea area, where the Laizhou Bay and Bohai Bay have been contaminated worse inshore, and better in other regions. The dynamic model for distribution of marine PH among multiphase environments in the Bohai Sea has been established, according to the basic principle of dynamic model for distribution of marine contamination among multiphase environments. The environmental capacities ($EC_O$) and surplus environment capacities ($SEC_O$) of PH have been estimated in the Bohai Sea according to the dynamic model. The results showed that: the $EC_O$ separately

are 29 169 t/a, 177 306 t/a and 298 446 t/a under the first, second and third, fourth class seawater quality standards requirement. And the $EC_O$ of Bohai Bay, Liaodong Bay, Laizhou Bay and Central Bohai Sea were 5 255 t/a, 8 869 t/a, 4 889 t/a and 10 156 t/a respectively under the first and second class seawater quality standards requirement. The model was rational and the simulation matched the survey value reasonably well. Thus we can conclude that first and second class seawater quality standards could be satisfied and more PH pollutants could be accepted in the Bohai Sea.

According to the contamination status of PH and analysis on environmental capacity, the national department of marine environment management should implement the total quantity control of PH pollutant discharge to the Bohai Sea, and discharge the pollutants scientifically according to the self-purification capacity, enhance management on marine exploitation in the zones inshore, and organically combine the marine pollution control with the inland pollution control.

## Acknowledgements

The paper was supported by the National Science Foundation of China projects (NSFC-40136020) and Shandong Natural Science Foundation projects (L2000E01).

## References

[1] Zhao Zh Y, Kong L H. Environmental status quo and protection countermeasures in Bohai marine areas. *Research of Marine Science*, 2000, 13 (2): 23-27.

[2] Zhang X L. Investigation of pollutant of Pb, Cd, Hg, As in sea water and deposit in Bohai Sea area. *Heilongjiang Environmental Jouknal*, 2001, 25 (3): 87-90.

[3] SOA. *Public Report of China Marine Environment in 2002*. SOA, Beijing, 2003.

[4] Yuan Y X. *Report of "research on environment quality and ecological variation of in Yellow Sea and Bohai Sea"*. Yellow Sea Fisheries Research Institute, Chinese Academy of Fisheries Sciences, Qingdao, 1996, 18-29.

[5] Ded W. Connell Prediction of Bioconcentration and Related Lethal and Sub Lethal Effects with Aquatic Organisms. *Marine Pollution Bulletin*, 1995, 31(4-12): 201-205.

[6] Yang J W. Theory and practice of the total control of pollutant discharge in coastal sea (in Chinese). *Marine Communication*, 2001, (2): 24-26.

[7] "Marine monitoring criterion" Editorial Board. *Marine Monitoring Criterion*. China Ocean Press, Beijing, 1999, 70-72.

[8] Lu B, Xiong J, Zheng S L. The distribution of petroleum hydrocarbon in the regions of Xiaongshan Bay. *Donghai Marine Science*, 1993, 11 (4): 67-74.

[9] GB3097-1997. National seawater quality standard.

[10] Oceanic and Fishery Administration of Shandong Province. *Public Report Marine Environment of Shandong Province in 2001* (in Chinese). Oceanic and Fishery Administration of Shandong Province, Jinan, 2002.

[11] Oceanic and Fishery Administration of Liaoning Province. *Public Report Marine Environment of Liaoning Province in 2001* (in Chinese). Oceanic and Fishery Administration of Liaoning Province, Shenyang, 2002.

[12] Oceanic Administration of Hebei Province. *Public Report Marine Environment of Hebei Province in 2001* (in Chinese). Oceanic Administration of Hebei Province, Shijiazhuang, 2002.

[13] Oceanic Administration of Tianjin. *Public Report Marine Environment of Tianjin in 2001* (in Chinese). Oceanic Administration of Tianjin, Tianjin, 2002.

[14] SOA. *Public Report of China Marine Environment from 1996*. SOA, Beijing, 1997.

[15] SOA. *Public Report of China Marine Environment from 1997*. SOA, Beijing, 1998.

[16] SOA. *Public Report of China Marine Environment from 1998*. SOA, Beijing, 1999.

[17] SOA. *Public Report of China Marine Environment in the End of 20$^{th}$ Century* (in Chinese). SOA, Beijing, 2000.

[18] Ge M, Wang X L, Yan J et al. The calculation of environmental capacities of nutrients of nutrients in Jiaozhou Bay (in Chinese). *Marine Science,* 2003, 27 (3): 36-42.

[19] Li K Q, Wang X L, Yan J et al. Calculation of environmental capacities of petroleum hydrocarbons pollutant in Jiaozhou Bay. *Marine Environmental Science*, 2003, 22 (4): 13-17.

[20] Ye C M. Conception of Multimedia Environment. *Advances in Environmental Science*, 1995, 3 (2): 1-9.

[21] Ye C M, Lei Z F, Yan H. Dynamic Model of N-(2,4-dimethylphenyl)-N' Methyl Formamidine and Other Organic Pollutant in Multimedia Environment. *Journal of Environmental Sciences*, 1997, 15(2): 193-197.

[22] Jerttu L Schnoor. Environmental Modeling. John & Sons Inc., New York, 1996, 185-229.

[23] An Y. *Research on the environmental capacity and transport of petroleum hydrocarbon pollutant in Jiaozhou Bay*. Ocean University of China, Qingdao, 2001.

[24] Wang Xiu Lin, An Yu, Zhang Jun. Contribution of Biological Processes to Self-purification of water with respect to Petroleum Hydrocarbon Associated with No.0 Diesel in Changjiang Estuary and Jiaozhou Bay, China. *Hydrobiologia*, 2002, 469: 179-191.

[25] Shi Xiaoyong, Wang Xiulin, Jiang Yu et al. Influence and bioconcentration of petroleum hydrocarbon associated with oil on and by plankton in a mesocosm experiment of East China Sea. *Proceeding of the Japan-China joint workshop on the cooperative study of the marine environment*. National Institute for Environmental Studies, Tokyo, 1999, 89-96.

[26] Wang Y C, Zhu C J, Sun B Y et al. Simulation experiments of crude oil purification in shallow sea area----the evaporation and degradation process of dispersed oil (in Chinese). *Chinese Journal of Oceanology and Limnology*, 1995, 26 (4): 389-396.

[27] Lin X P, Wu D X, Bao X W et al. Study on seasonal temperature and flux variation of the Bohai Strait. *Journal of Ocean University of Qingdao*, 2002, 32 (3): 355-360.

[28] Wei H, Tian T, Zhou F et al. Numerical study on water exchange of the Bohai Sea: simulation of half-life time by dispersion model. *Journal of Ocean University of Qingdao*, 2002, 32(4): 519-525.

[29] Wei H, Zhao L, Yu Z G et al. Variation of phytoplankton biomass in the Bohai Sea. *Journal of Ocean University of Qingdao*, 2003, 33(2): 173-179.

[30] State Environmental Protection Administration. *Environmental protection projects of the Bohai Sea*. State Environmental Protection Administration, Beijing, 2001.

[31] SOA. *The marine function area setting of China*. SOA, Beijing, 2002.

# Species Diversity and Abundance Distribution of Pelagic Siphonophores in Nan Wan Bay of Taiwan, China, in Late Autumn and Early Winter

ZHANG Jinbiao (张金标)[1], HWANG Jiangshiou (黄将修)[2], LIAN Guangshan (连光山)[1], TANG Senming (唐森铭)[1]

1 *Key Laboratory of Global Change and Marine-Atmospheric Chemistry, Third Institute of Oceanography, SOA, Xiamen* 361005, *Fujian, China*

2 *Marine Biology Institute, Taiwan Marine University, Jirong* 20224, *Taiwan, China*

**Abstract** Zooplankton surveys were carried out on November 2-3 and December 8-10, 2001 at 12 stations in the Nan Wan Bay of Taiwan, China. Altogether 92 quantitative zooplankton samples were collected from subsurface water and bottom water layers with two conical plankton nets (180 cm in length, 45 cm in opening diameter, 333 μm and 200 μm in mesh size). A total of 31 species of Siphonophores were identified, among them 7 species are new records in the waters around Taiwan Island, of which *Rocacea cymbiformis* is a new record in China. Dominated by *Chelophyes appendiculata*, *Bassia bassensis*, *Diphyes bojani*, *Diphyes dispar*, *Abylopsis eschscholtzi* and *Chelophyes contorta*, these species accounted for over 76 % and 63 % of the total abundance in November and December. The species number and Siphonophores abundance in December (25 species, 1.99 inds/$m^3$) were more than those in November (19 species, 0.438 inds/ $m^3$), and they were more in the surface water layer than in the bottom layer at most sampling stations. In early winter, the offshore high salinity water mass was a main factor influencing the distribution. The sampling efficiency for two plankton nets is discussed and the seasonal variation of species number and abundance in the Nan Wan Bay is compared with that in the neighboring waters.

**Keywords** marine zooplankton, Siphonophores, species diversity, abundance distribution, Taiwan, Nan Wan bay

The role of marine Siphonophores in the bio-oceanography and hydro-acoustics has long been recognized extensively, as well as their advantages and disadvantages in the food web[1-6]. In recent years many research publications have ascribed the "jellyfish bloom" to marine environmental changes, for example, the global warming, water eutrophication and overfishing. The variation of jellyfish abundance has received much attention. In this report the so-called "jellyfish" refer to the animals such as hydromedusa, Siphonophores, Scyphomedusae and Ctenophora, among which, the most important jellyfish is Siphonophores.

The Siphonophores recorded in the waters around Taiwan were *Ceatocymba dentata*, *Ceratocymba*

Received on June 7, 2005

*leuckarti*, *Abyla bicarinata*, Abyla *schmidti* and *Abyla trigona*. These 5 species were described by M. Sears in his "Dana Expedition" according to the specimens collected from the stations of northern, eastern and southern Taiwan as early as 1929 [7]. Almost half a century had passed when the species was first found by Chinese scientists. Another 3 species, *Lensia campanella*, *Lensia subtiloides* and *Abylopsis tetragona*, were first recorded by Chen Qingchao in his publication "Zooplankton and its distribution in the waters around Taiwan and in the northern South China Sea"[8]. Later on, 26 species of Siphonophores in the western waters of Taiwan were reported by Zhang Jinbiao[9]. These records make up a total of 31 species reported in the waters around Taiwan Island.

In this report the zooplankton samples were analyzed and reported with samples collected by the Institute of Marine Biology, the Marine University of Taiwan, during the study on the ecology of Kending coral reef of Taiwan in November and December, 2001. As results, the species and numerical distribution of Siphonophores and their relation to hydrographic environments were reported and the data can be fundamentally important both for biodiversity and for ecological study of Siphonophores in the waters around Taiwan Island.

## 1 Materials and Methods

### 1.1 Sampling

The zooplankton samples were collected from 12 stations (21° 52′ 12″ −21° 57′ 7″ N, 120° 43′ 13″ − 120° 51′ 0″ E, Fig. 1) in the Nan Wan Bay, Taiwan, during 2 cruises on November 2-3 and December 8-10, 2001. Two kinds of conical planktonic nets, which are 180 cm in length, 45 cm in opening diameter, and 333 μm and 200 μm in mesh size respectively, were used to tow samples in surface and bottom water layers for 10 min horizontally, respectively. Except for the station 12 where no samples were collected in the bottom water layer because it is shallow, most of the tows were done at the depth of 50 m. During the 2 cruises a total of 92 samples were obtained with 46 each by nets of

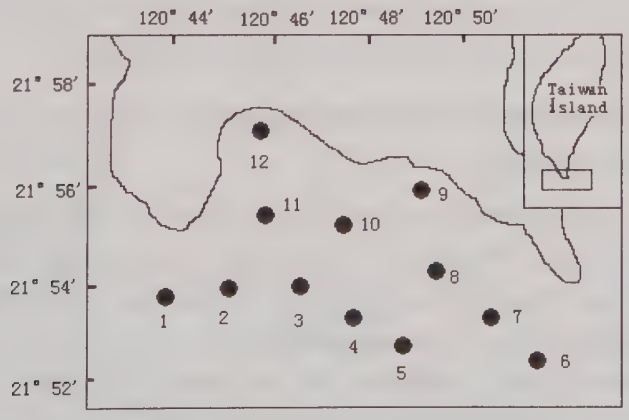


**Fig. 1 Locations of stations for Siphonophores sampling in the Nan Wan Bay, Taiwan**

different mesh sizes. Flow meters were used to measure the volume filtered and samples were fixed with 5 % Formalin solution before they were brought back to lab. Since macrozooplankton Siphonophores are larger, the abundance of jellyfish was only counted with samples from the net with a mesh size of 330 μm, while for species identification, the specimens from two different nets were used.

Water temperature and salinity data present in this report were collected by CTD, Model USA-YSI6600.

### 1.2 Data analysis

Index for Siphonophores Diversity is calculated with Shannon-Wiener formula ($H'$), Evenness ($J$) and Dominance ($Y$) [10-12].

$$H' = -\sum_{i=s}^{s} P_i \log_2 P_i, \qquad J = \frac{H'}{\log_2 s}, \qquad Y = \frac{n_i}{N} f_i$$

where $P_i$ is the ratio of numbers of the $i$th Siphonophores species to the total in a sample; $S$, the total species number in a sample; $n_i$, the average density of the $i$th species in a cruise; $N$, the total abundance of Siphonophores in the same cruise; $f_i$, the occurring frequency of the $i$th species in all stations of the same cruise.

## 2 Results

### 2.1 Species composition

By the data, 31 species of Siphonophores are identified, among which, 5 species of 2 families are Physonectae, and 26 species of 6 families are Calycohorae. Of 31 species, 7 species (Table 1, marked with asterisk) are the first records in the waters around Taiwan Island, among which, the species *Rosacea cymbiformis* is first recorded in China. Up to data, there are totally 38 Siphonophores in the waters around Taiwan Island when all Siphonophores, including the species that were not obtained in these two cruises, are accounted.

Table 1 shows that only 19 species occurred in November and it increased to 29 in December and that more species occurred in the surface water than in the lower water layer.

### 2.2 Distribution of total abundance and numbers of dominant species

#### 2.2.1 Distribution of total abundance

The abundance of Siphonophores was low (0.438 inds/m$^3$) in November and there was no difference between the surface water layer (0.435 inds/m$^3$ on an average) and bottom water layer (0.441 ind/m$^3$ on an average). From Fig. 2a, it is showed that the abundance is higher in the west waters both at surface and bottom water layer. The total abundance increased rapidly to 1.99 inds/m$^3$, which is 4.5 times higher in December than in November. The magnitude raised is high, almost 6 times (2.536 inds/m$^3$ on an average) in the surface water layer, while it is lower, only over 3 times (1.395 inds/m$^3$ on an average) in the bottom water layer where abundance was only half that of surface water though with

a high absolute value.

**Tab. 1 Species list of Siphonophores and its distribution in the Nan Wan Bay, Taiwan, in November and December**

| List of species | November | | December | |
|---|---|---|---|---|
| | surface | bottom | surface | bottom |
| *Physophora hydrostatica* Forskal | | + | + | |
| *Agalma okeni* Eschscholtz | | | + | + |
| *Agalma elegans* (Sars) | | | + | |
| *Nanomia bijuga* (Chiaje) | + | + | + | + |
| *Forskalia edwardsi* Kölliker* | | + | | |
| *Hippopodius hipopus* Forskål* | | | | + |
| *Vogtia glabra* Bigelow | | | + | + |
| *Amphicaryon ernesti* Totton* | | | + | |
| *Amphicaryon peltifera* (Haeckel)* | | | + | |
| *Rosacea plicata* Quoy et Gaimard | | | + | + |
| *Rosacea cymbiformis* (Chiaje)** | | | | + |
| *Sulculeolaria chuni* (Lens et van Riemsdijk) | + | + | + | + |
| *Sulculeolaria quadrivalvis* Blainxille | + | | + | + |
| *Sulculeolaria tropica* Zhang* | | | | + |
| *Lensia campanella* (Moser) | + | + | | |
| *Lensia hotspur* Totton | | | + | + |
| *Lensia subtilis* (Chun) | + | + | + | |
| *Lensia subtiloides* (Lens et van Riemsdijk) | + | | + | + |
| *Diphyes bojuni* (Eschscholtz) | + | + | + | + |
| *Diphyes chamissonis* Huxley | + | | + | + |
| *Diphyes dispar* Chamisso et Eysenhardt | + | + | + | + |
| *Chelophyes appendiculata* (Eschscholtz) | + | + | + | + |
| *Chelophyes contorta* | + | + | + | + |
| *Eudoxoides mitra* | + | + | + | + |
| *Eudoxoides spiralis* (Bigelow) | + | | + | + |
| *Sphaeronectes gracilis* (Claus) | | + | + | + |
| *Abyla schmidti* Sears | | | + | + |
| *Abylopsis eschscholtzi* (Huxley) | + | + | + | + |
| *Abylopsis tetragona*(Otto) | + | + | + | + |
| *Bassia bassensis* (Quoy et Gamard) | + | + | + | + |
| *Enneagonum hyalinum* (Quoy et Gamard)* | | | | + |

* : first species recorded in the waters around Taiwan

** : first species recorded in China Seas

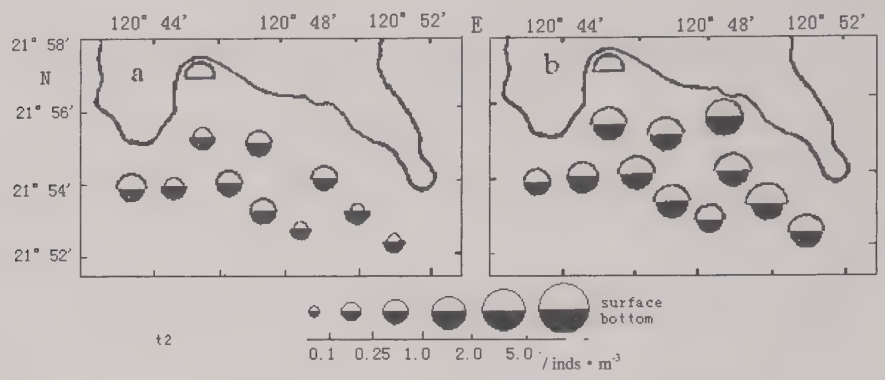


**Fig. 2 Horizontal distribution of Siphonophores abundance in November (a) and December (b)**

2.2.2 Distribution of Chelophyes appendiculata

Being the most abundant species from the surveys, the dominance of the species was 0.26 and 0.16 in November and December (Fig. 3a), respectively. The average abundance of the species was 0.154 inds/$m^3$ (35.5 % of the total) in December with a slightly lower abundance in the surface water layer (0.131 inds/$m^3$) than in the bottom water layer, while it increased markedly (0.342 inds/$m^3$ on an average, 17.2 % of the total) in November, showing a significant increment of abundance in the surface water layer (0.531 inds/$m^3$) compared with the lower water layer (0.136 inds/$m^3$). The abundance was

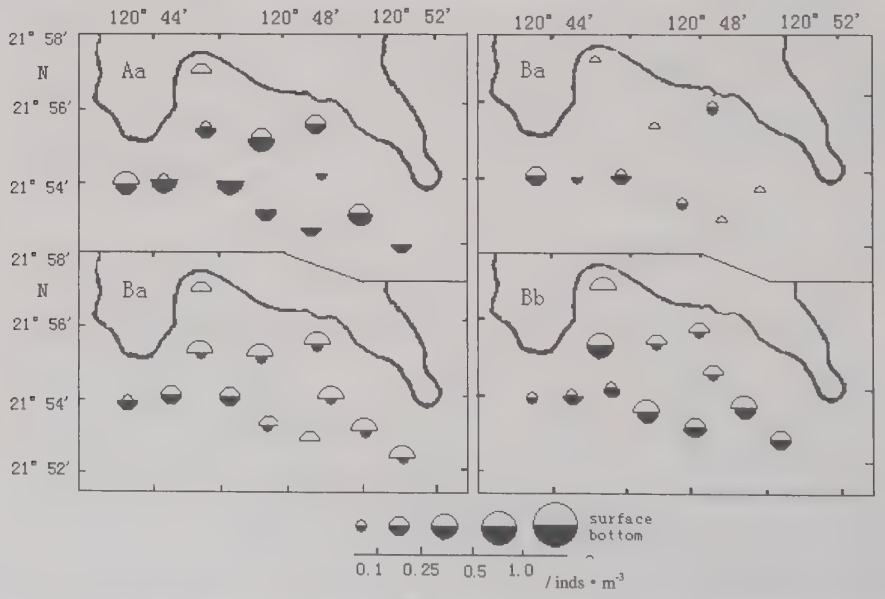


**Fig. 3 Horizontal distribution of *Chelophyes appendiculata* (A) and *Bassia bassensis* (B) abundance in November (a) and December (b)**

higher in in-shore waters than in offshore waters besides a much homogeneous distribution in bottom water layers (Fig. 3Ab).

*Chelophyes appendiculata* is a high-temperature and high-salinity cosmopolitan species[5], spreading widely in the three major oceans[13], the East China Sea, the Taiwan Straits and the north, the south and the center of South China Sea, dominating particularly in the center[14] and the south of South China Sea[15]. Reported by Alvarino, the distribution of Chelophyes *appendiculata* is not overlapped with *Chelophyes contorta* in the waters of Central America [16], while according to Rengarajan, these two species are common along the west coast of India except that *Chelophyes appediculata* is mainly found in the open sea and, the other, in the nearshore waters[17]. Stepanyants found that *Chelophyes appendiculata* is most dominant in the waters with salinity higher than 35.5 but *Chelophyes contorta* dominates in salinity from 34.0 to 34.5[18]. In this study we find little difference between their distributions, except that the abundance of *Chelophyes appendiculata* is higher than *Chelophyes contorta* in the Nan Wan Bay since the surveyed area was confined. As a result, it needs to be examined in much wider areas.

2.2.3 Distribution of Bassia bassensis

The abundance of the species was lower (0.044 inds/$m^3$ on an average) in November, showing no difference in abundance distribution between the surface water layer and the lower water layers, but more homogeneous in surface waters and higher abundance in offshore waters (Fig 3. Ba). The abundance increased markedly, reaching 0.217 inds/$m^3$ on an average (10.9 % of the total abundance in December) and it was significantly higher in the surface water (0.254 inds/$m^3$) than in the bottom (0.177 inds/$m^3$).

*Bassia bassensis* is also a high-temperature and high-salinity cosmopolitan species in the three major oceans[4, 14], and it dominates particularly in the tropical waters of west Pacific [19, 20]. Besides, it was found in the waters from the East China Sea to the south of South China Sea[5], where it mostly dominates in the central South China Sea [14].

2.2.4 Distribution of other species

Except for the above-mentioned species that dominated in November and December, *diphyes bojani*, *diphyes dispar*, *Abylopsis eschscholtzi* and *Chelophyes contorta* are also highly dominant species (Table 2), among them, the abundances of *diphyes bojani* and *Diphyes dispar* were higher whether in the surface or bottom water layers (10 % of the total abundance), where the abundance was higher in the surface water layer than in the bottom. In contrast, *diphyes bojani* distributed more homogeneously between surface and bottom water layers while *Diphyes dispar* showed a higher abundance in the nearshore waters than in the open sea (Fig. 4).

### 2.3 Distribution of diversity index

Diversity of Siphonophores was slightly lower in November (Fig. 5a) and there was no difference between the average diversity in surface (1.86) and bottom (1.96) water layers. However, the diversity was higher in the central area, reaching 3.0 at the station 10, compared with the lower value in the

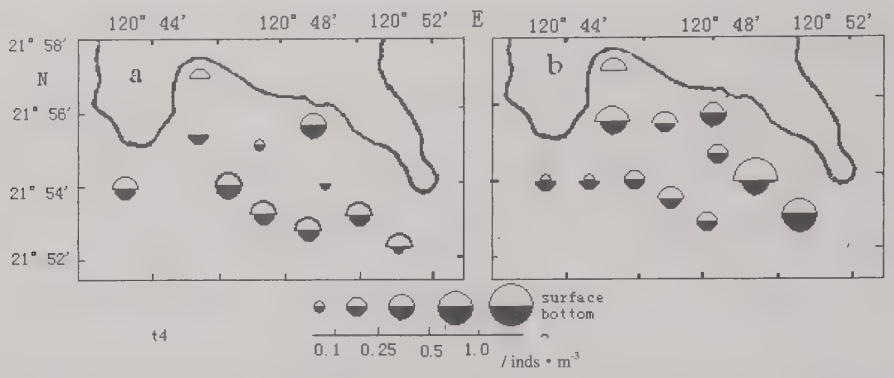


**Fig. 4 Horizontal distribution of *Diphyes bojani* (a) and *Diphyes dispar* (b) in December**

**Tab.2 Abundance and dominance of dominant Siphonophores in November and December**

| species | November | | | | December | | | |
|---|---|---|---|---|---|---|---|---|
| | Abundance / inds • $m^{-3}$ | | | Dominance | Abundance / inds • $m^{-3}$ | | | Dominance |
| | surface | bottom | average | | Surface | bottom | average | |
| *Chelophyes appendiculata* | 0.131 | 0.179 | 0.154 | 0.26 | 0.531 | 0.136 | 0.342 | 0.16 |
| *Bassia bassensis* | 0.044 | 0.043 | 0.044 | 0.06 | 0.254 | 0.177 | 0.217 | 0.11 |
| *Diphyes bogani* | 0.032 | 0.036 | 0.034 | 0.04 | 0.273 | 0.193 | 0.234 | 0.11 |
| *Diphyes dispar* | 0.013 | 0.035 | 0.024 | 0.02 | 0.271 | 0.190 | 0.232 | 0.12 |
| *Abylopsis eschscholtzi* | 0.031 | 0.032 | 0.031 | 0.04 | 0.141 | 0.113 | 0.128 | 0.06 |
| *Chelophyes contorta* | 0.037 | 0.049 | 0.043 | 0.06 | 0.112 | 0.084 | 0.099 | 0.04 |

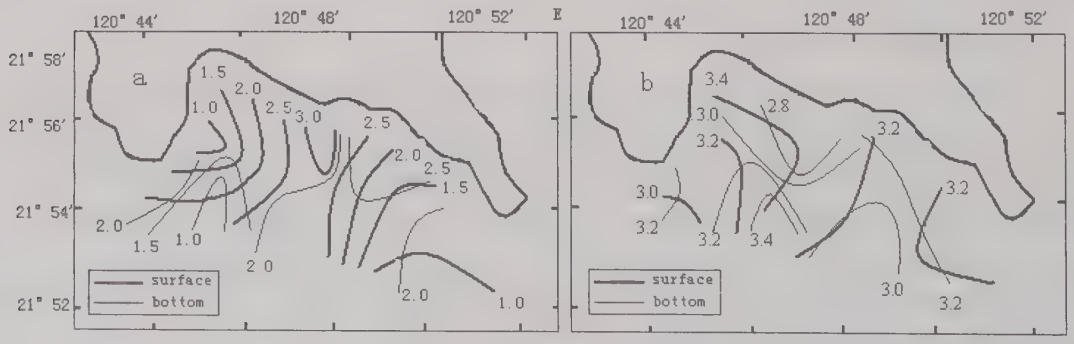


**Fig. 5 Horizontal distribution of Siphonophores by Shannon-Winer index in November (a) and December (b)**

southeast and northwest of the bay where it is less than 1 because less species were found. In the bottom

water layer, a slightly higher index was located in the central than at the east and west ends of the bay.

Diversity was higher in December than in November due to the increased species. It is showed that the species numbers are quite similar among the species with 3.24 and 3.14 in the surface and bottom water layers, respectively. Diversities in the surface water were much the same horizontally except for some higher value in the central bay and lower in the east and west parts of the bay in contrast to the bottom water layers where diversity was higher in the open sea and a slightly lower in the north.

Evenness was high during these two months. It averaged 0.87 (0.69-1.0) and showed higher in the surface (0.90) than the bottom water layer (0.84) in November except for a lower evenness in the surface water layer in the west and in the bottom water layer at the west and east ends of the bay. The evenness was much higher 0.88 (0.83-0.94) by average and showed little difference between surface (0.89) and bottom (0.81) water layers in December.

## 3 Discussion

### 3.1 Comparison with Siphonophores in the neighboring waters

From Table 3 we can find that the species number and abundance decrease more or less in the neighboring waters in contrast to the increase in the Nan Wan Bay since the turn of autumn to winter, demonstrating a unique pattern of seasonal alternations. Besides, viewed from the dominant species in autumn and winter, it is demonstrated that, when neritic species *Diphyes chamissonis*, *Lensia subtiloides* and *Muggiaea atlantica* dominated in the East China Sea, the Taiwan Straits and the north of South China Sea, only oceanic high-temperature and high-salinity species dominated in th Nan Wan Bay and central South China Sea. Thus, it is suggested that Nan Wan is geographically closer to the central South China Sea and both belong to the India-west Pacific-indo-Malayan Subregion [5].

**Tab. 3 Statistical comparison of the Siphonophores in the waters of Nan Wan Bay with that in the neighboring waters**

| Seas | East China Sea[21] | | West Taiwan Strait[22] | | East Taiwan Strait[8] | North of South China Sea* | | Central South China Sea[4] | | Nan Wan Bay | |
|---|---|---|---|---|---|---|---|---|---|---|---|
| Month and Season | Autumn | Winter | Autumn | Winter | Winter | November | December | Autumn | Winter | November | December |
| Species number | 26 | 37 | 28 | 19 | 19 | 26 | 28 | 54 | 52 | 19 | 29 |
| Abundance /inds • $m^{-3}$ | 1.81 | 1.56 | 9.00 | 0.11 | 0.95 | 4.03 | 1.55 | 1.51 | 1.24 | 0.438 | 1.99 |
| Dominant species | *Diphyes chamissonis*, *Muggiaea atlantica*, *Lensia campanella* | | *Diphyes chamissonis*, *Lensia campanella*, *Muggiaea atlantica* | | *Diphyes chamissonis*, *Lensia campanella* | *Diphyes chamissonis*, *Lensia campanella*, *Nanomia bijuga* | | *Chelophyes cntorta*, *Chelophyes appendiculata*, *Eudoxiodes mitra*, *Abylopsis tetragona*, *Bassia bassenisi*, *Eudoxoides piralis* | | *Chelophyes appendiculata*, *Bassia bassenisi*, *Diphyes bojani*, *Diphyes dispar*, *Abylopsis tetragona*, *Chelophyes cntorta* | |

Note: Nets with a mesh size of 505 μm were used except for that used in the Nan Wan Bay.

* from the manuscripts of Zhang Jinbiao and Xu Zhengzu.

### 3.2 Comparison of Siphonophores towed by different nets

Two types of nets with different mesh sizes were simultaneously used in zooplankton surveys. It is showed by Table 4 that more species were collected with the net mesh size 333 μm than the mesh size 200 μm, demonstrating a more efficient collection of Siphonophores with the mesh size 333 μm. Probably, the net with a bigger mesh size is much proper for the collection of macrozooplankon of larger Siphonophores. In China it is used to collect various zooplankton with a mesh size of 505 μm and so a comparative study using different nets is necessary for a better result.

It is also found from Table 4 that the obtained species were much more from the surface water layers than from the bottom water layer. This is also the case in the west of Taiwan Strait where species in shallow water (< 25 m) are more than that from deeper water layers (25-50 m) by vertical distribution of Siphonophores. It can be again confirmed that Siphonophores are the pelagic zooplanktonic animals.

**Tab. 4 Comparison of species number for Siphonophores collected with nets of different mesh sizes**

| Month | November | | | | December | | | |
|---|---|---|---|---|---|---|---|---|
| Mesh size / μm | 200 | | 300 | | 200 | | 300 | |
| Water layer | surface | bottom | surface | bottom | surface | bottom | surface | bottom |
| Species number | 13 | 12 | 15 | 13 | 17 | 15 | 25 | 23 |
| Combined species number | 15 | | 19 | | 18 | | 29 | |

### 3.3 Distribution of Siphonophores and its relations to the hydrographic factors

According to the behaviors of Siphonophores in the Nan Wan Bay, 31 species can be divided into 3 ecological groups: ( 1 ) nearshore warm water cosmopolitan group, which is composed of only 2 species, *Lensia subtitles* and *Diphyes chamissonis*, characterized by lower abundance with higher number near shore; ( 2 ) Oceanic warm water cosmopolitan group, which accounts for 84 % of Siphonophores and all dominant species in the Nan Wan Bay are in this group; ( 3 ) Oceanic equatorial stenocoenose group, which is composed of only 3 species, *Abyla schmidti*, *Rosacea plicata* and *Lensia companella*. Thus, it is clear that the species appearing in the Nan Wan Bay in November and December are the dominant oceanic warm water species whether viewed from species number or abundance. It is demonstrated that the waters in the Nan Wan Bay is controlled by oceanic water mass and it is confirmed again particularly when 12 species, of which 10 are the oceanic warm water cosmopolitan species and 2 the typical oceanic equatorial species, added in December. It is reported that the water in the Nan Wan Bay is controlled by the mixed water masses of medium salinity from the South China Sea, low salinity water from along the coast and Kuroshio current in autumn while it is dominated by waters only from the South China Sea and Kuroshio due to lack of coastal currents in winter [24]. As a result, the variations of Siphonophores from autumn to winter reflect a trend of the increasing influence of the oceanic water. Many hydrographic studies in the northeast of South China Sea have demonstrated that there is a branch of current, a so-called Kuroshio branch [25,26], which has the highest volume in winter [27], flowing westward or southwestward to the South China Sea through the Bashi Channel. The surveys conducted in the south of Taiwan evidenced a strongest influence of Kuroshio current in

winter [28]. As a result, it is considered that the increase in Siphonophores' species number and abundance is related to the influence of Kuroshio, which brings in more salinephile oceanic warm water and oceanic equatorial species. Also, data obtained by CTD show that the water temperature is much higher in November reaching 27.56 ℃ and 27.21 ℃ and it decreases evidently to 24.64 ℃ and 23.98 ℃ in December in the surface and bottom water layers, respectively, while for salinity it is low in November averaged only 33.25 and 33.59 and increases to 34.25 and 34.34, respectively, in the surface and bottom water layers. The change in water temperature and salinity also reflects the increasing influence of the oceanic water masses.

Compared with species of Siphonophore in the waters of eastern and western Taiwan Strait and in the north of South China Sea, 29 Siphonophores in the Nan Wan Bay of December are many, which demonstrates that Nan Wan is influenced much by high-temperature high-salinity waters. However, it is noted that the previously recorded typical oceanic equatorial species, such as *Ceratocymba leuckarti*, *Ceatocymba dentata*, *Abyla bicarinata* and *Abyla trigona*, were not found in these surveys. It is probably that these species were collected in the regions where Kuroshio passes by while the Nan Wan Bay is only an inshore cove. Another reason may be that December is only the beginning of winter and it is not the month when Kuroshio influences the most. However, further studies are needed to confirm these hypotheses.

## Acknowledgements

Financial support for this research was provided by the Foundation of NSC program of Taiwan and by the program of Fujian Nature and Science Foundation (D97009). The preparation of this manuscript was partly supported by the Start-up Research Foundation for Returned Overseas Personnel from the Ministry of Education, China.

## References

[1] Jennier E Purcell. Influence of Siphonophores behavior upon their natural diets: evidence for aggressive mimicry. *Science* N.Y., 1980, 209: 1 045-1 047.

[2] Jennier E Purcell. Dietary composition and diel feeding patterns of epipelagic Siphonophores. *Marine Biology*, 1981, 65: 83-90.

[3] George O Mackie, Phil R Pugh, Jennier E Purcell. Siphonophores biology. *Advance in Marine Biology*, 1987, 24: 98-262.

[4] Phil R Pugh. Gelatinous zooplankton —the forgotten fauna. *Progress in Underwater Science*, 1989, 14: 67-78.

[5] Zhang Jinbiao and Lin Mao. Study on the biogeography of Siphonophores in the South China Sea. *Acta Oceanologica Sinica,* 1997, 19(4): 121-131(in Chinese).

[6] Ma Xiping and Song Jun. Roles of medusa in marine food chain. *Marine Science*, 1998, 2: 38-42 (in Chinese).

[7] Mary Sears. Notes on Siphonophores 2.A revision of the Abylinae. *Bull. Mus. Comp. Zool. Harv.*, 1953, 109(1): 1-119.

[8] Chen Qingchao, Chen Minben, Huang jiangxiu. *Zooplankton species and its distribution in Taiwan Strait and in the north of South China Sea*(I). Taibei: Marine Science Research Center of Taiwan. 1998, 17-19 (in

Chinese).

[9] Zhang Jinbiao, Xu Zhaoli, Wan Yunlong et al. Hydromedusa and Siphonophores in western waters of Taiwan in winter and spring. *Taiwan Strait*, 1999, 18(1):76-82 (in Chinese).

[10] Ma Keping. Methods for bio-community measurement. Principles and Mythologies for Biodiversity study. *Biodiversity Committee of the Chinese Academy of Sciences*. 1994, 141-165(in Chinese).

[11] Sun Ruyong. *General Zoological Ecology*. Beijing Normal University Press, Beijing, 1987, 416-426 (in Chinese).

[12] Sheng Guoying and Shi Binzhang. *Marine Ecology* (2nd edition). Science Press, Beijing, 2002,153-188(in Chinese).

[13] Angeles Alvarino. Siphonophora of the Pacific with a review of the world distribution. *Bull. Scripps Inst. Oceanogr.*, 1971, 16:1-432.

[14] Lin Mao. Preliminary studies on Siphonophore Ecology in the central South China Sea. *Acta Oceanologica Sinica*, 1992, 14(2): 99-105 (in Chinese).

[15] Chen Qingchao, Zhang Guxian, Yin Jianqiang. *Zhenmu Shoal – Scientific Report of the Comprehensive Investigation in waters of China south territory*. Science Press, Beijing, 1987, 132-46 (in Chinese).

[16] Angeles Alvarino. Distribution of Siphonophores in the regions adjacent to the Suez and Panama Canals. *Fishery Bulletin US National Oceanic and Atmospheric Administration*, 72: 527-546.

[17] K. Rengarajan. Distribution of Siphonophores along the west coast of India and the Laccadive Sea. *Journal of the Marine Biological Association of India*, 1975, 17: 56-72.

[18] Sofia D. Stepanyants. Siphonophora of the central part of the Pacific Ocean. Exploration of the fauna of the Seas, XX(XXVIII), *Marine plankton* (Systematic and Faunisties). 1977, 54-81 (in Russian).

[19] Zhang Jinbiao, Cai Binji, Chen Ruixiang et al. Zooplankton in the surveyed waters, *Survey Report on the West Central Pacific by Marine Investigation Ship "Xiang Yang Hong 09"*. Oceanic Press, Beijing, 181, 118-136 (in Chinese).

[20] Lian Guanshan, Hou Shumin, Chen Xiaolin et al. Zooplankton. *Survey Report on the West Central Pacific by Marine Investigation Ship "Shi Jian"*. Marine Bureau of Oceanography of PRC, Oceanic Press, Beijing, 1981, 74-88 (in Chinese).

[21] Xu Zhaoli, Zhang Jinbiao, Jiang Mei. Study on the Siphonophores in the East China Sea. *Acta fisheriy Sinica*. 2003, 27(supl.), 82-90(in Chinese).

[22] Lin Mao. Ecological study on the Siphonophores in the west waters of Taiwan Strait. *Marine Bulletin*. 1989, 8(3): 65-71(in Chinese).

[23] Zhang Jinbiao, Lin Mao. Vertical distribution of Hydromedusa and Siphonophores in the west Taiwan Strait. *Taiwan Strait*. 2001, 20(1): 1-8 (in Chinese).

[24] Sun Yat Sen University of Taiwan. E*cological study in the waters south of Nuclear Station and near the Lan-yu island stockpile*. Sun Yat Sen University, 2003, 1.1-11.27 (in Chinese).

[25] Guo Zhongxin, Yang Tianhong, Cou Dezhong. Warm water current in the winter South China Sea and SW currents in the right side. *Tropical Marine Science*, 1985, 4(1): 1-9(in Chinese).

[26] Guohong Fang, Wendon Fang, Yue Fang et al. A survey of studies on the South China Sea upper ocean circulation. *Acta oceanographic Taiwanica*, 1998, 37(1):1-16.

[27] Huang Qizhou. Variations of Kurosio velocity .and volume in Bass Strait. *Tropical Marine*. 1983, 2(1): 35-41(in Chinese).

[28] Fan Kuanglung, Yu Chinyuan. A study of water masses in the seas of southern most Taiwan. *Aata Oceanographica Taiwanica*, 1981, 12: 94-111.

# Distribution Pattern of Heavy Metals in the Surface Sediments of the Jiaozhou Bay

CHEN Zhengxin (陈正新)[1], DONG Heping (董贺平)[1,2], LI Shaoquan (李绍全)[1],
YUAN Hongming (袁红明)[2], Wang Baojun (王保军)[1]

1 *Qingdao Institute of Marine Geology, Qingdao* 266071, *Shandong, China*

2 *Ocean University of China, Qingdao* 266003, *Shandong, China*

**Abstract** Grain size analysis and chemical analysis of heavy metals are made for 312 surface samples of the Jiaozhou Bay. Nineteen samples of the waste water taken from the sewage discharge outlets along the eastern coast of the bay are also analyzed for heavy metals. Results show that heavy metals are richer in the east and poorer in the west of the bay. Sedimentary dynamic studies reveal that the distribution of heavy metals in the surface sediments of the Jiaozhou Bay is under the control of hydrodynamics.

**Keywords** the Jiaozhou Bay, surface sediments, distribution pattern of heavy metals, sedimentary dynamics

## Introduction

Due to the joint influence of hydrodynamics and the impacts of biological and human activities, the distribution pattern of heavy metals in the coastal sediments becomes rather complicated. The question has raised attention from the world geocommunities since the 1970s. During the past 30 years, a lot of data have been accumulated [1-7]. The study of heavy metals in the sea bottom sediments began in the 1980s in China [8-13]. It includes the study of sources, occurrence, depositional mechanisms, and diagenetic changes of the elements [1-21] and their distribution in relation to coastal dynamics [22, 23], grain size distribution[24] and biological activities [25].

In the Jiaozhou Bay, the survey and research of heavy metal pollution began in 1980 [27, 28]. Case studies in the early stage were made for some elements with limited samples from small areas. During the past decades, many scholars [26-34] and research institutions have contributed to the studies of pollution in the Jiaozhou Bay. The studies have expanded from individuals to a number of elements, including As, Cd, Hg, Cr, Pb, Cu, Zn, as well as organisms, organic nitrogen, organic phosphorus, COD, BOD, DDT and sulfide. In this paper we try to find out the distribution pattern of heavy metals and its bearing on depositional dynamics so as to provide a basis for environmental pollution control in the Jiaozhou Bay.

Received on January 16, 2005

## 1 Regional Geo-Environment

The Jiaozhou Bay, located to the west of Qingdao city that lies in the coastal area of the Yellow Sea (Figure 1), is a semi-closed shallow bay. It is 33.3 km long from south to north and up to 27.8 km wide from east to west, with an area of 397 km$^2$. The average water depth is 7 m with the maximum of 64 m. Around the Jiaozhou Bay there are totally 12 small rivers emptying into it, such as the Longquan, Yanghe, Dagu, Moshui, Baisha and Haibo Rivers. Among them the Licun River and Haibo River are in fact the channels used for discharging sewage. There is little water flowing through them except in the flood season. According to statistic data, the wave is weak in the bay. It is less than 0.5 m high for about 264-300 days of a year and only for one day in a year it is over 1.5 m. The tide in the bay belongs to the regular semidiurnal tide. Waves are separated when they enter the bay, one goes through the Cangkou watercourse to the east, the second goes towards the west along the west side of the Middle Shoal and the third proceeds towards the north through the Central Watercourse (Figure 1). The highest tide level of the research area is 5.36 m and the lowest –0.70 m, with an average high tide level of 3.80 m. The greatest tidal range reaches 6.06 m (according to Huanghai Elevation). The speed of the flooding tide is in general 15 cm/s higher than that of the ebb tide. It could exceed 47 cm/s sometimes. The maximum of flooding tidal current usually appears 2-3 hours before the tide and the maximum of ebb current occurs 2-3 hours behind the high tide [35].

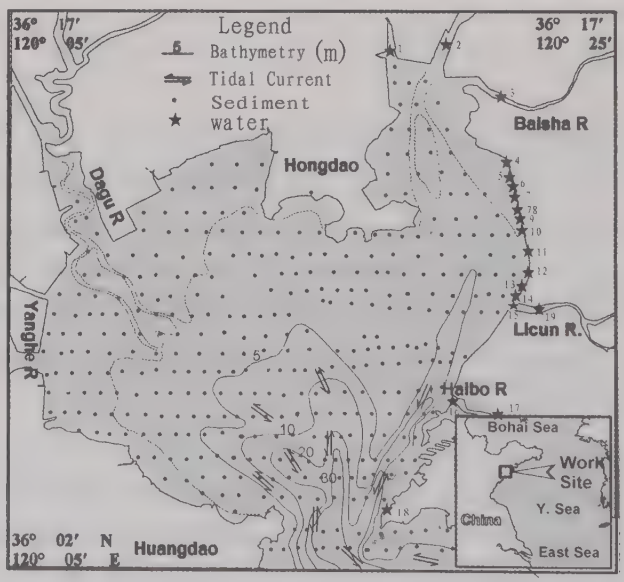


**Fig. 1 Map showing the location of the research area and the tidal current system and surface sediment samples in the Jiaozhou Bay. Water depths in meters**

Data analysis and shallow seismic profiling show that the Cangkou Fault goes through the Jiaozhou Bay and is the boundary of the Mesozoic in the west and the granite in the east. Late Mesozoic Intrusive

rocks occur in a wide area to the west of the Cangkou Fault. Rocks vary from the basic, medium-acidic, acidic to the partially alkali intrusions, which form the major part of the Laoshan Mountains. Faults are mainly developed in a NE — NNE direction, as a controlling factor over the structural and geomorphological patterns. The Jiaozhou Bay was resulted from the Holocene transgression. It is a stable area in steady uplifting in terms of its tectonic stability. There is only one layer of marine deposits in age of middle-late Holocene occurring in the Bay, which overlies the late Pleistocene fluvial or swamp deposits and the Mesozoic strata.

The basement around the Jiaozhou Bay is mainly composed of the Mesozoic strata and the Yanshan stage granite covered by unconsolidated Quaternary deposits. At the Jiaozhou Bay, there are almost artificial coasts. At the north bayhead, there are tidal riffles and seaside lowlands, which compose a fill-type estuarine coast. In the northwest, there are wide tidal flats and underwater riffles, and there is a silty-clayey coast; there are also wide tidal flats and underwater riffles at the front bayhead of Huangdao; only the part of seaside hills that run out into the bay forms a small-scale hard shore and develops marine abrasion physiognomy. In the bay, there are underwater riffles and marine plains, above which there are erosive geosynclines. There distribute erosive geosynclines from the bay mouth to the back of Tuandao–Huangdao, radiating four fingerlike channels, which are Cangkou, central, Daguhe river and Daoerhe river channels from the east to the west, to form the main flow passage for the ebb and flood tides. Among them, the Cangkou channel directly reaches the bayhead and connects to Baishahe River and Moshuihe River. Its 5-meter isobath channel length is 15 km, and the width is 500-2 000 m; it is the main sea-route of former Qingdao port. See Tables 1 and 2 below for all standard substances used and relative parameters.

## 2 Methods of Sampling and Analysis

### 2.1 Sampling

In 2002 and 2003, 312 surface sediment samples were taken from the Jiaozhou Bay following a grid of 1 km × 1 km (Figure 1) and analyzed were the grain size and heavy metal contents of the samples (As, Hg, Cd, Pb, Cr, Cu, Zn). In 2004, a total of 19 water samples were collected from the sewage discharge outlets along the east coast of the Jiaozhou Bay (Figure 1) and heavy metal contents analyzed.

The box sampler (capacity of 0.04 $m^3$) and clam snapper (capacity of 0.01 $m^3$) were alternately used for sampling of sediments. Sediments from the upper 0-5 cm were taken as surface samples.

Water samples were immediately treated with acid and sealed on the spot, and then analyzed in the laboratory the same day.

A DGPS positioning system with a precision of 2-15 m was used for sampling of surface sediments, and a portable GPS with a precision of 15 m for taking water samples.

### 2.2 Methods of analysis

Grain size analysis: After removal of organic matters, calcite and salt, the coarse fraction of sediments ( > 2 mm) was sieved. The fine fraction was analyzed with the Laser Grain-size Analyzer of

Mastersizer2000 produced by MALVERN Corp. of UK. Sediments were separated into classes every 1/4 Φ.

Heavy metal analysis: Take a sample of (0.1±0.000 1) g and put it into a sealed pot of polytetrafluorethylene. Add 1 ml of nitric acid (1:1) and 3 ml of hydrofluoric acid. After routine treatment under different temperatures, measure the contents of Cu, Pb, Zn, Cd, Cr using the Plasma Mass Spectrometer (IPC-MS).

Take a sample of 0.100 0-0.500 0 g and put it in a 25 mL colorimetric pipe. Add 10ml of aqua fortis to dissolve the sample. The solution Ai is used for analysis of Hg with a Cold-atomic Fluorescencemeter.

Take a sample of 0.300 0-0.500 0 g and put it in a 25 colorimetric pipe. Add 10ml of aqua fortis (1:1) to dissolve the sample. The solution is used for measuring As with a Cold-atomic Fluorescencemeter.

All samples were analyzed by the Qingdao Test Center for Marine Geology of Chinese Geological Survey.

## 3 Results and Data Analysis

### 3.1 Characteristics of the surface sediment

The surface sediments of the Jiaozhou Bay can be subdivided into four areas (Figure 2). The sandy area consisting of the sands of 0-2 Φ in median diameter mainly includes the watercourses such as the Cangkou, the Central and the Western Watercourses, and around the entrance of the bay; The area of sandy silt and silt, which vary from 2 to 4 Φ in median diameter, includes the upper reaches of the watercourses, the Dagu River Mouth and the offshore area of the Wutou River Mouth; Clayey silt and silt of 4-6 Φ in median diameter occur in the area between watercourses and to the north of the

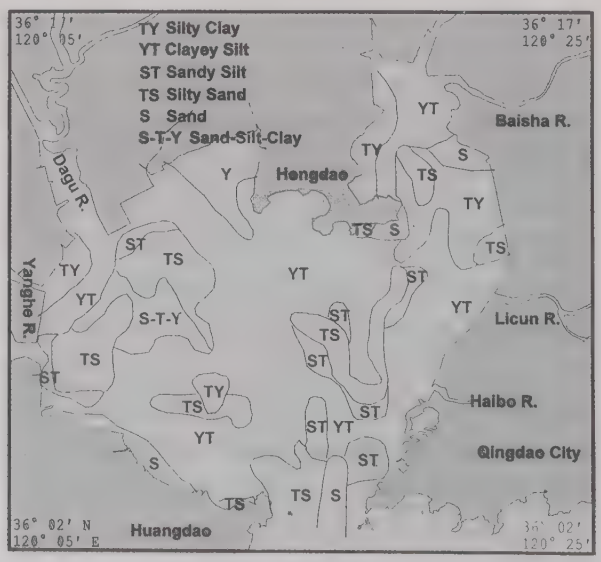


**Fig. 2 Distribution of surface sediments in the research area**

Cangkou watercourse, and the east nearshore area of the bay; the area of silty clay and mud, which vary from 6-9 Φ in median diameter, includes the northwest part of the Jiaozhou Bay, the Chaohai Salt Field, and the south side of the Dagu River Mouth (Figure 2).

### 3.2 Contents and characteristics of heavy metals

#### 3.2.1 Arsenic (As)

Arsenic has been detected in the surface sediments of the Jiaozhou Bay. The contents vary from the highest of $12.6\times10^{-6}$ to the lowest of $2.33\times10^{-6}$ with an average of $7.164\times10^{-6}$. It is $0.001\ 3\times10^{-6}$ in bottom water and $0.007\ 5\times10^{-6}$ in the pore water of sediments in the research area (Table 1). The As content changes in a range of $0.002\ 3\times10^{-6}$-$0.125\times10^{-6}$ in waste water (Table 2).

#### 3.2.2 Cadmium (Cd)

The average content of Cd is $0.081\ 7\times10^{-6}$, with the highest up to $1.0\times10^{-6}$. It is $0.000\ 6\times10^{-6}$ in bottom water and $0.022\ 7\times10^{-6}$ in the pore water of sediments in the research area (Table 1). The Cd content varies from $0.000\ 1\times10^{-6}$-$0.003\ 2\times10^{-6}$ in waste water samples (Table 2).

#### 3.2.3 Mercury (Hg)

The average content of Hg is $0.087\ 5\times10^{-6}$ in the surface sediments of the Jiaozhou Bay. The highest value reaches $4.1\times10^{-6}$ and the lowest is $0.007\times10^{-6}$. It is $0.000\ 05\times10^{-6}$ in bottom water and $0.000\ 04\times10^{-6}$ in the pore water of sediments (Table 1). The content of Hg in waste water changes from $<0.000\ 02\times10^{-6}$-$0.006\ 2\times10^{-6}$ (Table 2).

#### 3.2.4 Lead (Pb)

The average value of Pb is $32.3\times10^{-6}$ with its highest up to $109\times10^{-6}$ and the lowest down to $12.3\times10^{-6}$. It is $0.000\ 9\times10^{-6}$ in bottom water and $0.016\ 7\times10^{-6}$ in the pore water of sediments (Table 1). The Hg content is $0.001\ 7\times10^{-6}$-$0.061\times10^{-6}$ (Table 2) in waste water samples.

#### 3.2.5 Chrome (Cr)

The average content of Cr is $45.1\times10^{-6}$, with the highest up to $130.0\times10^{-6}$ and the lowest down to $1.95\times10^{-6}$. It is on an average $0.002\times10^{-6}$ in bottom water and $0.001\times10^{-6}$ in the pore water of sediments(Table 1). The Cr content detected from waste water is in a range of $0.000\ 3\times10^{-6}$-$0.906\times10^{-6}$ (Table 2).

#### 3.2.6 Copper (Cu)

The average Cu content is $24.93\times10^{-6}$, with the highest up to $211.0\times10^{-6}$ and the lowest down to $4.45\times10^{-6}$. It is on an average $0.001\ 9\times10^{-6}$ in bottom water and $0.017\times10^{-6}$ in the pore water of sediments (Table 1). The Cu content in waste water changes from $0.053\times10^{-6}$-$4.824\times10^{-6}$ (Table 2).

#### 3.2.7 Zinc (Zn)

The average content of Zn is $69.68\times10^{-6}$ in the surface sediments. The highest value detected reaches $384.0\times10^{-6}$ and the lowest is around $10\times10^{-6}$. It averages $0.009\ 6\times10^{-6}$ in bottom water and $0.055\ 4\times10^{-6}$ in the pore water of the sediments (Table 1). The Zn content in waste water is in a range of $0.023\times10^{-6}$-$0.564\times10^{-6}$ (Table 2)

**Tab. 1 The comparison of standards and repetition analysis**

| Item | Analysis Method | Detection Limit | Unit | Qualification rate / % | |
|---|---|---|---|---|---|
| | | | | First Class Standard Substance | Repetition |
| As | Atomic Fluorescence Spectroscopy (AFS) | 1 | μg/g | 100 | 100 |
| Cd | Inductively Coupled Plasma- Mass Spectroscopy (ICP-MS) | 20 | ng/g | 100 | 100 |
| Cr | Inductively Coupled Plasma- Mass Spectroscopy (ICP-MS) | 5 | μg/g | 100 | 100 |
| Cu | Inductively Coupled Plasma- Mass Spectroscopy (ICP-MS) | 1 | μg/g | 100 | 100 |
| Hg | Atomic Fluorescence Spectroscopy (AFS) | 2 | ng/g | 100 | 100 |
| Pb | Inductively Coupled Plasma- Mass Spectroscopy (ICP-MS) | 2 | μg/g | 100 | 100 |
| Zn | Inductively Coupled Plasma- Mass Spectroscopy (ICP-MS) | 2 | μg/g | 100 | 100 |

**Tab. 2 The reference datasheet of the first class standard substances(Unit×$10^{-6}$)**

| Monitored sample | | As | Cd | Cr | Cu | Hg | Pb | Zn |
|---|---|---|---|---|---|---|---|---|
| GSD1a | Standard value | 2.7 | 0.11 | 126 | 29.0 | 0.031 | 31 | 90 |
| 10501 | Measured value1 | 3.7 | 0.103 | 134 | 29.3 | 0.031 | 28 | 89 |
| 10520 | Measured value2 | 3.5 | 0.109 | 142 | 28.7 | 0.029 | 27 | 89 |
| 10522 | Measured value3 | 3.0 | 0.118 | 152 | 29.5 | 0.036 | 28 | 90 |
| GSD11 | Standard value | 188.0 | 2.300 | 40 | 78.6 | 0.072 | 636 | 373 |
| 10517 | Measured value1 | 194.5 | 2.302 | 49 | 77.4 | 0.072 | 573 | 374 |
| 10519 | Measured value2 | 169.5 | 2.104 | 46 | 74.3 | 0.075 | 580 | 363 |
| GSD9 | Standard value | 8.4 | 0.260 | 85 | 32.1 | 0.083 | 23 | 78 |
| 10515 | Measured value1 | 7.8 | 0.254 | 82 | 37.9 | 0.081 | 24 | 77 |
| 10521 | Measured value2 | 7.8 | 0.247 | 77 | 31.8 | 0.075 | 21 | 72 |
| 10523 | Measured value3 | 8.1 | 0.254 | 85 | 35.6 | 0.073 | 22 | 77 |
| GSD11 | Standard value | 25.0 | 1.120 | 136 | 22.6 | 0.280 | 27 | 46 |
| 10516 | Measured value1 | 25.3 | 1.040 | 146 | 20.4 | 0.277 | 29 | 42 |
| 10518 | Measured value2 | 24.4 | 1.034 | 154 | 20.5 | 0.272 | 28 | 43 |
| 10524 | Measured value3 | 21.6 | 1.114 | 156 | 22.6 | 0.272 | 29 | 44 |

## 4 Discussion

### 4.1 The relation of heavy metal content to grain size of sediments

The distribution pattern of heavy metals shows that the Jiaozhou Bay could be divided into two

parts taking the Cangkou Watercourse as a boundary. Heavy metals are richer in the eastern part and poorer in the western part. High contents of heavy metals are related to some small bays in the east and the north, in particular the area close to sewers and rivers mouths which are used for discharging sewages ( Figs. 3-9 ) The sediments are mainly clayey silt, silty clay, and clay with a median grain size of 5-9 Φ.

Arsenic mainly distributes in the clayey silt and silty clay areas off the east coast of the Bay, the bay northeast to the Chaohai Salt Flat, the Dagu River Mouth, the eastern part of the Hongdao Bay and the north side of the Oil Harbor of the Huangdao Port. The highest values occur in the area extending from the Licun River Mouth to Zhonggang (Figure 3). The areas with As content higher than $10\times10^{-6}$ mostly consist of silty clay (median grain size of 6-9 Φ). The correlation coefficient between heavy metals and median grain size is 0.57 (Table 3). In the west, the samples with As contents of $4\times10^{-6}$-$6\times10^{-6}$ are mostly from silt and clayed silt(median grain size of 4-6 Φ), and those with As contents over $9\times10^{-6}$ mainly from clay and silty clay(median grain size of 7-9 Φ), and both lie in the still water area of the Jiaozhou Bay. The correlation coefficient between As and Φ is 0.55 in the east and 0.37 in the west.

The distribution of Cd in surface sediments shows no obvious correlation with grain size and the correlation coefficient is as low as 0.16-0.17 (Table 3). Cd distributes in a scattered pattern without definite tendency. Although the distribution of Cd has no relation with grain size, it is dependent on geographical positions. The areas with high Cd content distribute mainly from the eastern Licun River south to the entrance of the Jiaozhou Bay, sewage discharge outlets and close to rivers mouths. The surface sediments there are mostly silt and clayey silt. Cd is also found in the northern part of the Central Watercourse and the inner part of the bay north to the Big Bridge where silty clay and mud deposited (Figure 4).

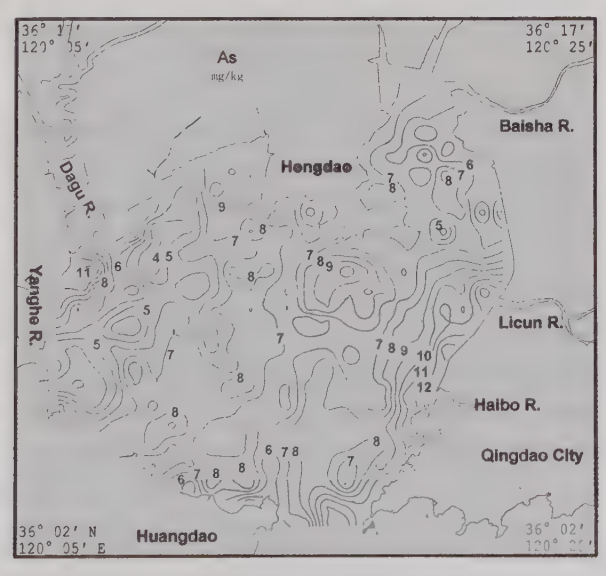


**Fig. 3 Distribution of As content in surface sediments of the Jiaozhou Bay**

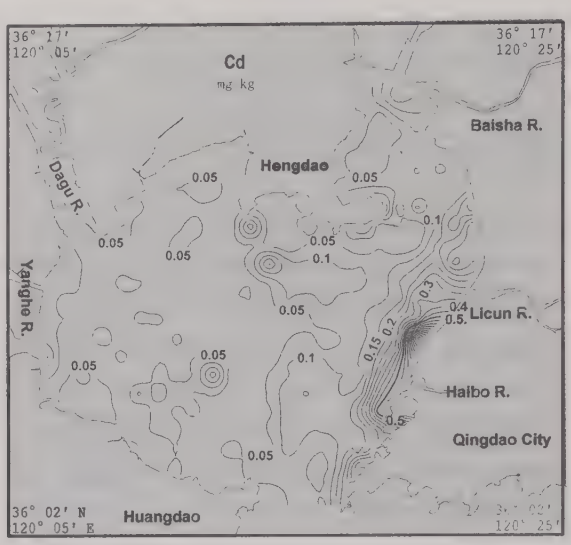


**Fig. 4 Distribution of Cd content in surface sediments of the Jiaozhou Bay**

**Tab. 3 Contents of heavy metals in surface sediment of Jiaozhou Bay ($\times 10^{-6}$)**

| Sample | | As | Cd | Hg | Pb | Cr | Cu | Zn |
|---|---|---|---|---|---|---|---|---|
| Surface sediments | Average value | 7. 164 | 0. 0817 | 0. 0875 | 32. 3 | 45. 1 | 24. 93 | 69. 68 |
| | Highest value | 12. 6 | 1. 0 | 4. 1 | 109 | 130 | 211 | 384 |
| | Lowest value | 2. 33 | Not detectable | 0. 007 | 12. 3 | 1. 95 | 4. 45 | 10 |
| Bottom water* | Average value | 0. 0013 | 0. 0006 | 0. 00005 | 0. 0009 | 0. 002 | 0. 0019 | 0. 0096 |
| Pore water of sediment* | Average value | 0. 0075 | 0. 0227 | 0. 00004 | 0. 0493 | 0. 001 | 0. 0167 | 0. 0554 |

*: Ye Siyuan. Report on sedimentary environment survey in offshore Qingdao. 2004.

In the east part of the research area, the high-content of Hg distributes mainly along a narrow area (Figure 5) from the northern end to the southern entrance of the Jiaozhou Bay. It has quite good correlation with the median grain size of the sediments. The correlation coefficient is 0.58 (Table 3). The sediments with Hg content over $(0.1\text{-}0.25)\times 10^{-6}$ are mainly silty clay with a median grain size of 6.0-7.25Φ. In the west part, Hg occurs in the bay near the Chaohai Salt Field, where silty clay and clayey silt dominate. The distribution of Hg is in a scattered pattern there, and the correlation coefficient between heavy metal content and median grain size drops down to 0.26 (Table 3). The difference of the Hg distribution pattern between the west and east parts of the research area means that the sources as well as the transportation mechanism of Hg are different in the two areas. Hg comes from industrial and domestic sewages in the east. Hg shows similar enrichment at the Licun River Mouth (Figure 5) and Pb is enriched in the sea areas where the No. 4 waste water sample was taken (Figure 6). It occurs mainly in the forms of ion, colloid, and organic complex compound in polluted water. They are easy to be absorbed by clay minerals, colloid and organic complex compound at the boundary of fresh water and seawater. Though Hg is carried into the sea by fresh water too in the west, it may enter the sea as

residual particles. After being sorted by seawater, they deposited in silt and sandy silt as particles. High-content of Hg could be found in coarser sediments. Therefore, there is no correlation between Hg content and grain size.

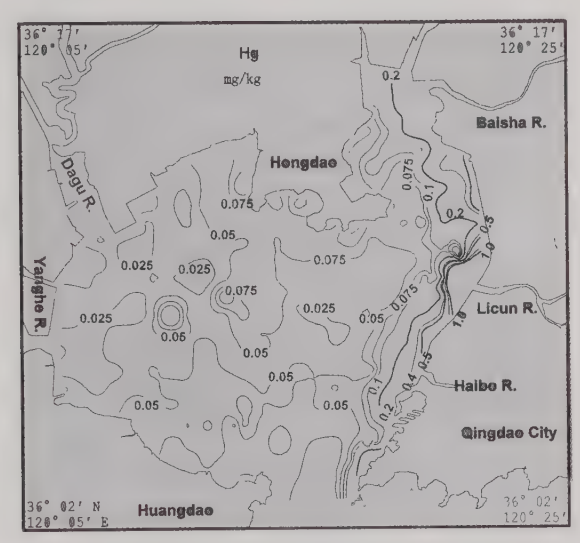


**Fig. 5 Distribution of Hg content in surface sediments of the Jiaozhou Bay**

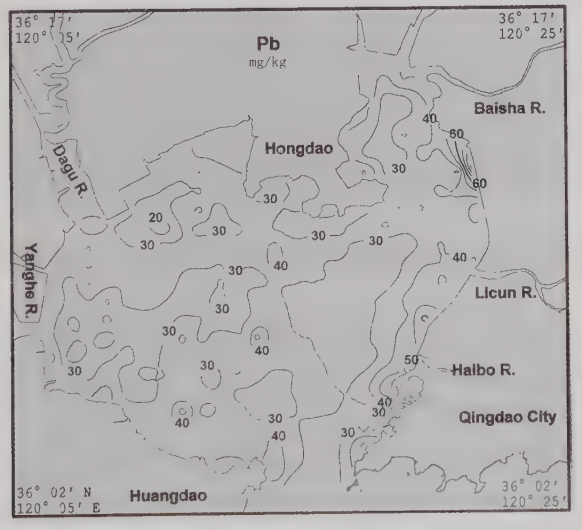


**Fig. 6 Distribution of Pb content in surface sediments of the Jiaozhou Bay**

The content of Pb shows a positive correlation with the median grain size of sediments and the correlation coefficient reaches 0.57 in the eastern part of the research area (Table 3). Most of the samples with a high concentration of Pb are from fine sediments with the median grain size between 6-7

Φ. Samples with Pb content higher than $40\times10^{-6}$ distribute mainly in the coastal water, in particular in the sea area near the chemical works in the north, the area north to the Cross-Sea Bridge in the north, and the area north to the Oil Harbor in the Huangdao Port (Figure 6). In the western part, high-contents of Pb can be found in the sediments from fine sand to silty clay, and the correlation coefficient drops to 0.37 (Table 3). This indicates that the distribution pattern and origin of Pb are similar to those of Hg.

Cr with the content more than $80\times10^{-6}$ distributes mainly in the sea areas between Dagang Port and the Licun River Mouth (Figure 7). The sediments are mainly clayey silt with silty clay as minor. The samples with Cr more than $60\times10^{-6}$ are from the northern end of the bay, the area north to the Oil Harbor of the Huangdao Port, the Western Watercourse and the northern part of the Central Watercourse (Figure 7). High contents of Cr occur in the sediments of sandy silt, silt, clayey silt and silty clay. The distribution pattern of Cr is similar to that of Cd.

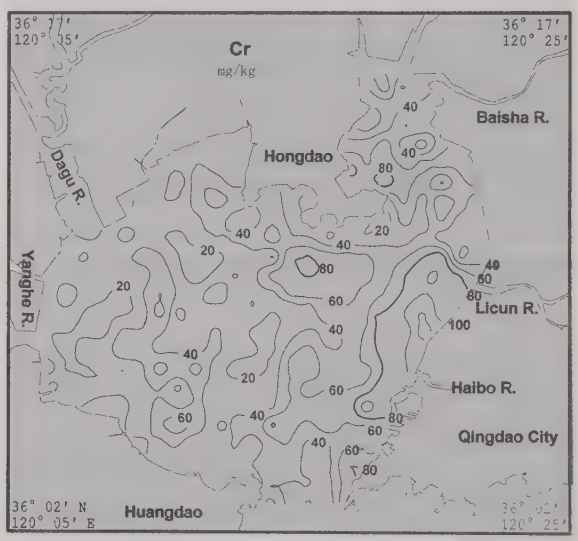


**Fig. 7 Distribution of Cr content in surface sediments of the Jiaozhou Bay**

Samples with the Cu content more than $35\times10^{-6}$ are mainly found in coastal waters (Figure 8). Hosting sediments are clayey silt and silty clay (6-7.25 Φ) in the east. The content of Cu has a close correlation with median grain size, and the correlation coefficient between Cu content and grain size is 0.52 in the eastern part (Table 3). The correlation coefficient is only 0.31 (Table 3) and the value of content is much lower in the west. Cu is similar to Hg and Pb not only in the distribution pattern and depositional characters, but also in geographical locations. It is shown in Figure 10 that Cu is enriched in the No. 4 waste water sample, and in the clayey silt and silt at the Licun River Mouth and Mianyan River Mouth. That the sediments in these areas are basically similar further proves that these metals came from the same source.

Statistic data show that the change in Zn content is proportional to the median grain size of the sediment, and the high content of Zn concentrates mostly in fine deposits. In the eastern part of the

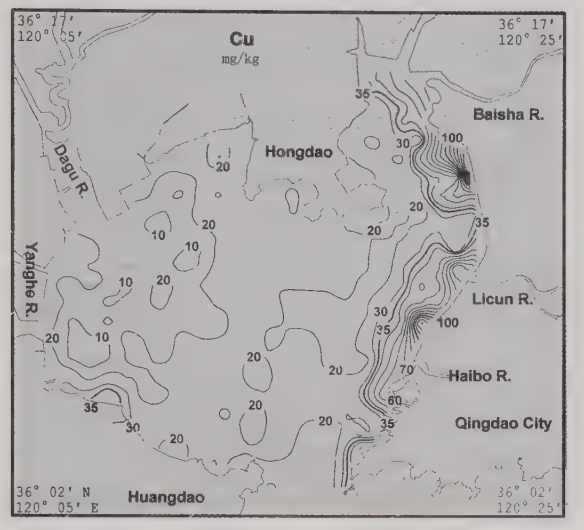


**Fig. 8 Distribution of Cu content in surface sediments of the Jiaozhou Bay**

Jiaozhou Bay, the high content of Zn is found in clayey silt and silty clay and the correlation coefficient is 0.61 (Table 3). In the western part, the high content of Zn distributes mostly in silt and clayey silt and the correlation coefficient is 0.57 (Table 3). In addition, there shows a high concentration of Zn at the Licun River Mouth and the offshore area near the Tuandao Sewage Treatment Plant in the east part of the bay. Zn is concentrated as well at the north end of the bay, to the north of Huangdao and the area between the Central Watercourse and the West Watercourse in a zone extending from south to north. It is obvious that the enrichment of Zn at the Licun River Mouth and the surrounding area of the Tuandao Sewage Treatment Plant is caused by the pollutant sources (Figure 9). In other areas, the distribution pattern and depositional process of Zn are similar to As.

### 4.2 Distribution of heavy metals in waste water

There are tens of sewers along the coast of the bay from the Qianhaixi through the east coast to the Tuandao Sewage Treatment Plant. Samples taken from sewage (Samples 1, 4, 6, 7, 8, 10, 11, 12, 13, 15, 17, and 19) obviously contain higher heavy metals (Table 2, Figure 10). The contents of As are $0.023\times10^{-6}$ and $0.125\times10^{-6}$ respectively in the No.4 and No.13 samples, which are over tens times and nearly one hundred times as much as the contents in the bottom water ($0.001\ 3\times10^{-6}$). The contents of Cd in the samples No.4 and No.18 are $0.003\ 2\times10^{-6}$ and $0.0013\times10^{-6}$ respectively, which are 3-6 times as much as that in the bottom water ($0.000\ 55\times10^{-6}$). Cu, Cr and Pb are also very high in the samples of 4, 5, 6, 12,13 and 14 (Table 2) (Figure 10) and the highest record of Cu reaches $4.824\times10^{-6}$ in the sample No.4. In addition to Cu and Pb, Zn is as high as $0.529\times10^{-6}$ in the Moshui River(sample No. 2 ), Cu and Zn reach $0.176\times10^{-6}$ and $0.188\times10^{-6}$ respectively in the Mianyang River. Other heavy metals in river water are relatively lower than those in waste water. For example, the contents of Cr, As, Cd and Hg in waste water samples of the Haibo River are as high as $0.000\ 4\times10^{-6}$, $0.011\times10^{-6}$, $0.000\ 1\times10^{-6}$ and

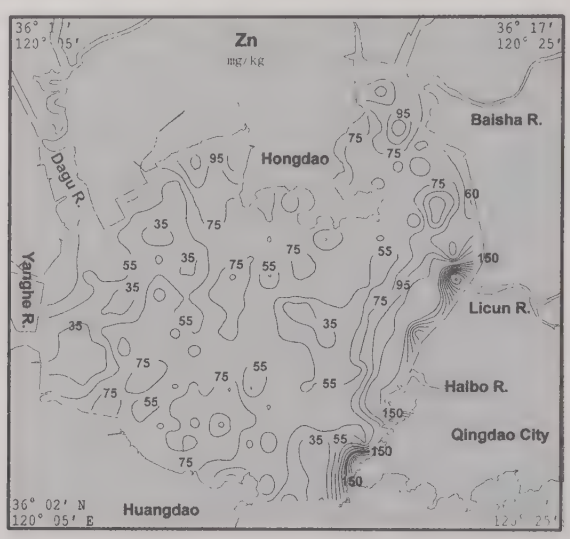


**Fig. 9 Distribution of Zn content in surface sediments of the Jiaozhou Bay**

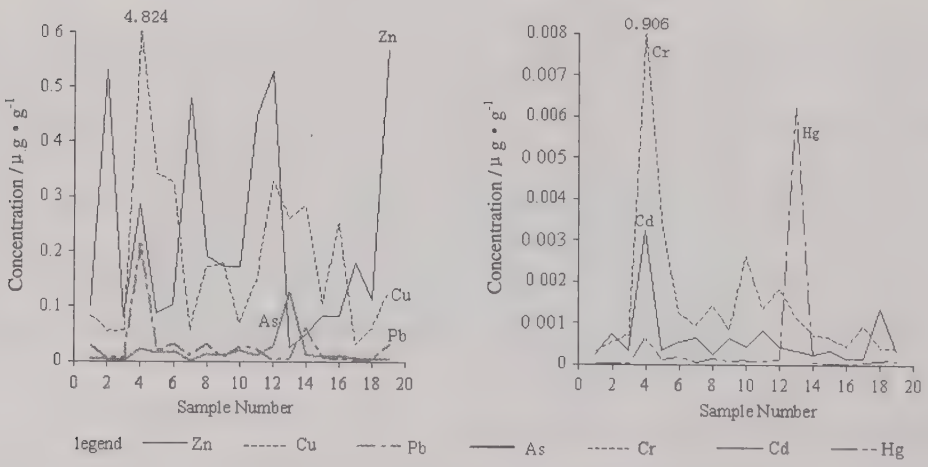


**Fig. 10 Contents of heavy metals in the waste-water samples**

$0.000\ 03\times10^{-6}$ respectively, and from the waste water sample of No.4, the contents of Cr, As, Cd and Hg reach $0.906\times10^{-6}$, $0.023\times\ 10^{-6}$, $0.003\times10^{-6}$ and $0.000\ 6\times10^{-6}$ respectively (Table 2) (Figure 10). Therefore, the heavy metal content of waste water from sewers is higher than that of river water. The content of heavy metals of the No. 4 sample is specially high compared to the others. Anyway, sewers are still one of the major pollutant sources even if their volume is not large, but the heavy metal concentration in the sewages is high. River water is another important pollution source for the waste water disposed into rivers has a low content of heavy metals after treatment, but the water volume is large. Both the waste water and river water are important pollutant sources of the Jiaozhou Bay.

Due to less industrialization on the west coast of the Jiaozhou Bay, the water from the Longquan

River, the Caowen River, the Yang River, the Dagu River and the others emptying into the bay from the west coast has a lower content of heavy metals. As a result, the heavy metals in the sediments of the western part are much lower than those of the eastern part of the Jiaozhou Bay.

During the period of 1993—1995, Chai Songfang measured the Hg content of seawater taken from the area of river mouths along the west coast of the Jiaozhou Bay in the low-water season (May), high-water season (August), and normal level season (October) respectively, and found that the average content of Hg is $0.03\times10^{-9}$ in the high-water season, and $0.019\times10^{-9}$ in the low-water season[32] . This indicates that the pollutant came mainly from rivers, and the provision of the pollutant is higher in the high-water season. So the content of heavy metals is directly proportional to the amount of water from rivers.

### 4.3 Relation of heavy metals' distribution to water dynamics

The Jiaozhou Bay is a semi-closed basin with one exit or inlet. The waves will proceed mainly along the three watercourses after they enter the bay. Tide moves back and forth. The flooding tide is generally moving faster than that of the ebb. Sedimentation is controlled by water dynamics. The tidal action in the Cangkou watercourse is obvious in control of the distribution of heavy metals. On the one hand, it acts as the barrier to prevent the pollutants moving from the eastern coast of Jiaozhou Bay to the west. While the contents of Hg, Cd, Cu, Pb and Zn are quite high in the east, they keep low in the area to the west of the Cangkou watercourse (Figures 3-9). There are some high-content anomalies of heavy metals indeed in the west, they have nothing to do with the east, but the deposits from the rivers in the west. On the other hand, the tidal current along the Cangkou Watercourse is a dynamic force to take the pollutants, which do not deposit in time, away to the Yellow Sea. The dense isolines of heavy metal concentration along the east coast are the result of deposition of heavy metals after transportation (Figures. 3-9).

It is found that the enriched heavy metals of Cd, Hg, Pb, Cu, Cr, As and Zn are all deposited in a zone, which is 1-3 km in distance from the coast (Figure 11), in NNE direction. Next to the enriched zone in the west, i.e. the zone 3-8 km away from the eastern coast, is a zone with the lowest concentration of heavy metals. This further proves that the tide current along the Cangkou Watercourse plays an important role in protecting the Jiaozhou Bay from pollution. It forces the pollutants from the eastern coast to move to the Yellow Sea and prevents them from moving across the boundary to the west, and as a result, the Jiaozhou Bay is protected from further pollution.

## 5 Conclusions

( 1 ) The offshore area on the east coast of the Jiaozhou Bay, which is 1-3 km away from the coast, is the zone rich in heavy metals, especially in the area around sewers and rivers mouths. The content of heavy metals is low in the western part of the Bay.

( 2 ) Heavy metals in the east are mainly from industrial and domestic wastes, but those in the western part of the bay mainly from rock weathering, agriculture and aquiculture. The sources are doubtlessly the major factors, which control the distribution pattern of heavy metals. The metals are

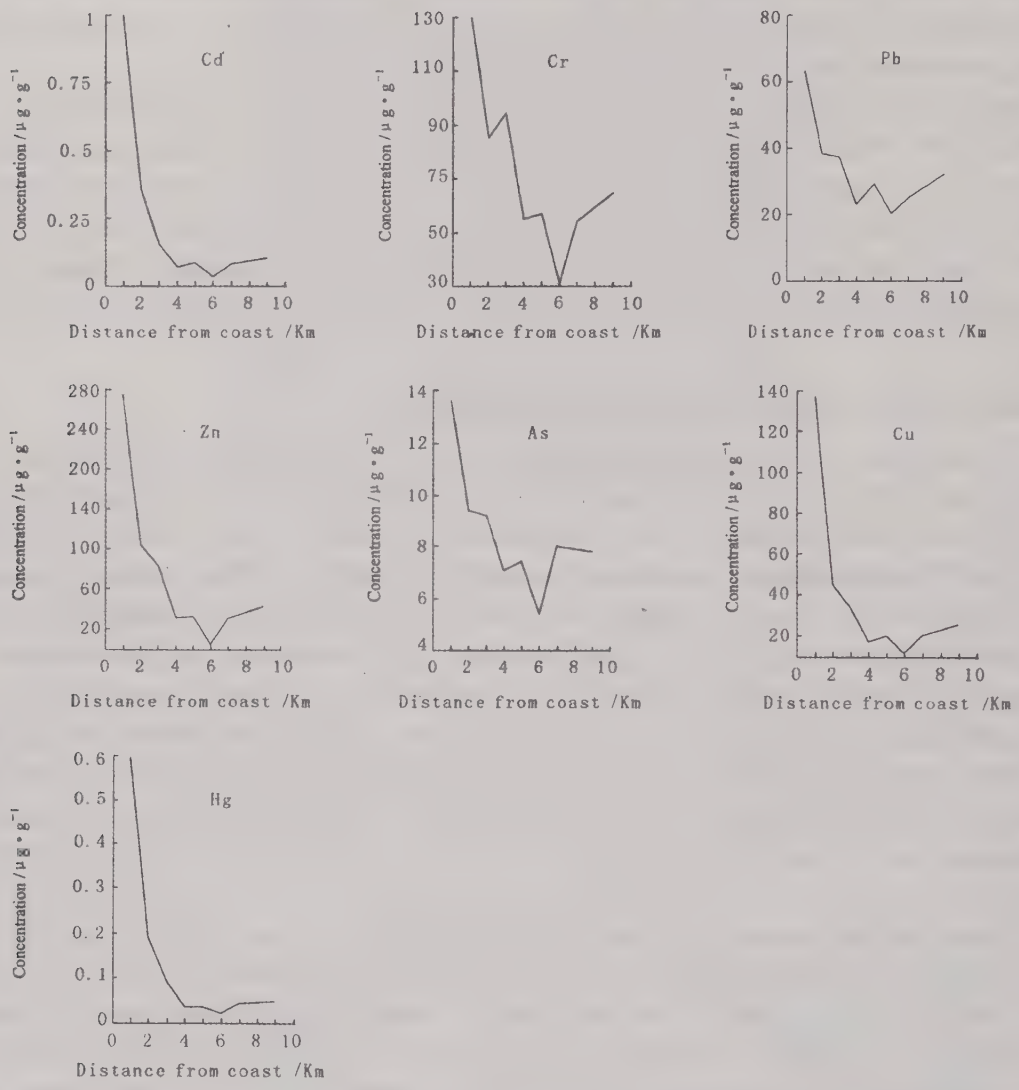


**Fig. 11 Heavy metals in surface sediment samples versus the distances of the samples from the coast**

carried by fresh water. When they move into the sea, the chemical and physical reaction between the fresh and seawater is the factor to cause sedimentation. The forms of deposition depend upon the chemical characteristics of heavy metals and the environments.

( 3 ) The hydrodynamic system controls not only the distribution pattern of sediments, but also the pattern of heavy metals. The Cangkou Watercourse is the boundary of the western part and the eastern part of the Jiaozhou Bay. The strong tidal current through it becomes a barrier to block the exchange of sediments and heavy metals from the east to the west, and vise versa. That is the reason why the distribution patterns of sediments as well as heavy metals are different from east to west. The back and forward motion of tide current is also the factor to protect the Jiaozhou Bay from pollution.

( 4 ) The distribution of heavy metals has certain correlation with the grain size of sediments in the

eastern part. The higher contents of As, Hg, Pb, Cu, and Zn distribute mostly in fine sediments. The coefficient of correlation is 0.52-0.61 with the median grain size of sediments. The correlation is not so obvious in the western part, but the tendency of change is detectable.

## Acknowledgements

This paper is part of the outcomes of the projects on "1:50,000 Environmental Geological Survey and Assessment of Qingdao" and "Geological Environmental Quality Evaluation and Sustainable Developments of Ecology & Economy of Qingdao". Thanks should go to the members of these projects. I would also thank Profs. Liu Jian and Lan Xianhong for their help and support to this paper.

## References

[1] Jenne E A. Trace element sorption by sediments and soils – sites and process. In: *Molybdenum in the Environment*. Marcel Dekker, NewYork, 1977, 425-553.

[2] Hoeck M, Runte K H. Heavy metal concentrations in a sediment corn from the tidal flats Northwest of Buesum. *Meynianam*, Kiel, 1996, 48: 35-48.

[3] Doschinsky A , Gerber H, Szemeitat A. Experiments on the influence of technical activities in the deep - sea on heavy metal cycles. *ISOPE, GOLDEN*, CO(USA), 1997, 1 :445-450.

[4] Schwedhelm E, Irion G. Heavy metals and nutrients in sediments of the German tidal flat areas. Cour Forschunginst Senckenb, 1985, 73 : 119.

[5] Renner R M , Glasby G P , Szefer P. Endmember analysis of heavy metal pollution in surface sediments from the Gulf of Gdansk and the southern Baltic Sea of Poland. *Applied Geochemistry*, 1998, 13(3): 313-318.

[6] Palanques A, Sanchez Cabeza J A, Masque P et al. Historical record of Heavy metals in a highly contaminated Mediterranean deposit : The besot prodelta. *Marine Chemistry*, 1998, 61(3−4): 209-217.

[7] Hallberg R O. Heavy metals in the sediments of the Gulf of Bothnia. *Ambil*, 1979, 8 (6): 265-269.

[8] Chen Zhenlou et al. Spatial Distribution and Accumulation of Heavy Metals in Tidal Flat Sediments of Shanghai Coastal Zone. *Acta Geographica Sciences*, 2000, 55(6): 641-651.

[9] Huang Hua-Rui, Pang Xue-Zhong. Heavy metals in sediments of tidal zone from southwest Bohai Sea. *Marine Sciences,* 1992, 5: 94-66.

[10] Huang Huarui, Pang Xue-Zhong. The heavy metals in sediments of intertidal zone southwest of Bohai Sea. *Marine Science*, 1992, 5: 44-46.

[11] Liu Changling, Zhang Jing, Yu Zhi-Gang. Study on the characteristics of the aerosol and atmospheric flux of the heavy metals over the Yellow Sea. Marine Environmental Science, 1998, 17(4) : 126.

[12] Zhu Jian. The quality evaluation of heavy metal in tidal flat bed of Shanghai Pudong area. *Journal of East China Normal University (Natural Science)*, 1991, (3) :79-85.

[13] Li Renwei. Contamination of sediments and environmental sedimentology. *Advance in Earth Sciences*, 1998, 13 (4): 398-402.

[14] Jones B, Turki A. Distribution and speciation of heavy metals in surface sediments from the Tees estuary, Northeast England. *Marine Pollution Bulletin*, 1997, 34 (10): 768-779.

[15] C U Sero J, Gracia I. Speciation of heavy metals in sediments from salt marshes on the Southern Atlantic Coast of Spain. *Marine Pollution Bulletin*, 1997, 34 (2): 123-128.

[16] Gerritse R G, Wallbrink P J , Murry A S. Accumulation of phosphorus and heavy metals in the Peel Harvey estuary in Western Australia: results of a preliminary study. *Estuarine, Coastal and Shelf Science,* 1998, 47: 679-693.

[17] Attrill M J, Thomes R M. Heavy metal concentrations in sediment from the Thames estuary, U K. *Marine Pollution Bulletin*, 1995, 30 (11): 742-744.

[18] Emmerson R H C, O 'reilly Wiese S B, Macleod C L. et al. A multivariate assessment of metal distribution in intertidal sediments of the Black water estuary, U K. *Marine Pollution Bulletin*, 1997, 34 (11): 960-968.

[19] Liao Ziji. The Pollution and Migration of Heavy Metals in Environment. Science Press, Beijing, 1989, 233-235.

[20] Weng Huan-Xin et al. Approach to Effective Species of Heavy Metals in Coastal Surface Sediments. *Chinese Journal of Geology*, 2002, 37(2): 243−252.

[21] Liu Qing , Wang Zijian and Sha Hongxiao. Research progress in heavy metal speciation and toxicity and bio-availability of heavy metals. *Chinese Journal of Environmental Science,* 1996, 17(1): 89−92.

[22] Li Ran, Li Jia, Zhao Wen-Qian, Review of the Study on the Heavy Metal Pollution in Water Environment of China. *Sichuan Environment*, 1997, 16(1):18-22.

[23] Xu Shi-Yuan, Tao Jing, Chen Zhen-Lou et al . Dynamic accumulation of heavy metals in tidal flat sediments of Shanghai. *Oceanologic & Limnologic Science*, 1997,28( 5): 509-515.

[24] Shao MiHua, Wang ZhengFang. The research of chemical forms and distributive characteristic of Co, Ni, Fe, Mn in suspend grains of sea areas around Yangzi River's mouth. *Proceedings of Environmental Science*, 1991, 11 (4):423-438.

[25] Cai Agen , Wang Kun , Yang Yi-Ping. The amounts and distribution of heavy metals in bed and biological bodies of intertidal in Jinjiang city. *Journal of Xiamen University*, 1998, 37 (4): 569-575.

[26] Cui Yi , Chen Bi-Juan , Song Yun-Li et al. Heavy metals content in sea water and marine organisms at Jiaozhou Bay. *Chinese journal of applied ecology*, 1997, 8( 6): 650-654.

[27] Wang Shuchang et. al. The distribution and Keeping Forms of Lead in Water of the Northeast Jiaozhou Bay. *Marin Corpus*, 1980, 3(1): 51-63.

[28] Sun Bingyi et al. The distribution and Keeping Forms of Zinc in Water of the Northeast Jiaozhou Bay. *Marin Corpus*, 1980, 3(2): 50-58 .

[29] Shi Zhili et al. a Study of Zinc and Lead in Surface sediments of the Northeast Jiaozhou Bay. *Journal of Shandong College of Oceanology*, 1982, 12(4): 27-36.

[30] Lu Xiaoqiao et al. The distributive rules of the content of Hg and its forms in Jiaozhou Bay. *Qingdao University Proceedings*, 1990, 20(4):107-113.

[31] Meng Ke, Sun Tingzhi,. The judgment of the content distribution of heavy metals in sediments and the pollutants in eastern coast of Jiaozhou Bay. *Qufu Normal University Proceedings*, 1996, 22 (1): 77-82.

[32] Chai Song-Fang, The research of total content of Hg and its distributive characteristic in sea water of Jiaozhou Bay. *The oceans of Yellow Sea and Bohai Sea,* 1998, 16(4): 60-63.

[33] Yin Xiaocai et al. The research of heavy metals' distribution in surface sediments of Jiaozhou Bay. *Qingdao University Proceedings*, 2001, 14(1): 76-79.

[34] Chen Xian-Fen, The survey of environmental pollution in Jiaozhou Bay. *Marine Bulletin*, 1991, 10(4): 72-77.

[35] The Port & Bay Office of the 1st Marine Institute of National Marine Bureau. *Natural environments of Jiaozhou Bay.* Ocean Publishing House, Beijing, 1984, 65-79.

# Study on Treating Halobios Pollution by Hydroxyl Radical

BAI Mindong (白敏冬)[1], XIAO Yu (肖 宇)[1], XU Xiaohong (许小红)[2], WU Chundu (吴春笃)[2], ZHOU Xiaojian (周晓见)[3]

1 *Physics Department, Dalian Maritime University, Dalian* 116026, *Liaoning, China*

2 *School of Biological and Environmental Engineering, Jiangsu University, Zhenjiang* 212013, *Jiangsu, China*

3 *Natural Science Research Institute of Kobe University of Japan, Kobe* 657-8501, *Japan*

**Abstract** The high ratio concentration hydroxyl solution is produced by strong discharge, and applied to the prevention of invasive species in ship ballast water and red tide. This paper introduces the plasma process of hydroxyl radical production, the production process of high ratio hydroxyl solution, and the application to treating ballast water and red tide.

**Keywords** hydroxyl radical, ballast water, red tide, prevention

Human beings are facing a serious environmental crisis which is even threatening their existence. Therefore, many scholars propose the concept of advanced oxidation method (technology or process, abbr. AOP or AOT). The advanced oxidation method includes the process of producing hydroxyl radicals ($OH^{\cdot}$) and a series of chain reactions excited by $OH^{\cdot}$. The radicals can attack various kinds of pollutants and microorganisms in water and finally decompose them into $CO_2$, $H_2O$ and inorganic salts, which realizes Zero Emission and Zero Pollution and solves environmental problems once and for all [1-6]. Because $OH^{\cdot}$ radicals have very high oxidation electrode potential ($E_0$=2.80 V) and is a strong oxidant, it is extremely easy to oxidize and decompose varied organic matter and living beings. The chemical reaction is a free radical one and the reaction speed is extremely fast. The reaction rate constant of C-H, C-C bonds is mostly above $10^9$ L/mol·s, even in or above the diffusing rate limit value ($10^{10}$ L/ mol·s) [7]. $OH^{\cdot}$ radical can bring out a series of chain reactions ,which destroys the small living beings completely or fully damages them , leading to the decomposition of them into $CO_2$ , $H_2O$ and mini-inorganic salts. The half-life of surplus $OH^{\cdot}$ radical is 20-40 mins and is finally changed to $H_2O$ and $O_2$ [8] which have no pollution to environment.

With the development of industry, fishery and transportation business and the excessive discharge of coastal sewage, the water body near the shore is eutrophicated and the large area of red tide has frequently taken place in our country, which seriously threatens marine resources and economy [9]. Another heavy threat to marine environment is the introduction of marine species into new environments by ship's ballast water. Till now, 500 more invasive species are confirmed from ballast water. These introduced marine organisms will cause calamitous destruction to environment and threaten the foundation of sustainable development at regions having rapid economic development[10,11].

Received on June 15, 2005

For this reason, scientists have carried out a lot of exploratory researches on the marine biological pollution problems and proposed many suggestions and methods, but problems such as feasibility, economy, security or secondary pollution still exist [12]. Recently, Bai Xiyao [13] et al. utilize the method of strong ionization discharge under high pressure, gain a high ratio concentration hydroxyl radical solution and study the treatment of ballast water and red tide [14,15]. The result indicates that hydroxyl radical has many advantages such as low drug dose, fast reaction speed, low operation costs, no secondary pollution to the ocean environment etc., which is an effectual measure to solve the problem of harmful microorganisms pollution.

## 1 Biochemical Processes

Hydroxyl radical has a strong oxidation effect, and interrelated reaction is a kind of dissociation radical one. Hydroxyl radical effects on microorganism in the ocean are shown in Fig.1.

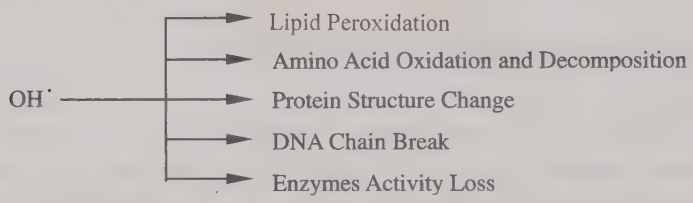


**Fig. 1 Sketch of OH· oxidized effect on ocean microorganisms**

### 1.1 Lipid peroxidation

The cell membrane or biomembrane with a thickness of 4-7 nm, is mainly composed of protein including enzyme, lipid (primarily phosphatide and amylose), water, metal ions and so on, in which phosphatide is a key structural unit and mainly consists of phosphoglyceride. The phosphoglyceride has a saturated fatty acid molecule and an unsaturated one. The unsaturated fatty acid molecule commonly links with the second carbon atom of glycerin, which is easy to carry on a series of reactions with hydroxyl radicals such as the lipid-bond break, carbon chain break and hydrolyze of unsaturated fatty acid as follows ( 1 ) [16].

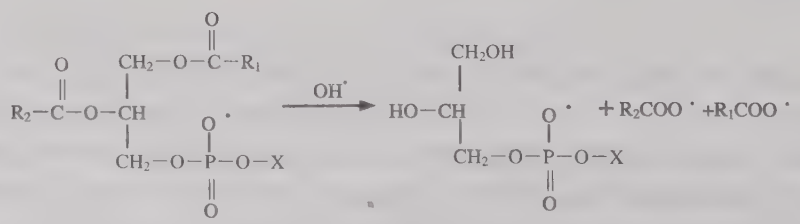


( 1 )

The above compound can be further oxidized and hydrolyzed to –OH, as in ( 2 ).

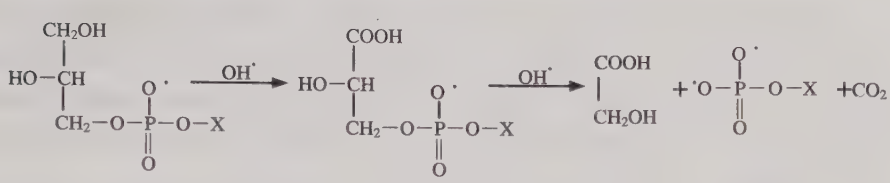

(2)

Hydroxyl radicals oxidize the unsaturated bond in -$R_2$ chain, as in ( 3 ).

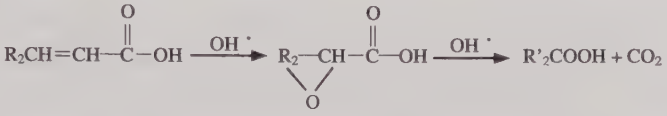

(3)

Cell membrane separates the inside and outside environments of cell, and its permeation and selectivity is the life base. Lipid peroxidation causes the cell membrane destruction and the content overflowing, finally leading to the cell death.

### 1.2 Amino acid oxidation and decomposition

Protein, a most important substance to keep the life function, is composed of the amino acid linked with the peptide bonds. The amino acid is oxidized and decomposed by hydroxyl radicals shown in ( 4 ) [17].

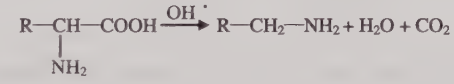

(4)

### 1.3 Protein structure change

Hydroxyl radicals cause the peptide bonds to break and the protein to denaturalize. Some amino acids have the activated radical of sulfhydryl -SH to form the disulfide bonds, which is an important chemical bond to keep the space structure of protein. Hydroxyl radical makes the disulfide bond be oxidized and broken to change the space structure of protein, resulting in the proteins to be denaturalized or the enzymes to lose the activity, finally leading to the cell death. The reaction of disulfide bond break is as follows ( 5 ) [16].

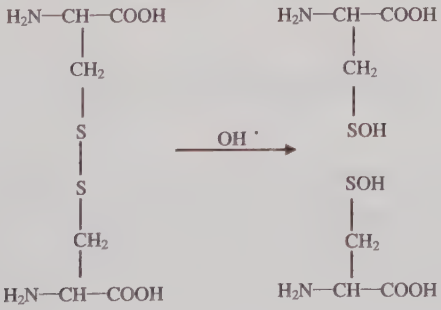

(5)

### 1.4 DNA Chain break

DNA is an important genetic molecule in the body of invasive marine species. Hydroxyl radicals

combine with DNA to form DNA Addcuts, which is a forepart damage to DNA, resulting in some changes in DNA structure such as the alkaline radical replacement and loss, the chain break and so on. Hydroxyl radicals mainly act on the C8 of adenine (A) and guanine (G) as well as the 5th and 6th double bond of pyridine alkaline radical. Also DNA is directly damaged to destroy its structure and function leading to the cell death.

### 1.5 Enzymes activity loss

There are constantly many complicated chemical changes inside organisms, which occur under the catalytic action of all kinds of enzymes[18]. The function of enzymes includes removing of harmful substance and protecting organisms from suffering from environmental pollution as well as taking physiological functions, adjusting physiological processes and catalyzing varied metabolizability. Enzyme has a unique biological characteristic: rapidly react under mild conditions such as normal temperature, normal pressure and nearly neutral pH conditions and so on. However, as a kind of protein, enzyme can denaturalize and lose the activity, finally leading to the cell death when getting from environmental pollution attack.

## 2 Plasma Processes For $OH^{\cdot}$ Radical Formation

By using the ionization discharge method, the reduced electric field intensity E/n forming discharge in the plasma reactor microgap is more than 400 Td at normal temperature and pressure. The electrons achieve an average energy of above 12 eV from the field, which is enough to ionize $O_2$ and $H_2O$ shown in Fig. 2.

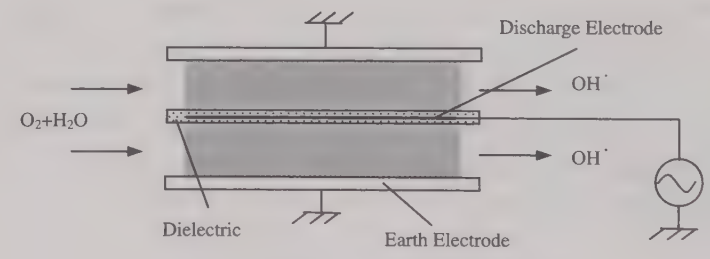


**Fig. 2 Sketch of forming $OH^{\cdot}$ by strong ionization discharge**

In a strong electric field, the plasma processes in which $O_2$ and $H_2O$ molecules are excitated to produce $OH^{\cdot}$ and $e_{aq}^{-}$ radicals are complicated. Describing them respectively according to different raw material gases, a $OH^{\cdot}$ radical formation process with mainly $O_2$ molecules ionization is found in (6) [19].

$$O_2 + e \longrightarrow O_2^+ + 2e \quad (6)$$

$O_2^+$ and $H_2O$ molecules form hydration ions in the strong electric field. The reaction is as (7).

$$O_2^+ + H_2O + M \longrightarrow O_2^+(H_2O) + M \quad (7)$$

The decomposition of hydration ions is the main approach to forming $OH^{\cdot}$ radicals by $O_2$ molecules ionization as follows.

$$O_2^+(H_2O) + H_2O \longrightarrow H_3O^+ + O_2 + OH^{\cdot} \quad (8)$$

$$O_2^+(H_2O) + H_2O \longrightarrow H_3O^+(OH) + O_2 \quad (9)$$

$$H_3O^+(OH) + H_2O \longrightarrow H_3O^+ + H_2O + OH^{\cdot} \quad (10)$$

During the strong ionization discharge process, it is possible to make 2.70 hydration ions to form $OH^{\cdot}$ injecting per 100 eV energy[19]. The plasma processes shown in ( 11 ) are $OH^{\cdot}$ and $e_{aq}^-$ radicals formation processes mainly through $H_2O$ molecules ionization and excitation and over-excitation.

$$2H_2O + e \longrightarrow H_2O^+ + H_2O^* + 2e \quad (11)$$

The dissociation of $H_2O^*$ molecules at the excited state:

$$H_2O^* \longrightarrow H^{\cdot} + OH^{\cdot} \quad (12)$$

The dissociative ionization of $H_2O^+$:

$$H_2O^+ + H_2O \longrightarrow H_3O^+ + OH^{\cdot} \quad (13)$$

The reaction of $H_2O$ adhesion, decomposition and ionization is as follows.

$$H_2O + e \longrightarrow e_{aq}^- \longrightarrow H^{\cdot} + OH^- \quad (14)$$

As a kind of radicals, hydration electron （$e_{aq}^-$） has special chemical character and stimulates many chemical reactions. Per 100 eV energy injected into the discharge electric field is possible to produce 2.80 $OH^{\cdot}$ and 2.75 $e_{aq}^-$ [14].

$OH^{\cdot}$ formation is not in ionization space but the reaction of the activated pieces results in cluster way [20, 21]. In the plasma reactor strong electric field, ionization discharge brings about excitation and ionization of $O_2$ and $H_2O$ molecules. Per 100 eV energy injected may produce 5.5 $OH^{\cdot}$ and 2.75 $e_{aq}^-$.

## 3 Application of Hydroxyl Radicals to the Prevention of Halobios Pollution

### 3.1 Application to the treatment of invasive species in ship's ballast water

The introduction of harmful species is one of the four major threats to ocean, and the ship's ballast water discharging is the main way leading to harmful organisms' travel between geographically alternative water bodies. Until now, 500 more invasive species have been confirmed from ballast water. Invasive harmful organisms lead to the calamitous destruction to the input sea area, hamper economic progress and endanger residents' health.

The international organizations of the scientific research institutions of many countries are organizing the scholars to study and control the introduced harmful organisms in ballast water. In 2003, IMO passed the "International Convention on the Control and Management of Ship's Ballast Water and Sediment", which makes the ballast water management a mandatory procedure. Scientists research on ballast water treatment methods such as heating, ultraviolet irradiation, hydrogen peroxide oxidization and so on [12,13]. But these methods have some shortcomings in feasibility, economy and security, etc. Their role in preventing invasive harmful organisms is tiny. MEPC and Glo Ballast think that there is no

effective way to treat ballast water now[17].

The process flow chart of hydroxyl radicals treating ballast water is shown in Figs. 3, 4 by Dalian Maritime University. The method is to adopt strong ionization discharge, make $H_2O$ and $O_2$ react to active particles such as hydroxyls in the unit 3, dissolve them in the water by high spreading quality efficiency means and finally get high ratio concentration hydroxyl solution[22]. Hydroxyl solution is injected into the liquid/liquid /dissolver 16 and then deal with ballast water. In the 20 t/h pilot-scale system experiment, monitoring in 4 meters from the liquid/liquid dissolver, the result indicates that when the hydroxyl ratio concentration is 0.63 mg/L the microorganisms death rate is 100 % as shown in Fig. 5, the removal efficiencies of nitrate , ammonium, COD are respectively 98.4 %, 99.5 %, 100 %, the turbid degree drops by one time and DO increases by 77. 2 %, which improves water quality to a great extent[23] as shown in Table 1 and realizes treating ballast water during transporting.

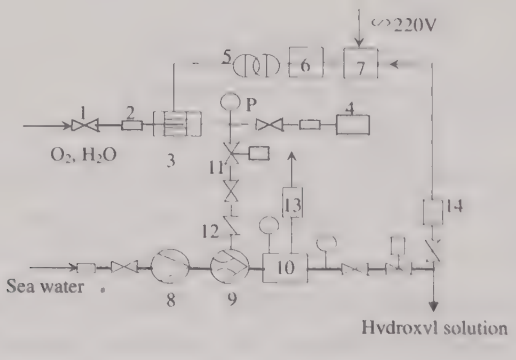


**Fig. 3 Experiment system for hydroxyl solution**

1. Valve, 2.Flowmeter, 3.OH· plasma reactor, 4.Dissolved OH· monitor, 5.Transformer, 6.Inverter, 7. Controller, 8.Pump;,9.Gas/ liquid dissolver, 10.Gas/liquid separator, 11.Electric valve, 12.Check valve, 13.Eliminator of residual OH ,14.Dissolved OH· analysis

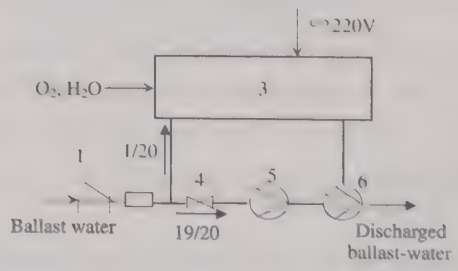


**Fig. 4 Experimental system flow chart for treatment of ship's ballast water**

1. Mechanical filter, 2.Flowmeter, 3. Experiment system for hydroxyl solution, 4.Valve, 5. Pump, 6. Liquid - liquid dissolver

### 3.2 Application to the treatment of red tide

In our country the red tide frequency trends to rise year after year. The red tide took place 79 times in 2002 and 119 times in 2003, which caused enormous losses to marine environment and aquiculture.

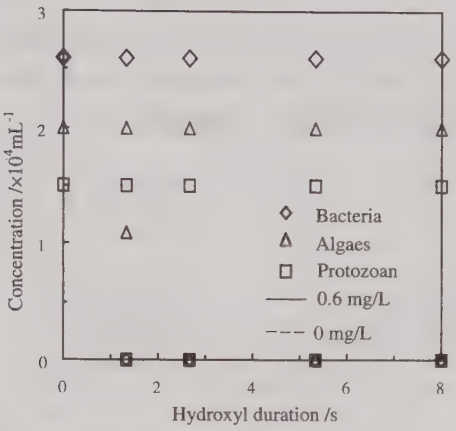


**Fig. 5 Hydroxyl duration vs. organism concentration**

**Tab. 1 Experimental data of effect on ballast water quality by hydroxyl radicals**

| Items | Hydroxyl radical solution / mg • $L^{-1}$ | |
|---|---|---|
| | 0 | 0.63 |
| Nitrate / μg • $L^{-1}$ | 156.8 | 184.1 |
| Nitrite / μg • $L^{-1}$ | 66.6 | 1.1 |
| Ammonium / μg • $L^{-1}$ | 79.8 | 0.4 |
| COD / mg • $L^{-1}$ | 0.54 | —— |
| DO / mg • $L^{-1}$ | 7.47 | 13.24 |
| Salinity | 31.351 | 31.349 |
| pH | 8.13 | 8.12 |
| Conductance | 47.3 | 47.58 |

In the past 20 years, there are 4 700 kinds of drugs to control red tide which have achieved a satisfactory result in the microcosmic test. However, when testing is done in a bigger sea area, there are only few effective drugs and also exist the problems such as too big drug dozes and long-term pollution to the ocean. These methods for controlling the microcosmic red tide are still in the studying stage.

On the basis of the earlier small experiment at the laboratory, Environmental Engineering Institute of Dalian Maritime University and the First Institute of Oceanography, SOA jiontly carried on an enclosure experiment on hydroxyl drug killing red tide organisms in the Longkou sea area in the Jiaozhou Bay as shown in Fig. 6 [24].

Measured results show that the efficiency is up to 99 89 % to kill 31 marine microorganisms, up to 100 % to kill bacteria, and that the chlorophyll and bacterium's corpora have been totally decomposed and become such harmless materials as $CO_2$, $H_2O$, $O_2$ and inorganic salts, etc., and that DO in the sea water is resumed. From Fig. 7, it can be seen that hydroxyl concentration vs. algae death rate, hydroxyl

ratio concentration is between 0.6 mg/L-0.8 mg/L killing *diatoma ,dunaliella and* P. *subcordiformis.* Hydroxyl concentration value is 0.8 mg/L to kill tiny algaes whose death rate is above 99 %. To achieve the 100 % death rate of *diatoma ,dunaliella* and *P. subcordiformis*, hydroxyl ratio concentrations should be respectively up to above 0.9 mg/L, 1.16 mg/L, 1.12 mg/L.

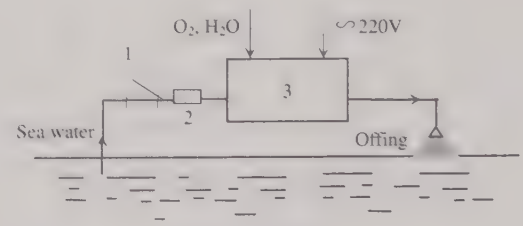


**Fig. 6 Flow chart of treatment of red tide**

1. Mechanical filter, 2.Flowmeter, 3. Experiment system for hydroxyl solution

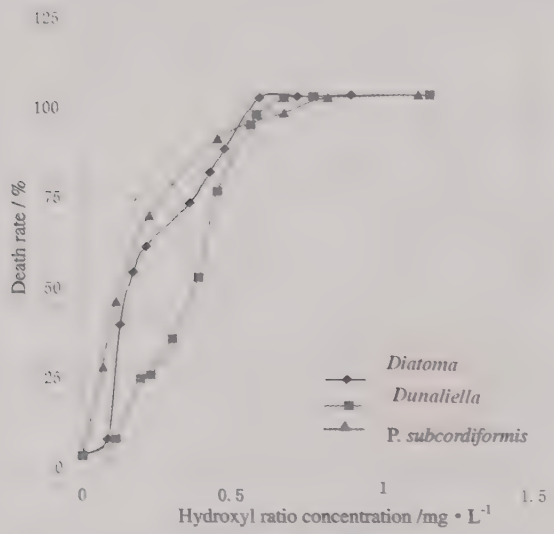


**Fig. 7 Hydroxyl ratio concentration vs. algae death rate**

The hydroxyl has an extremely strong oxidization ability and low drug consumption. The chemical reaction between hydroxyl and organisms of red tide belongs to the free radical reaction. Reaction speed of killing red tide is extremely fast. The final product of remaining hydroxyl is $O_2$ and $H_2O$, which doesn't have such problems as poisonous leftovers, etc. Experimental result indicates that treating red tide with hydroxyl is also a feasible, effective and ideal method.

## 4 Conclusions

There is always an academic study focus on how to gain the high concentration hydroxyl radical

solution. With the new advances of gas electronics, plasma chemistry, atom and molecule physics and dielectric material and so on, it is hopeful to solve this difficult and noticeable problem. The article uses the single molecular engineering method at atom and molecule levels, produces high density of hydroxyl radicals according to the designed model in advance [20, 25], and then make the high concentration (100 mg/L) and highly productive (> 100 t/h) hydroxyl radicals solution.It will become an effective, cheap, green, and ideal method to deal with the invasive harmful organisms. The experimental result shows:

( 1 ) Hydroxyl radicals are characterized by fast reaction speed, strong oxidization ability and no secondary pollution, which accords with the 8 principles of advanced oxidation technology[8]. They are incomparable in controlling the marine biological pollution.

( 2 ) In utilizing strong ionization discharge to make high density hydroxyl radicals solution, raw materials are only $H_2O$ and $O_2$, which don't adopt catalysts and produce waste materials and adjunctions.

( 3 ) The surplus hydroxyl radical is reduced into water and oxygen after being oxidized and decomposed in 20-40 mins, which exerts no pressure on the environment. Using hydroxyl radical is a feasible and effective ideal method without residuals for controlling ocean harmful biological pollution.

## Acknowledgments

The study has been funded by Key Project of National Foundation Research from the Ministry of Science and Technology of China, (2002CCC00900), outlay:30,0000, Key and General Projects of National Natural Science Foundation of China (NSFC: 60371035), outlay:26,0000, and Key and General Projects of National Natural Science Foundation of China (NSFC: 60471036), outlay:21,0000.

## Renferences

[1] Hoigne J, Bader H. The Role of Hydroxyl Radical Reactions in Ozonation Processes in Aqueous Solutions. *Water Res.*, 1976, 10(2): 377.

[2] Glaze W H, Kang J W, Chapin D H. The Chemistry of Water Treatment Processes Involving Ozone-Hydrogen Peroxide and Ultraviolet Radiation. *Ozone Sci. & Eng.*, 1987, 9(4): 335.

[3] Duguet J P. Application of Combined Ozone-Hydrogen Peroxide for the Removal of Aromatic Compounds from a Groundwater. *Ozone Sci. & Eng.*, 1990, 12(3): 281.

[4] Staehelin J, Hoigne J. Decomposition of Ozone in Water:Rate of Initiation by Hydroxide Ion and Hydrogen Peroxide.Environ. *Sci. & Tech.*, 1982, 16(3): 676.

[5] Matte ws R W. Photooxidation of Organic Material in Aqueous Suspensions of Titanium Dioxide. *Water Res.*, 1990, 24(5): 653.

[6] Petrier C, Lamy M L, Francony A et al. Sonochemical Degradation of Phenol in Dilute Aqueous Solutions:Comparison of the Reaction Rates at 20 and 487 kHz. *J.Phys.Chem.*, 1994, 98(5): 1 051.

[7] Muhammad A M, Abdul G, Salman A M. Water purification by electrical discharges. *Plasma Source Sci.*

*Technol*, 2001, 10: 82-91.

[8] Sun X B, Zhao Q X, Cao G M et al.. Characteristic and application of advanced oxidation method. *Water supply and drainage of China* (in Chinese), 2002, 18(5): 33-35.

[9] Anderson D M. Turning back the harmful red tide. *Nature*, 1997, 388:513-514.

[10] Ruiz G M, Rawlings T K, Dobbs F C, et al. Global spread of microorganisms by ships. *Nature*, 2000, 408: 49-50.

[11] Penemrante B M,Bardsley J N, Hsiao M. Kinetic analysis of nonthermal plasma used for pollution control. *J Appl Phys*, 1997, 36: 5 007-5 016.

[12] Lin H P. Ballast water management. *Sea transportation of the world* (in Chinese), 2001, 24(3): 40-41.

[13] Bai X Y, Zhang Z T, Bai M D et al. Research actuality and development of non- equilibrium plasma chemistry. *Science Bulletin* (in Chinese), 1999: 65-69.

[14] Bai X Y, Bai M D, Zhou X J. Research on treating red tide by hydroxyl solution. Nature (in Chinese), 2002, 24(1): 26-32.

[15] Bai Mindong, zhang Zhitao, Bai Xiyao et al. "The killing of organisms in ship's ballast water using hydroxyl radicals", *Oceanologia et Limnologia Sinica (china)*, 2003, 34(5): 484-489.

[16] Kong F X. *Environmental biology*. Higher Education Publishing Company, Beijing, 2000, 68-94.

[17] Shen R Q, Gu Q M. Biochemistry tutorial. Higher Education Publishing Company, Beijing, 1993, 1-233.

[18] Chen S G, Zhou R Q. *Enzymology*. Fudan University Publishing Company, Shanghai, 2001.

[19] Bernie M PENETRANTE, J Norman BARDSLEY, Mark C HSIAO. Kinetic Analysis of Non-Thermal Plasmas Used for Pollution Control. *Jpn. J. Appl. Phys*, 1997, 36(7B): 5 007-5 017.

[20] Bai C L, Su M. Single molecule chemistry and physics. *Science and technology research and development* (in Chinese), 2000, 21(4):12-15.

[21] Xu X J, Zhu D C. *Gas discharge physics*. Fudan University Publishing Company, Shanghai, 1996.

[22] Bai M D, Bai X Y, Zhang Z T et al. Simulation test research on killing microorganisms in ballast water by strong oxidation free radicals. *Traffic and environmental protect*, 2003, 24(2): 1-4.

[23] Zhou X J, Liu X W, Deng S F. 20t/h pilot-scale system experiment research on killing microorganisms in ship's ballast water by hydroxyl radicals. *Ocean Engineering* (in Chinese), 2004, 22(2): 79-82.

[24] Bai X Y, Zhou X J, Lv J B. Test on killing red tide microorganisms at Jiaozhou Bay. *Dalian Maritime University Journal* (in Chinese), 2003, 29(2): 47-50.

[25] Bai X Y, Zhang Z T, Han H et al. 2002. Research situation and progress of non-equilibrium plasma chemistry. *Chinese Science Bulletin* (in Chinese), 47(7): 529-530.

# A New Way to Study Water-Vapor Absorption Coefficient

ZHOU Liangming (周良明), GUO Peifang (郭佩芳), TAN Yingyu (谭映宇)
*Department of Oceanography, Ocean University of China, Qingdao 266003, China*

**Abstract** In the visible spectrum, the atmospheric attenuations to sunlight mainly include aerosol scattering, atmospheric molecule Rayleigh scattering and ozone absorption, while in the near-infrared spectrum (from 650 nm to 1 000 nm), we must take water-vapor absorption into account. Based on the atmospheric correction theory, using spectrum irradiance data measured by Instantaneous Ground spectrometer, ozone content measured by Microtops II ozone monitor, water-vapor content and aerosol optical thickness measured by sun photometer, we give a new way to study water-vapor absorption to sunlight, and the result shows that the main peak values of water-vapor absorption coefficients are 0.025 $cm^{-1}$, 0.073 $cm^{-1}$, 0.124 $cm^{-1}$, 0.090 $cm^{-1}$, 0.141 $cm^{-1}$ and 0.417 $cm^{-1}$, which respectively lie at 692 nm, 725 nm, 761 nm, 818 nm, 912 nm and 937 nm.

**Keywords** atmospheric attenuation, water-vapor, ozone, aerosol scattering, Rayleigh scattering

## Introduction

Atmospheric correction is one of the most important problems for satellite ocean color remote sensing, and the key to atmospheric correction is to acquire the ingredients of atmosphere, from content to distribution. For ocean color remote sensing, the range of spectrum we concern is from 400 nm to 760 nm, so we mainly take into account the Rayleigh scattering, aerosol scattering and ozone absorption when computing atmospheric correction.

The influence of water-vapor absorption in the near-infrared spectrum causes an apparent spectral variation, which will lead to an error in atmospheric correction. This effect is dependent on the water-vapor content of the atmosphere. If the water-vapor content is known, a simple procedure is provided to remove the degradation of the atmospheric correction. Uncertainty in the water-vapor content will limit the accuracy of the correction algorithm.

The absorption of water vapor is little in the visible spectrum, while in the near-infrared spectrum, it is large by comparison. The optical thickness of water-vapor absorption is proportional to its content. Generally, the optical thickness of water-vapor absorption may be presented as

$$\tau_w = k_w U_w \quad (1)$$

where $k_w$ is the absorption coefficient (in $cm^{-1}$), and $U_w$ is the water-vapor content (in cm).

Received on June 9, 2005

The Environmental Protection Agency (EPA) [1] provides spectral irradiance from 300 nm to 700 nm. The spectral irradiance at 550 nm is 1.903 mW/cm$^2$/nm, this gives a choice to select wavelength elsewhere.

## 3 Atmospheric Attenuation in the Visible Spectrum

### 3.1 Ozone absorption

The ratio of ozone absorption versus thickness $\tau_{oz}$ is related to the ozone absorption coefficient $k_{oz}(\lambda)$ by Gordon (1969) [2]

$$\tau_{oz} = k_{oz} \frac{l}{1000} \tag{2}$$

where $l$ is the ozone path length in cm-atm, a thickness ozone is millimeters when compressed to sea level pressure and temperature, which can be measured by Microtops II ozone monitor.

The ozone absorption coefficient $k_{oz}(\lambda)$ was taken from Nicolet (1984) [3]

$$k_{oz} = (3.116 \times 10^{-3})\lambda^{-4.9325\lambda + 4.9325} \tag{3}$$

### 3.2 Aerosol scattering

The aerosol is basically assumed to be a combination and/or Mie scattering, where dust is the aerosol is considered to a layer of 2 km of thickness over the sea surface with about 50 % of the Rayleigh scattering molecules above the aerosol. The aerosol optical properties in the sea coastal environment are very significant.

The aerosol optical thickness $\tau_a$ varies with wavelength according to Kasten (1966) [4]

$$\tau_a(\lambda) = \tau_a(\lambda_0)(\lambda - \lambda_0)^{-\beta} \tag{4}$$

where the exponent $\beta$ is assigned to be close 1.

Moreover [5] use photometer measurements $\tau_a$ in mid-visible band (0.5 mm, 0.7) and (1.020 mm, according to these data $\tau_a$ we can compute $\tau_a$ with all more wavelength using (4).

### 3.3 Rayleigh scattering

The Rayleigh optical thickness being almost [6] processes in the general purpose. The optical value $\tau_R$ is computed according to Stum (1981) [7]

$$\tau_R = \frac{}{} \tag{5}$$

where $\lambda$ is in micrometers, $p$ is the station pressure and the parameter $\Delta p$ of the actual pressure with respect to the standard is set equal to $\pm$ 15 hPa.

After getting $\tau_{oz}$, $\tau_a$ and $\tau_{ray}$ we can provide the optical thickness at wavelength $\lambda$ in the visible spectrum, which is marked as $\tau_\lambda$

$$\tau_\lambda = \tau_{oz} + \tau_a + \tau_{ray} \tag{6}$$

According to Gordon and Voss (1999)[4], the direct transmittance $T$ is

$$T = \exp(-\tau M) \tag{7}$$

where $\tau$ is the total optical thickness in both visible and near-infrared spectra, that is

$$\tau = \tau_v + \tau_w \tag{8}$$

and $\tau_w$ and $\tau_v$ are presented in ( 1 ) and ( 6 ) respectively.

In ( 7 ), $M$ is the air mass, which was taken from Fargion G S and Mueller J L ( 2000) [5]

$$M = \sec\theta - 0.0018167(\sec\theta - 1) - 0.002875(\sec\theta - 1)^2 - 0.008083(\sec\theta - 1)^3 \tag{9}$$

where $\theta$ is the solar zenith angle.

The relation between the direct incident irradiance above sea surface $E_{s,d}$ and the extraterrestrial dolar irradiance $\bar{F}_0$ is followed as (Gordon and Voss, 1999)

$$E_{s,d} = \bar{F}_0 \exp(-\tau M) \tag{10}$$

According to ( 1 ), ( 8 ) and ( 10 ), the absorption coefficient of water-vapor is confined as follows

$$k_w = \frac{\ln(E_{s,d} / \bar{F}_0)/M - \tau_v}{U_w} \tag{11}$$

## 2 Data Processing and Results

From June to August, 2003, we made in-situ observations at 136 points in the Bohai Sea. These data include ozone content, sea surface pressure, water-vapor content and aerosol optical thickness at 440 nm, 500 nm, 675 nm, 870 nm and 1 020 nm. Fig 1 is the curve of Rayleigh scattering optical thickness. Fig.2 shows the aerosol optical thickness with different wavelengths. Fig.3 is the ozone absorption thickness curve. Then we get the water-vapor absorption coefficient $k_w$ (presented as in Fig.4). The main peak values of water-vapor absorption coefficients are 0.025 $cm^{-1}$, 0.073 $cm^{-1}$, 0.124 $cm^{-1}$, 0.090 $cm^{-1}$, 0.141 $cm^{-1}$ and 0.417 $cm^{-1}$, which respectively lie at 692 nm, 725 nm, 761 nm, 818 nm, 912 nm and 937 nm.

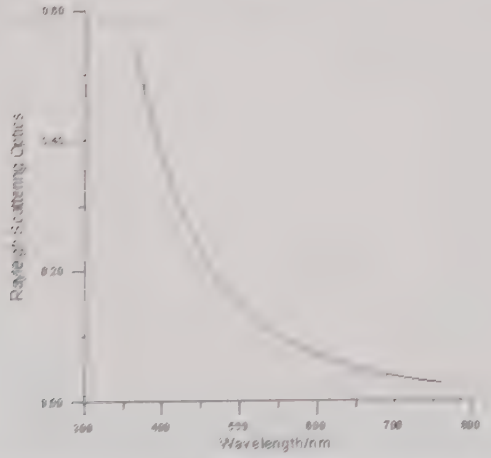


**Fig. 1 Rayleigh scattering optical thickness varies with wavelength, where the pressure is 1 016 hPa**

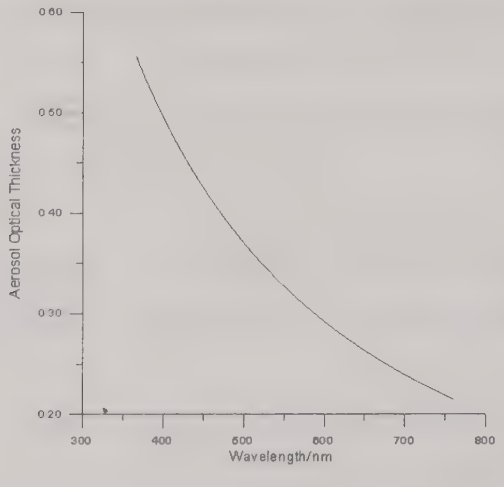


**Fig. 2 Aerosol optical thickness varies with wavelength**

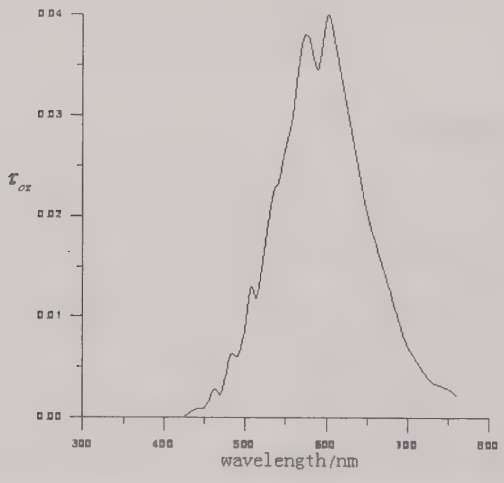


**Fig. 3 Ozone optical thickness, where the ozone content is 318.9DU**

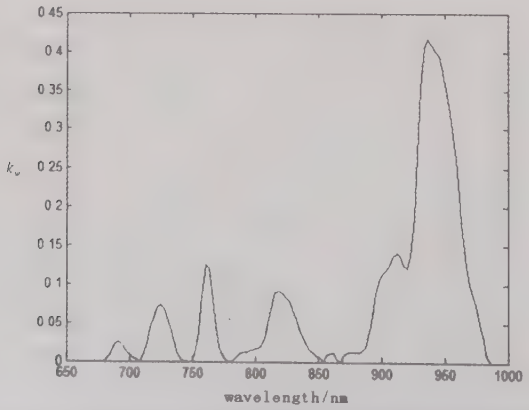


**Fig. 4 The curve of water-vapor absorption coefficient**

## 3 Concluding remarks

In this paper, we present a new way to study water-vapor absorption coefficient, and the result corresponds with the conclusions given by predecessors. This way and work will facilitate studying atmospheric attenuation and atmospheric correction of ocean color remote sensing.

## Acknowlegements

Financial support was provided by The National High Technology Research and Development Program of China (863 Program): No 2001AA633030 and 2001AA633080.

## References

[1] Gordon H R. Remote Sensing of Ocean Color: A Methodology for Dealing with Broad Spectral Bands and Significant out-of-band Response. *Applied Optics,* 1995, 34(36): 8 363-8 374.

[2] Nicolet M. The Solar Spectral Irradiance and Its Action in the Atmospheric Photodissociation Processes, *Planet Space Sci.* 1981, 29: 951-974.

[3] Sturm B. Ocean Color Remote Sensing Using Nimbus CZCS Data. *In oceanography from space edited by J.F.R.Gower,* 1981, 267-288.

[4] Gordon H R and Voss K J. MODIS Normalized Water-leaving Radiance Algorithm Theoretical Basis Document, Version 4, *Under Contract Number NASS-31363*, 1999, 1-25.

[5] Fargion G S, andMueller J L. Ocean Optics Protocols for Satellite Ocean Color Sensor Validation, Revision 2. *NASA/TM-2000-209960*, 2000, 4-189.

# Biogeochemistry of Nutrient Elements in the Changjiang (Yangtze River) Estuary

WANG Baodong (王保栋), TU Jianbo (屠建波)
*First Institute of Oceanography, SOA*, Qingdao 266061, *Shandong, China*

**Abstract** Based on the biogeochemical studies on nutrient elements in the Changjiang estuary, the main results and recent progresses are reviewed in this paper, such as the nutrient fluxes into the sea, the mixing behaviors, the distribution characteristics and transportation as well as the biogeochemical behaviors of nutrients in the plume frontal region. The exploring directions and research emphases in the future are proposed.

**Keywords** nutrient, biogeochemistry, the Changjiang estuary

## Introduction

The estuarine and coastal waters are nutrient-enriched and the nutrient ratios have been altered as a result of the changed riverine input due to land-use change and anthropogenic nutrient emission over the last century [1, 2]. Estuarine and coastal ecosystems respond to such changes in nutrient budgets by shifting population dynamics of phytoplankton and hence of the rest of the food web, leading to changes in top-down as well as bottom-up control of community structures [3]. Since land input signals from large river systems undergo a much smaller modification prior to reaching the ocean compared to those of small rivers [4], coastal regions impacted by major rivers carrying substantial nutrients loads provide settings in which to examine a broad spectrum of nutrient conditions and their relationship to biological processes. The biogeochemical characteristics of large river estuaries and their potential influence on the coastal ecosystems have been recently reviewed [4, 5].

The Changjiang (Yangtze River), the world's third largest river after the Amazon and the Nile, discharges to the East China Sea (ECS) $9.32\times10^{11}$ $m^3$/a of freshwater [6] and an SPM load of $4.32\times10^8$ t/a (mean from 1950 to 2000) [7]. Seventy-one percent of the freshwater discharge occurs in the wet season (May to October) and only 29 % in the dry season (November to April)[6]. The huge Changjiang drainage basin is located in a heavily populated temperate area with a total area of $1.94\times10^6$ $km^2$ and settlements of 400 million people [6]. The Changjiang is the major pathway of nutrients, which channels anthropogenic impacts in the catchment to the estuary.

High levels of nutrients have caused severe eutrophication in the estuarine and the extended coastal waters and harmful algal blooms (HABs) are frequently observed in the area. The ECS is the sea where most severe HABs occur among the four China Seas. The incidents of HABs in the ECS accounts for 45 % of the total recorded number in China Seas [8]. The frequency of HABs occurrence in the ECS increased rapidly since the 1990s, and the durations and sizes of affected area increased continually. For instance, 51 individual HAB occurrences were observed in 2002 mainly in the estuarine and adjacent

Received on January 11, 2005

coastal areas of the ECS, which is 10 times more than the average value in the 1990s [8]. Toxic species of HABs were often observed in the ECS such as Alexandrium and Gymnodrium, and kills in zoobenthos and fish kills especially for aquaculture in the coastal areas were often reported [8]. The occurrence of HABs damages the nearby fishing ground (e.g. the well-known Zhoushan fishing ground) and events of oxygen depletion (hypoxia) in near-bottom water off the Yangtze River mouth, which was first recorded in the 1950s, have become more serious in recent years [9].

Since the biological processes and the ecological environment in the Changjiang estuary and its adjacent waters are influenced significantly by the inputs of nutrient elements from the Changjiang, it is essential to find problems through analyzing and summarizing the previous work, and then adjust and forecast the research direction of future study.

## 1 Nutrient Fluxes from the Changjiang into the Sea

The inflow from the Yangtze River is the major source of nutrients to the Changjiang estuary and coastal waters. Nutrient concentrations as well as nutrient loads of the Yangtze River, notably DIN, increased exponentially and by a factor of seven from the 1960s to the end of the 1990s, mainly due to the increasing amount of fertilizer application and effluents from cities in the river basin [10]. Liu et al. [11] found that the concentration of DIN increased by a factor of seven from 15 μmol/L in 1968 to 118 μmol/L in 1997. Compared to the result of Liu et al., although there were some differences in the nutrient fluxes of the Changjiang estimated by different investigators (Tab.1) due to the differences in sampling time, place, methods of analysis as well as the annual and seasonal variations of the nutrients fluxes, it is widely believed that the nutrient fluxes from the Changjiang into the sea have been increasing significantly since the 1960s.

**Tab. 1 Nutrient fluxes from the Changjiang River (t/a)**

| DIN / $\times 10^5$ | $NO_3$–N/$\times 10^5$ | $PO_4$–P / $\times 10^3$ | $SiO_3$–Si / $\times 10^6$ | References |
|---|---|---|---|---|
| 3.15 | 5.40 | 5.69 | 3.17 | Liu et al.[11] |
| 7.84 | 6.91 | 15.10 | 2.22 | Shen[12] |
| — | 8.40 | — | — | Edmond et al.[13] |
| 6.25 | 4.27 | 16.40 | 2.47 | Zhang[14] |

## 2 Behaviors of Nutrient Elements during Estuarine Mixing

There is no common pattern about estuarine mixing behaviors of nutrients because of different processes involved in the estuarine mixing in different estuaries. By analysis of the field data in the Mississippi estuary and laboratory simulation, Bien et al.[15] found that silicate demonstrated obvious removal, and they pointed out that the existence of electrolyte and suspended particulate matter were essential for the chemical removal of silicate. This opinion of chemical removal was supported by the

results of Burton et al.[16]. They found that nearly 10 %-30 % of silicate was removed during estuarine mixing in the estuaries of the Southampton River, the Conway River and the Alde river in U.K. as well as the Vellar River in India; and it was confirmed by laboratory experiments that the absorption onto the suspended particulate matter and the existence of electrolyte played a dominant role in the chemical removal of dissolved inorganic silicate, whereas the biological removal was minor.

In contrast, Wollast and De Broen [17], Fanning and Pilson [18] believed that the biological removal of silicate was dominant during estuarine mixing. Wollast et al. surveyed the Scheldt River estuary in Belgium and found that silicate was removed in large quantities. They considered that the inorganic removal played a minor role.

With regard to the Changjiang estuary, the mixing behaviors of nutrients have been studied by many investigators and different conclusions were obtained. Huang et al.[19], Ye et al.[20] and Wang et al.[21] reported significant correlation between the nitrate or silicate concentrations and the salinity in the Changjiang estuary, and thus they concluded that nitrate and silicate demonstrated conservative behavior. For instance, Wang et al.[21] obtained the coefficients of -0.96 ($n$ = 139) and -0.99 ($n$ = 204) for nitrate–salinity and silicate–salinity correlations, respectively, and thus they concluded that nitrate and silicate concentrations were mainly controlled by dilution process. However, Shen et al.[22] considered that there were biological removals of nutrients in the Changjiang estuary. They found that the physical mixing played a dominating role in the nutrient transportation from the estuary to the sea, but at the same time biological removal occurred through phytoplankton uptake due to the high biomass of phytoplankton in the upper water of the Changjiang estuary.

In the previous observations, phosphate demonstrated some remobilization, depending upon water stage and particle populations [13, 14, 23]. However, nitrate demonstrated either conservative behavior [13, 23] or in excess of the conservative mixing relationship[14]. Similarly, silicate demonstrated both conservative behavior (1980 – 1981 cruises) and an overall remobilization (1988 cruise) in the Changjiang estuary [13, 23].

The conflicting distribution modes of DIN and silicate in different seasons and different years in the Changjiang estuary imply that both biotic and abiotic events may affect their behaviors during estuarine mixing and the actual distributions of DIN and silicate would depend on how and to what extent biological (uptake and regeneration) and abiotic (adsorption/desorption) counterbalance each other [14].

## 3 Biogeochemical Characteristics in the Plume Frontal Region

The plume front is an important front existing in estuary. The diluted water diffused from river into sea is usually called the plume water, and the interface between the outer seawater and the plume water is called the plume front. The spatial scale of the plume front depends primarily on the runoff into estuary and secondly on the variations of currents outside the river mouth. The plume front in the Changjiang estuary is a salinity front and usually lies in the salinity region of 20-28 with a characteristic value of 25 [24]. The plume front is obvious in the flood season and usually locates at 123° E, whereas it moves back to nearby the river mouth during dry season [24]. The plume front is an area of high primary productivity due to low concentration of suspended particulate matter (less than 100 mg/L) and high

transparency (up to 5 m) which provides an essential condition for the photosynthesis of phytoplankton; whereas the nutrients in the Changjiang Diluted Water (CDW) provide a favorable nutritional basis for the photosynthesis of phytoplankton. At the same time the moderate salinity could satisfy, to some extent, the growth of both the high salinity species and the low salinity species of phytoplankton. All these factors promote the formation of high productivity zone in the plume front region.

Based on the field observation, Zhou et al.[25] found that there were three kinds of fronts in the Changjiang estuary in summer, *i.e.*, the shear front formed by the difference of the flow velocities nearby the marginal beach, the suspended sediment front at the river mouth formed at the interface between the estuarine water and the plume water, and the plume front at the interface between the plume water and seawater. The features in nutrient distributions were different in different frontal areas. In the suspended sediment frontal area, the nitrate distributions were characterized by the large horizontal gradient but small vertical gradient. In the plume frontal region, however, in addition to the large horizontal gradient of nitrate concentration, there was also large vertical gradient which resulted in the vertical stratification. The plume front restricted the nutrient transportation from the estuary to the open sea to some extent by acting as a barrier. Thus the nutrient concentration on the shoreward side was evidently higher than that on the seaward side of the front. For example, during a cruise to track the plume front in the Changjiang estuary on August 26, 1988, Zhou et al.[25] observed that the concentrations of phosphate and silicate on the shoreward side were 2 and 4 times as those on the seaward side of the front, respectively. The nitrate concentration was about 20 μmol/L on the shoreward side of the front, whereas it was below the detecting limit on the seaward side of the front.

The plume front functioning as a barrier not only restricts the transportation of nutrients, but also differentiates ecological environments on both sides of the front. It was observed that there were more freshwater species on the shoreward side of the front but more saline water species on the seaward side of the front[25]. With regard to phytoplankton species quantity, there were usually more saline water species than fresh water species. Thus the total species of the phytoplankton on the seaward side of the front were more than that on the shoreward side. Therefore, the nutrients on the seaward side of the front were more changeful in concentrations and distributions, because different biological species have different modes and processes of nutrient uptake. This is the indirect impact of plume front on nutrients through restricting the biological activity.

Hu et al.[24] found that on the shoreward side of the plume front, the phytoplankton could not grow rapidly because of light limitation due to the high concentration of suspended particulate matter. Therefore the nutrients were less disturbed by the phytoplankton and thus the nitrate and silicate demonstrated well conservative behaviors. However, within the plume front, the light availability is no longer a limiting factor and the phytoplankton could grow rapidly to form an area with high pH and high DO nearby the margin of the plume front. An acidified reductive condition with low pH, low DO and Eh was formed in the sediments through decomposition of organic matter by chemical or microbiological processes after the sinking of large quantities of debris and organics produced by the biological activities. In addition, the existence of the pycnocline in summer, which limits convection, and exchange of water aggravates the reductive degree of the bottom environment. This is the so-called biogeochemical filtrating effect that exists in the plume front, which may change not only the chemical constitution of

the sediments, but also the material composition of the sediments as well as the biogeochemical condition. Not only are the nutrients, organic matter and carbonates deposited on the bottom by way of the biogeochemical filtrating effect, some chemical elements (e.g. heavy metals) are also transferred through the biological uptake.

## 4 Distribution and Transport of Nutrients in the Changjiang Estuary

There are many research reports about the distribution and variations of nutrient elements in the Changjiang estuary and its adjacent areas. Huang et al.[26] found that the Changjiang Diluted Water has the tendency of expanding simultaneously towards the south and the north as indicated by the horizontal distributions of phosphate and total phosphorus. Based on the field data obtained in the Changjiang estuary, it was pointed out that some of the nutrients in the Changjiang Diluted Water were transported to the northeast of the Changjiang estuary throughout the year [27]. Based on the cruise data during 1984—1985 and the field data in the Yellow Sea and the East China Sea (including the Changjiang estuary) in 1997—1999, Wang [28,29] concluded that there was a large area with high nutrient concentrations in the northeast of the Changjiang estuary throughout the year, and the source of nutrients was from the left-turning of the main body of the Changjiang Diluted Water in the flood season, whereas in the dry season the nutrients mainly came from the inflow from the Subei Coastal Current Water having high nutrient concentrations and the inflow of a small part of the Changjiang Diluted Water. Thus he put forward the viewpoint that the Changjiang Diluted Water extends simultaneously in two directions, *i.e.*, the Changjiang Diluted Water firstly flows southeastward along the estuarine trend to the river mouth, then it is divided into two parts: one part flows across the Hangzhou Bay and Zhoushan Islands and extends southward continually along the coast or extends southeastward, the other part flows northward or northeastward into the south of the southern Yellow Sea. The water quantities and proportion of the north and the south sections of the diluted water are different in different seasons.

## 5 Nutrient Limitation in the Changjiang Estuary and its Adjacent Areas

Inside the river mouth of the Changjiang estuary, primary productivity is limited by light availability due to the high turbidity as well as the intense hydrodynamic condition of the water, whereas nutrients do not limit the primary productivity [22]. However, in the area outside of the river mouth, N/P ratio is much greater than the Redfield ratio due to the input of the freshwater having a very high N/P ratio (up to 125) and thus the primary productivity is P-limited in this region [22, 29-31]. It is N-limited in the area 500 km more away from the estuary [30].

Based on the *in situ* incubation experiment, Hu et al.[32] put forward a criterion for nutrient limitation in the Changjiang estuary, *i.e.*, the growth of the phytoplankton is P-limited when $N/P > 30$, and N-limited when $N/P < 8$. By applying the above criterion, Wang et al. [29] analyzed the field data of the total shelf areas of the Yellow Sea and the East China Sea in 1997—1999 and concluded that the P-limited area in summer covered the south-west of the Yellow Sea, the area to the west of 126° E from 33° N in the north to 30° N in the south, and the coastal area of the East China Sea, which was the

largest among the four seasons; in spring, the P-limited area covered the coastal area west of 123° E from 34° N in the north to 29° N in the south, which was the second in the P-limited area; in autumn, the P-limited area was confined to a narrow band in the coastal area of ECS; whereas there was no P-limited area in winter. Moreover, they found also that the area with the highest N/P ratio was not inside the estuary, but located at 124.5° E, 32° N. This area locates just at the plume frontal region. The phytoplankton uptake large quantities of nutrients in the plume frontal region and the phosphate were nearly exhausted, whereas the inorganic nitrogen was abundant. This resulted in an extremely high N/P ratio in the surface water and led to P-limited growth of the phytoplankton.

Based on the analysis of the field data of phytoplankton, nutrients, temperature and salinity in the Changjiang estuary and its adjacent areas obtained in May, 1999, together with the results from the *in situ* incubation experiment and laboratory simulation experiment, Pu et al.[33] studied the nutrient limitation of phytoplankton in the Changjiang estuary. Based on the results obtained as well as by taking into consideration the rate of freshwater input, its flowing direction and the stratification, they divided the Changjiang estuary into four sections: the area near the river mouth where the deficiency of light availability is the primary limiting factor with phosphate as the potential limiting nutrient; the diluted area where phosphate is the limiting nutrient, and it is relatively deficient by more than 0.5-1.0 μmol/dm$^3$; the area influenced by the Taiwan warm current, the phosphate is relatively deficient by less than 0.5 μmol/dm$^3$; the area influenced by the Yellow Sea Coastal Current where the light availability is the primary limiting factor with phosphate as the potential limiting nutrient.

## 6 Summary

At present, the temporal-spatial distributing characteristics of nutrients in the Changjiang estuary have been understood explicitly. However, there is still some controversy about the nutrient transformation. Although the plume front theory could explain some phenomena about the nutrient distribution, it is still faulty and cannot give out a satisfied quantified explanation. We still know little about the biogeochemical processes of the nutrients in the Changjiang estuary, especially the processes at various interfaces. It is essential to know profoundly these key processes, and then establish budget models or dynamic models of biogeochemical cycles of nutrient elements, by which we can better understand the eutrophication process and the formation mechanism of the harmful algal blooms in the Changjiang estuary and its adjacent areas, to support decision-making for the protection of coastal ecological environment.

## Acknowledgments

The paper was supported by the National Science Foundation of China projects (40076022) and the National Basic Research Program of China ( 001CB409703).

## References


[1] Nixon S W. Coastal eutrophication: A definition, social causes, and future concerns. *Ophelia,* 1995, 41: 199-220.

[2] Paerl H W. Coastal eutrophication and harmful algal blooms: Importance of atmospheric deposition and ground-water as "new" nitrogen and other nutrient sources. *Limnol. Oceanogr.,* 1997, 42: 1 154-1 165.

[3] Landry M R et al. Iron and grazing constraints on primary production in the central equatorial Pacific: An EqPac synthesis. *Limnol. Oceanogr.,* 1997, 42: 405-418.

[4] Dagg M, Benner R, Lohrenz S et al. Transformation of dissolved and particulate materials on continental shelves influenced by large rivers: plume processes. *Cont. Shelf Res.,* 2004, 24: 833-858.

[5] Mckee B A, Aller R C, Allison M A et al. Transport and transformation of dissolved and particulate materials on continental margins influenced by major rivers: benthic boundary layer and seated processes. *Cont. Shelf Res.*, 2004, 24: 899-926.

[6] Chen Z, Li J, Shen H et al. Yangtze River of China: historical analysis of discharge variability and sediment flux. *Geomorphology*, 2001, 41: 77-91.

[7] Chen J Y & Chen S L. Ecological environmental changes in the Yangtze River estuary and suggestions for countermeasure. *Water Resources Hydropower Engineering,* 2003, 34(1): 19-25 (in Chinese).

[8] Guan D M, Zhan X W. Red tide disaster in coastal water of China and its prevention suggestions. *Mar. Environ. Sci.*, 2003, 22(2): 60-63 (in Chinese with English abstract).

[9] Li D and Daler D. Ocean pollution from land-based sources: East China Sea, China. *Ambio.*, 2004, 33(1-2): 107-112.

[10] Duan S W, Zhang S. Material fluxes and their variations from the Changjiang River into the sea. In: *Land-Sea Interaction in Estuaries of the Changjiang River, Zhujiang River and their Adjacent Sea Areas.* Edited by Zhang S & Shen H T, China Ocean Press, Beijing, 2001, 10-26 (in Chinese).

[11] Liu Xincheng, Shen Huanting, Huang Qinghui. Concentration variations and flux estimation of dissolved inorganic nutrient from the Changjiang River into its estuary. *Oceanologia et Limnologia Sinica,* 2002, 33(5): 332-340 (in Chinese with English abstract).

[12] Shen Zhiliang. A Study on the effects of the Three Gorges Project on the distributions and changes of the nutrients in the Changjiang River estuary. *Oceanologia et Limnologia Sinica*, 1991, 22(6): 540-546 (in Chinese with English abstract).

[13] Edmond J M, Spivack A, Grant B C et al. Chemical dynamics of the Changjiang River estuary. *Cont Shelf Res*, 1985, 4: 17-36.

[14] Zhang J. Nutrient elements in large Chinese estuaries. *Continental Shelf Res,* 1996, 16: 1 023-45.

[15] Bien G S, Contois D E, Thomas W H et al. The removal of soluble silica from fresh water entering the sea. *Geochem et Cosmochem Acta*, 1958, 14: 35-54.

[16] Burton J D. *Basic Properties and Processes in Estuarine Chemistry.* Burton J D, Liss P S. *Estuarine Chemistry*. Academic Press, London, New York, 1976, 31-36.

[17] Wollast R, De Broeu F. Study of the bahaviour of dissolved silica in the estuary of the Scheldt. *Geochimica et Cosmochimica Acta,* 1971, 35: 613-620.

[18] Fanning K A, Pilson M E Q. The lack of inorganic removal of dissolved silica during river-ocean mixing. *Geochimica et Cosmochimica Acta*, 1973, 37 (11): 2 405-2 415.

[19] Huang Shanggao, Yang Jiadong, Ji Weidong, et al. Spatial and temporal variation of reactive Si, N, P and their relationship in the Changjiang estuary water. *Taiwan Strait*, 1986, 5(2): 114-123 (in Chinese with English abstract).

[20] Ye Xiansen, Zhang Yong, Xiang Youtang. Characteristic of nitrate Distribution in the Changjiang River estuary and its cause of formation. *Marine Science Bulletin*, 2000, 19(1): 89-92. (in Chinese with English abstract)

[21] Wang Zhengfang, Yao Longkui, Ruan Xiaozheng. Distribution and characteristics of nutrients (N, P, Si) in the estuary of Changjiang River. *Oceanologia et Limnologia Sinica*, 1983, 14(4): 324-332 (in Chinese with English abstract).

[22] Shen Zhiliang, Lu Jiaping, Liu Xingjun. Distribution feature of nutrients in the Changjiang Estuary and the impact of the Three Gorges project on it. *Collected Works of Marine Science*, 1992, 33: 107-129 (in Chinese with English abstract).

[23] Tian R C, Hu F X, Martin J M. Summer nutrient fronts in the Changjiang (Yangtze River) estuary. *Estu.Coast. Shelf Sci.,* 1993, 37: 27-41.

[24] Hu Fangxi, Hu Hui, Gu Guochuan (eds). *The Sudy of the Changjiang Fronts*. The East China Normal University press, Shanghai, 2002, 88-95 (in Chinese with English abstract).

[25] Zhou Juzhen, Gu Guochuan. Variation of nutrients and the impact of fronts during summer in Yangtze River. *Guangzhou Environmental Science*, 2002, 17(1): 1-5 (in Chinese with English abstract).

[26] Huang Ziqiang, Ji Weidong. Characteristics of the variations of Phosphorus (TP, organic phosphorus and the phosphate) and their relationship in the Changjiang River estuary. *Acta Oceanologica Sinica*, 1994,16(1): 51-60 (in Chinese with English abstract).

[27] Chemistry Department of Shandong College of Oceanology. Integrated research report in the area adjacent to the Changjiang River estuary and Chejudo island (Chapter 4: Marine Chemistry). *Shandong Colloege of Oceanology Sinica*, 1986, 16(1): 132-210 (in Chinese with English abstract).

[28] Wang Baodong. On the extension and nutrient transportation of the Changjiang River diluted water. *Journal of Oceanography of Huanghai & Bohai Seas,* 1998, 16(2): 41-47 (in Chinese with English abstract).

[29] Wang Baodong, Wang X L and Zhan R. Nutrient conditions in the Yellow Sea and the East China Sea. *Estu.Coast. Shelf Sci.,* 2003, 58: 127-136.

[30] Harrison P J, Hu M H, Yang Y P et al. Phosphate limitation in estuarine and coastal waters of China. *J. Exp. Biol. Ecol.*, 1990, 140: 79-87.

[31] Wong G T F, Gong G C, Liu K K et al. Excess nitrate in the East China Sea. *Estuarine, Coastal Shelf Science*, 1998, 46: 411-418.

[32] Hu Minghui, Yang Yiping, Xu Chunlin et al. Phosphate limitation of phytoplankton growth in the Changjiang estuary. *Oceanologia Sinica,* 1989, 11(4): 439-443 (in Chinese with English abstract).

[33] Pu Xinming, Wu Yulin, Zhang Yongshan. Nutrient limitation of phytoplankton in the Changjiang Estuary II: Condition or nutrient limitation in spring. *Acta Oceanologica Sinica*, 2001, 23(3): 57-65. (in Chinese with English abstract).

# Red Tide Frequency Analysis Using the Extreme Value Theory

XIE Zhonghua (谢中华)[1], WANG Hongli (王洪礼)[2], SHI Daoji (史道基)[2], SUN Jing (孙 景)[2]
1 *Tianjin University of Science and Technology, Tianjin* 300222, *China*
2 *Tianjin University, Tianjin* 300072, *China*

**Abstract** In recent years, the red tide erupted frequently, and caused a great economic loss. At present, most literatures emphasize the academic research on the growth mechanism of red tide alga. In order to find out the characters of red tide in detail and improve the precision of forecast, this paper gives some new approaches to dealing with the red tide. By the extreme values, we deal with the red tide frequency analysis and get the estimation of T-times red tide level $U_{(T)}$, which is the level once the consistence of red tide alga exceeds on the average in a period of T times.

**Keywords** Red tide, Generalized extreme values distribution, Empirical distribution, Kernel density

## Introduction

In recent years, frequent occurrences of red tide have caused a great economic loss on breeding seafood, fishing, human health, and damaged coastal tourism and ocean ecological environment badly. In order to reduce the damage by red tide, to forecast red tide accurately has already become an important subject. However, recent researches have focused on the mechanism and properties of red tide. Most papers [1-3] that were reported researched and analyzed one or several red tides occurring in specified waters, and not many red tide observations. Thus we could not know the character of red tide or forecast it precisely. In order to solve this problem, this paper has given the theorical method of frequency analysis according to many red tide observations.

## 1 Observations Collections

Considering the big areas influenced and the long lasting-time when the red tide occurred, we should establish many observation stations in the waters where red tides occurred, observe several times in the morning, noon and evening of one day, and then record observations for analysis. This paper considered the observations of many red tides of the same observing station at specified waters.

Because we need an amount of observations, Gaussian random numbers are considered in this paper instead of real observations. Assume the cell consistency of red tide algal is said to follow the Gaussian

Received on January 11, 2005

distribution with the mean 2 and the variance 1. 100 Gaussian random numbers of this kind are used as 100 observations of red tide. We could obtain 21 observations in a week (3 observations one day) at the same station during every red tide period. Maxima contrasted from 21 observations constitute a sequence of $(x_1, x_2, \cdots, x_{100})$. Then we discuss the extreme value distribution which this sequence is said to follow.

## 2 Density Function Estimation

Let $X$ be any $x_i, i = 1,2,\cdots,100$, it can be known by [4] that $X$ is said to follow GEV (generalized extreme value) Distribution, denoting:

$$X \sim G(x;\theta) \tag{1}$$

Where $\theta = (\mu, \sigma, \xi)$ is an unknown parameter obtained by ML (the method of maximum likelihood).

### 2.1 Formulation density function

A df (density function) estimation which the observations are said to follow needs to be obtained before ML. There are two methods, one is to formulate empirical density function, and the other is to formulate kernel density[5,6]. The function formulated is known as true density function of observations. Then do ML and obtain the proper df. Because the previous one is a discrete function, we discuss kernel density function and construct a smoothing df as follows

$$\hat{f}_b(x) = \frac{1}{nb}\sum_{i\le n} k\left(\frac{x - x_i}{b}\right) \tag{2}$$

Where $b > 0$ is the bandwidth $k(x) = \frac{3}{4}(1 - x^2) I(-1 \le x \le 1)$.

The value of $b$ in Eq. (2) has an effect on the properties of kernel density function. It can be followed that $\hat{b} = 0.5940$ by [6, 7]. Corresponding kernel density functions are shown in Fig. 1.

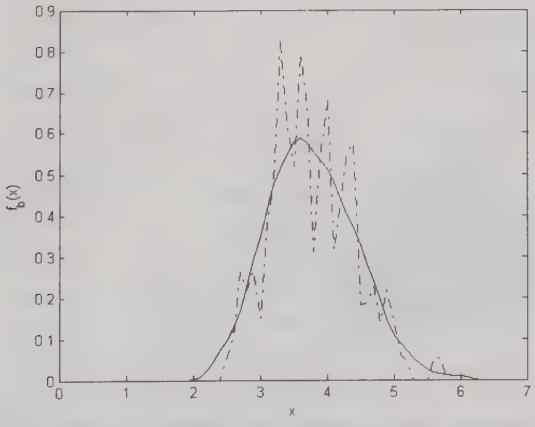


**Fig. 1 Two kernel density functions for $b$=0.594 (solid) & for $b$=0.1120 (dotted)**

### 2.2 Parameter estimation

The parameter in Eq. (1) is obtained by ML.

If $\xi = 0$, $X$ is said to follow the Gumbel distribution, and if $\xi \neq 0$, $X$ is said to follow Frechet ( $\xi > 0$ ) and Weibull ( $\xi < 0$ ) distribution. Correspondingly, the expression of the Log-likelihood is

$$l(\theta) = -n\log\sigma - \sum_{i=1}^{n}\left(\frac{x_i - \mu}{\sigma}\right) - \sum_{i=1}^{n}\exp\left\{-\left(\frac{x_i - \mu}{\sigma}\right)\right\} \quad (3)$$

$$l(\theta) = -n\log\sigma - \sum_{i=1}^{n}\left[1 + \xi\left(\frac{x_i - \mu}{\sigma}\right)\right]^{-1/\xi} - (1+1/\xi)\sum_{i=1}^{n}\log\left[1 + \xi\left(\frac{x_i - \mu}{\sigma}\right)\right] \quad (4)$$

Suppose $\xi = 0$, we can get the ML estimator of $\theta$ by Eq.(3) as follows

$$\hat{\theta}_1 = (3.4753, 0.5471)$$

Suppose $\xi \neq 0$, we then obtain the following result by Eq. (4)

$$\hat{\theta}_2 = (3.5248, 0.5677, -0.1661)$$

We can know that if $\xi = 0$, $X$ is said to follow the Gumbel distribution with the parameter $\hat{\theta}_1$, and if $\xi \neq 0$, $X$ is said to follow the Weibull distribution with the parameter $\hat{\theta}_2$. We choose the more proper one from these two distributions.

### 2.3 Model checking

Probability Plots, quantile plots, return level plots and density plots are all useful for assessing the quality of a fitted generalized extreme value model. Suppose the distribution by ML is denoted by $\hat{G}(x)$, let $x_{(1)} \leq x_{(2)} \leq \cdots \leq x_{(n)}$ be a sequence of the sample. Thus, the probability plot consists of the pairs

$$\left\{\left(\frac{i}{n+1}, \hat{G}(x_{(i)})\right); i = 1,2,\cdots,n\right\}$$

The quantile plot consists of the pairs

$$\left\{\left(\hat{G}^{-1}\left(\frac{i}{n+1}\right), x_{(i)}\right); i = 1,2,\cdots,n\right\}$$

If the sample is said to follow the GEV distribution, then both the probability and quantile plots should consist of the points that are approximately linear.

The return level plot consists of the locus of points $\{(T, U_{(T)})\}$.

In this case, $U_{(T)}$ is the estimated T-times return level:

$$U_{(T)} = \hat{G}^{-1}(1 - 1/T)$$

Diagnostic plots for the GEV distribution are shown in Fig. 2. It can be seen directly that Weibull

distribution with the parameter $\hat{\theta}_2$ can be well fitted to the sample distribution, but Gumbel distribution with the parameter $\hat{\theta}_1$ is worse. Accurate normality is needed for precision.

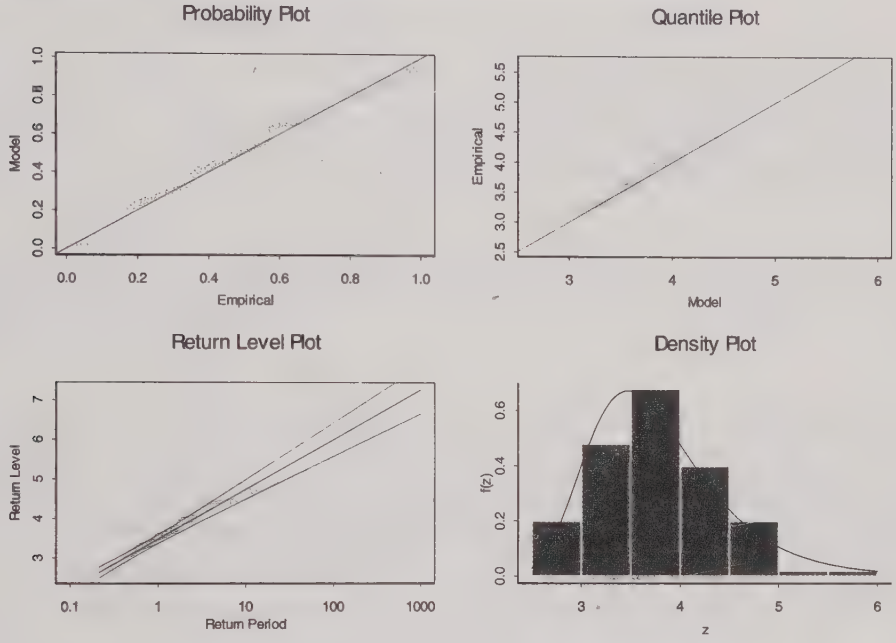


( a ) Diagnostic plots for Gumbel distribution with the parameter $\hat{\theta}_1$

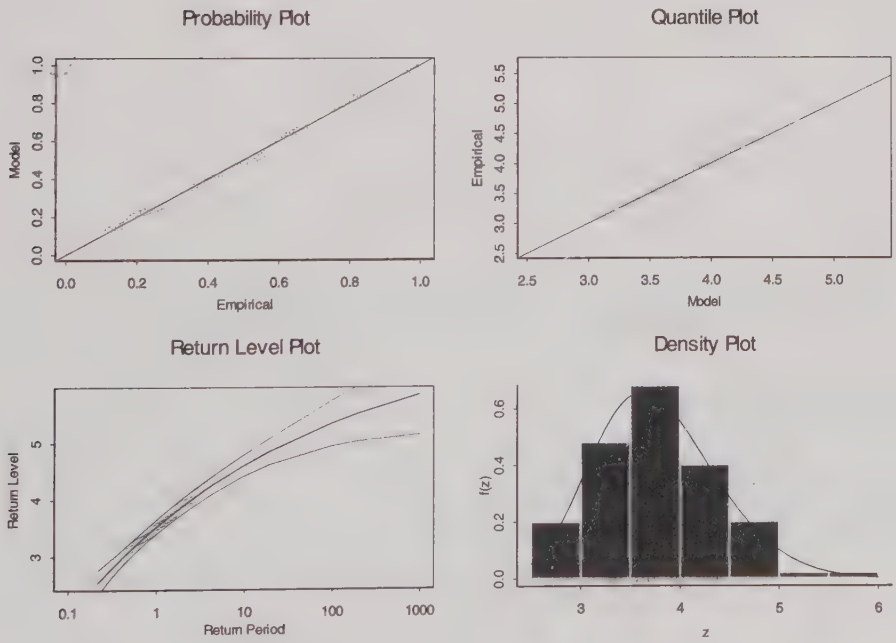


(b)Diagnostic plot for Weibull distribution with the parameter $\hat{\theta}_2$

**Fig. 2 Diagnostic plots for the GEV distribution**

Suppose $X \sim G_\theta(x)$, $g_\theta$ is the density function. Let us consider the $L^2$ norm

$$d(\hat{f}_b, g_\theta) = \| \hat{f}_b - g_\theta \|_{L^2}^{1/2} = \left( \sum_{x \in A} \left[ \hat{f}_b(x) - g_\theta(x) \right]^2 \right) \quad (5)$$

According to Fig.1, assume $A = \{0, 0.1, 0.2, 0.3, \cdots, 7\}$

Apply Eq.(5) to $\hat{\theta}_1$ and $\hat{\theta}_2$, we could define the optimal $G_\theta(x)$ as the $G_\theta(x)$ which gives the minimum $d(\hat{f}_b, g_\theta)$. We obtain the following results in Tab. 1:

**Tab. 1 Value of $d(\hat{f}_b, g_\theta)$**

| Parameter | $d(\hat{f}_b, g_\theta)$ |
|---|---|
| $\hat{\theta}_1$ | 0.355721 |
| $\hat{\theta}_2$ | 0.228432 |

We choose Weibull distribution with the parameter $\hat{\theta}_2$ from Table 1, that is, $X$ is said to follow Weibull distribution with the parameter $\hat{\theta}_2$. We can see this result from Fig. 3.

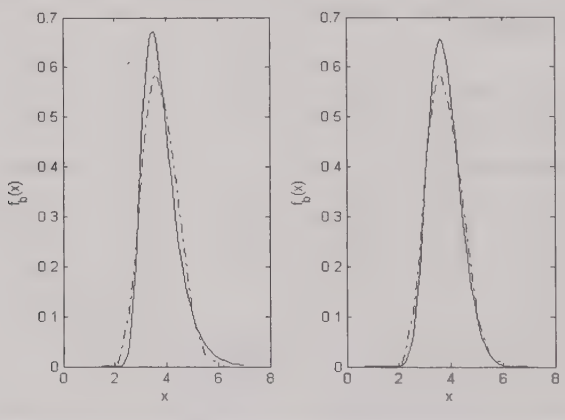


**Fig. 3 Density functions: Left: Gumbel distribution with the parameter $\hat{\theta}_1$ (solid) and $\hat{f}_{0.5940}(x)$ (dotted), Right: Weibull distribution with the parameter $\hat{\theta}_2$ and $\hat{f}_{0.5940}(x)$ (dotted)**

## 3 T-times Return Level

In previous sections, we obtained $X \sim G_{\hat{\theta}_2}(x)$

Here, we can obtain T-times return level by [4] as follows

$$\begin{aligned} U_{(T)} &= G_{\hat{\theta}_2}^{-1}(1 - 1/T) \\ &= \mu - \frac{\sigma}{\xi}\left[1 - \{-\log(1 - 1/T)\}^{-\xi}\right] \\ &= 3.4188096\left[1 - \{-\log(1 - 1/T)\}^{0.1660516}\right] + 3.5247730 \end{aligned} \quad (6)$$

Apply $T = 10,30,50,80,100$ to Eq. (6), we can obtain the corresponding T-times return level, and the results are shown in Tab. 2.

**Tab. 2 T-times return level**

| Times | 10 | 30 | 50 | 80 | 100 |
|---|---|---|---|---|---|
| $U_{(T)}$ | 4.591 | 4.995 | 5.155 | 5.290 | 5.351 |

Observations of 5, 13, 20, 23, 46, 51, 53, 58, 66, 86 are above this level. As to $U_{(10)} = 4.5908$, only the 13rd observation is above this level of $U_{(100)} = 5.3509$. Then we conclude that the scale of the 13rd red tide is scarce.

## 4 Conclusion

In this paper, the red tide frequency analysis is given, and we obtain the GEV distribution which observation is said to follow and the T-times return level $U_{(T)}$. Then we can know the properties of red tide occurrence more clearly, and judge the scales of red tide occurred by it, and forecast the scales of red tide with some forecast of red tide methods, in order to provide it better and reduce loss.

## Acknowledgements

This study is supported by the National Natural Science Foundation of China under No. 10472077.

## References

[1] David W Townsend, Neal R Pettigrew. Offshore Blooms of the Red Tide Dinofla- gellate, Alexandrium sp., in the Gulf of Maine. *Continental Shelf Research*, 2001, 21(4): 347-369.

[2] Kudela R M, Cochlan W P. Nitrogen and Carbon Uptake Kinetics and the Influence of Irradiance for a Red Tide Bloom off Southern California. *Aquatic Microbial Ecology*, 2000, 21(1): 31-47.

[3] Wang Hongli, Li Chao. The Research of the Nonlinear Dynamics Behaviors of the Red Tide Algal Model with Nutrimental Limited. *Ocean Technology*, 2003, 22(1): 40-44.

[4] Stuart Coles. An Introduction to Statistical Modeling of Extrem Values. *Springer*, 2001.

[5] B W Silverman. Density Estimation for Statistics and Data Analysis. *Chapman and Hall, London*, 1986.

[6] S J Sheather & M C Jones. A Reliable Data-Based Bandwidth Selection Method for Kernel Density Estimation. *Journal of the Royal Statistical Society*, 1991 , B 53: 683-690.

[7] A Ronald Gallant. Kernel Density and Regression Estimation. 2000.

# Study on the Adsorption of Metal Ions by Immobilized Marine Algae with the Existence of Clay

ZHENG Shenghua (郑盛华), WANG Xian (王 宪), CAI Zhenzhen (蔡真珍), CHEN Lidan (陈丽丹), QIU Haiyuan (邱海源), HUANG Zhiwei (黄智伟), QIAN Aihong (钱爱红)
*College of Oceanography and Environmental Science, Xiamen University, Xiamen* 361005, *Fujian, China*

**Abstract** The process of adsorption of metal ions by immobilized marine algae with the existence of clay was investigated. It can be noted from the results that, after mixing with clay, the adsorption rate increases rapidly with the increasing amount of the marine algae. When pH=5, the best ratio between the clay and the marine algae is 1:4 for $Pb^{2+}$. The result of *in situ* handling of the waste water containing heavy metals shows that the average adsorption rates of heavy metal irons $Cu^{2+}$, $Cd^{2+}$, $Pb^{2+}$ and $Ni^{2+}$ are all over 70 %.

**Keywords** clay, marine algae, metal ions, adsorption

## Introduction

Biosorption is a process that utilizes biomass to absorb heavy metals and is particularly useful for the removal of contaminants from industrial waste water. Since the adsorption effect on heavy metal ions by clay is worse than marine algae powder [1-6], people mostly use marine algae powder as sorbent, but clay is much cheaper than marine algae powder, people often mix clay and algae powder with a certain ratio in order to reduce the cost and to improve the adsorption effect in practical application[7-11]. Therefore, it is of great importance to find out the best ratio of the mixture to treat the waste water containing heavy metal irons.

In this study, immobilized *Laminaria japonica* and solution containing the metal ion $Pb^{2+}$ are chosen as biosorbent and adsorption object, separately. The aim of this study is to try to discuss the adsorption efficiency at different ratios between clay and marine algae, and to make the immobilized cells applicable in the practical waste water handling.

## 1 Materials and Methods

### 1.1 Main devices

ICP-AES (E-984, Hilger Co., U.K.); Centrifuge (80-2, Shanghai Medical Instruments (Group) Corp.); Shaker (HY-4, the Guohua Electronic Machines Company of Changzhou).

Received on July 4, 2005

### 1.2 Main reagents

Plumbum Nitrate, calcium chloride, sodium hydroxide, hydrochloric acid, nitric acid, formaldehyde, formicacid, methanol. All the reagents used are of analytical reagent grade and come from the Third Firm of General Agent Factory of Shanghai.

### 1.3 Biosorbent

*Laminaria japonica* powder and clay are obtained from the Qingdao Mingyue Marine Algae Co. and Fujian Longyan Bentonite Co. respectively. *Sargassum fusiforme* is obtained from the coast of Xiamen. The algae are pre-treated by 0.2 M calcium chloride for 12 h. The calcium chloride treated biosorbent is rinsed several times with deionised water. It is then dried at 80 ℃ in an oven, sieved and stored in a desiccator for later use.

### 1.4 Method

#### 1.4.1 Crosslinking of marine algae

Follow the procedure of Wang [12]. Twenty-five grams of dried algae powder are contacted with 500 mL of formaldehyde (HCHO) and 1 000 mL of formic acid (HCOOH). The reaction mixture is shaken on a rotary shaker for 6 h at 150 r/min. The resulted algae are then filtered and followed by sequential distilled water, 0.2 M sodium carbonate, and final distilled water washes. Algae are dried at 80 ℃ for 10 h and finally for 2 h at 110 ℃. The algae of 80-120 mesh are sieved for later use.

#### 1.4.2 Pre-treatment of clay

The clay is treated with 1 M HCl for 30 minutes to remove impurity, and the reacting temperature is kept constant at 80 ℃. Then the clay is rinsed by denoised water, and the solution is adjusted neutral by using $Na_2CO_3$. After filtering and dehydration, the filter cake is dried at 120 ℃. They are ground and passed through a sieve of 150 mesh for later use.

## 2 Results and Discussion

### 2.1 The adsorption on the heavy metal by the mixture of clay and algae

The treated *S. fusiforme* and *L. japonica* are mixed with clay at the ratio 1:8, 1:4, 1:2, 1:1, 2:1 and 4:1, respectively, and the total mixture should not exceed 0.5 g. Follow the study of Wang [13]. The adsorption rate is the best when pH is adjusted to 5, so pH of 0.2 mM heavy metals solutions are adjusted to 5, and the mixture is added into them. Then the solution is shaken for 4 h, the topper fining liquor was extracted, and centrifugated for 8 min, then the leaving concentration of the heavy metals in the topper fining liquor is detected with the aid of ICP-AES with standard addition recovery of 95.2 %-105.0 % and RSD less than 5.6 %.

The adsorption effect by clay is not as good as marine algaes. We mainly use marine algaes as the sorbent to adsorb heavy metals. It can be noted from the experiments' results (Fig. 1) that the adsorption

rate increases as the amount of the algae powder increases. For $Pb^{2+}$, the adsorption effect is the best when the ratio between the clay and the biomass is 1:4, and the adsorption rate is able to reach 99.95 %. For *S. fusiforme*, the adsorption effect is best when the ratio between the clay and the algae is 1:4, and the adsorption rate is 92.62 %.

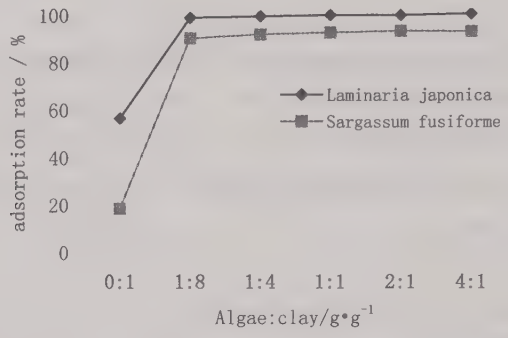


**Fig. 1 The adsorption efficiency of mixture of algae and clay with different ratios**

It can be noted from the results that, after mixing with clay, the adsorption rate increases with the increasing amount of the marine algae. When pH=5, the best ratio between the clay and the marine algae is 1:4.

## 2.2 The experiment of in situ Handling of the Waste Water

The sketch map of *in situ* handling of the waste water is showed in Fig. 2. In the experiment, the quantity of the algae biosorbent is adjusted by the concentration of the heavy ions in the waste water, the waste water is adjusted to appropriate pH, and the flowing speed is regulated so that the heavy metals can be adsorbed sufficiently.

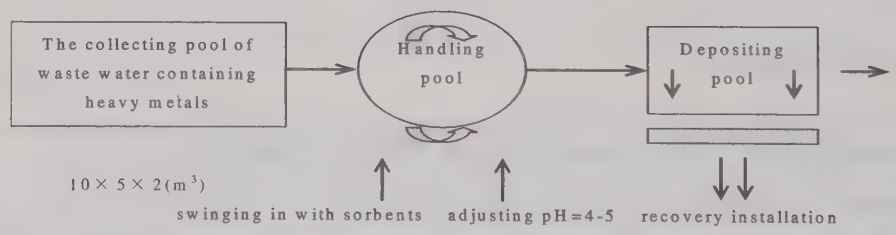


**Fig. 2 The sketch map of in situ handing of the waste water containing heavy metal ions**

Although diversities in the adsorption rate among the four heavy metal ions can be found from Fig. 3, the average adsorption rate is greater than 70 %. In other words, the concentration of heavy metal ions in the waste water will be reduced about 2/3. The difference of adsorption rates may be caused owing to the different existing forms of these four kinds of metals under special conditions, or due to other factors such as prior adsorption.

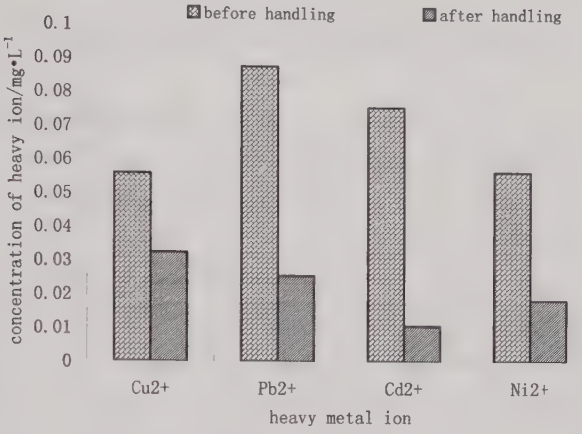


**Fig. 3 The concentration of heavy metal before and after handling in *in situ* experiments**

## 3 Conclusion

( 1 ) The adsorption efficiency of the mixture of the clay and the marine algae increases with the increasing amount of the marine algae. When pH=5, the optimum ratio between clay and biomass is 1:4.

( 2 ) The average adsorption rate is greater than 70 % in *in situ* handling of the waste water containing $Cu^{2+}$, $Pb^{2+}$, $Cd^{2+}$, $Ni^{2+}$.

( 3 ) The priorest adsorption ion is $Cd^{2+}$, and the order is $Cd^{2+}$>$Pb^{2+}$> $Ni^{2+}$>$Cu^{2+}$.

### Acknowledgements

We gratefully acknowledge the financial support for this project from the Advanced Technology Fund of Xiamen.

## References

[1] Dong D, Li Y and Hua X. Investigation of Fe, Mn oxides and organic material in surface coatings and Pb, Cd adsorption to surface coatings developed in different natural waters. *Microchemical Journal,* 2001, 70(1): 25-33.

[2] Wilson A R, Lion L M, Nelson Y M et al. The effects pH and surface composition on Pb adsorption to natural freshwater bilfilms. *Environ. Sci. Technol*, 2001, 35: 3 182-3 189.

[3] Percival S L, Knapp J S, Edyvean R et al. Biofilm development on stainless steel in mains water. *Wat. Res.*, 1998, 32(1): 243-253.

[4] Wimpenny J. Ecological determinants of biofilm formation. *Biofouling*, 1996, 10(1-3): 43-63.

[5] Costern J W, Cheng K, Geesey G G et al. Bacterial bilfilms in natural and disease. *Ann. Rev. Microbio*, 1987,

42: 435-464.

[6] Hsieh K M, Lion L W, Shuler M L et al. Bioreactor for the study of defined interactions of toxic metals and bilfilms. Appl. Environ. *Microbiol*, 1985, 50(5): 1 155-161.

[7] Sekhar K C, Subramanian S et al. Removal of metal ions using an industrial biomass with reference to environmental control. *Int. J. Miner. Process*, 1998, 53: 107-120.

[8] Ye Jinshao, Yi Hua and Peng Hui. Study on Biosorption of Heavy Metals. *Urban Environmental & Urban Ecology*, 2001, 14(3): 30-32.

[9] Gupta V K, Shrivastava A K and Neeraj J. Biosorption of chromium(VI) from aqueous solutions by green algae Spirogyra species. *Wat. Res*, 2001, 35(17): 4079-4085.

[10] Yin P H, Yu Q m, Jin B et al. Biosoption removal of cadmium from aqueous solution by using pretreated fungal biomass of cultured from starch wastewater. *Water Research*, 1999, 25(8): 1960-1963.

[11] Chen L D, Wang X, Xu L R et al. Thermodynamic analysis of heavy metals biosorptionby two macroalgae. *Marine Science Bulletin*, 2004, 6(1): 47-52.

[12] Wang J L. Biosorption of copper (II) by chemically modified biomass of *Saccharomyses Cerevisiae*. *Process Biochemistry*, 2002, 37: 847-850.

[13] Wang X, Chen L D, Xu L R et al. Mechanism and affecting factors of macroalgae biosorption to metal ions. *Journal of Oceanography in Taiwan Strait*, 2003, 22(2): 262-268.

[14] Qian A H, Wang X Deng Y Z et al. Heavy metal biosorption sites of laminaria japonica, *Marine Science Bulletin*, 2005, 7(1): 87-91.

# Toxic Effects of Phthalates on Ocean Algae

QIU Haiyuan (邱海源), WANG Xian (王 宪)

*College of Oceanography and Environmental Science, Xiamen Univ., Xiamen* 361005, *Fujian, China*

**Abstract** This article discusses the interaction of phthalates and ocean algae based on the standard appraisal method of chemical medicine for algae toxicity. Through the experiments on the toxic effects of dimethyl (o-) phthalate (DMP), diethyl (o-) phthalate (DEP), dibutyl (o-) phthalate (DBP) on ocean algae, the 50 % lethal concentration of the three substances in 48 h and 96 h for *plaeodectylum tricornutum*, *platymonas* sp, *isochrysis galbana*, and *skeletonema costatum* is obtained. Tolerance limits of the above ocean algae of DMP, DEP, and DBP are discussed.

**Keywords** toxic effect, ocean algae, phthalate

Phthalates are widely used synthesized organic substances all over the world, with an increasing output globally. Because phthalates are in dissociation state in plastic products, it is easier for them to enter the water. In addition, their output increase and wide use enable them to exist in atmosphere, water and soil [1]. Phthalates have become one of the most widely distributed environmental contaminates throughout the world. DMP, DEP and DBP have been defined as preferentially controlled contaminates by the U.S. Environmental Protection Agency and the General Environmental Monitoring Station of China [2]. Toxic effects of organic substances have been researched by some scholars. Defee[3] et al. reported that: 96h$E_{50}$ of DBP on Fathead minnow is 0.85 mg/L. Research of Thoren[4] showed that: 100 μg/L di(2-ethyl hexyl)-phthalate (DEHP) could increase the locomotion effects of arthropods; however, when the concentration is as high as 500 μg/L, it could decrease the locomotion effects of arthropods. But, under the two above-mentioned concentrations, dibutyl (o-) phthalate (DBP) could decrease the locomotion effects of arthropods. 96h$E_{50}$ of dimethyl (o-) phthalate (DMP) for Chlorella is 313 mg/L[5], which was researched by RCEES/CAS. Organic contaminates in water environments are generally seened as a kind of restrained factor for algae, whose concentration abides by Shelford's law of tolerance[6] when above the limit of tolerance. Within the limit of tolerance, they make the number of kinds of algae decrease and the quality decline. Firstly, algae gather together under the influence of organic substances, resulting in algae moving along with the food chain of biology or a series of biochemical reactions together with all kinds of enzymes in the bodies of algae, making organic substances degradated or transformed. This article researches the toxic effects of DMP, DEP and DBP on ocean algae, which is explained mainly by their 50 lethal concentrations.

## 1 Material and Method

### 1.1 Main devices

Spectrophotometer: Model 721; Model 800 Centrifuge; Stainless Standard Sieve Ⅰ (300 mesh,

Received on December 10, 2004

Aperture 0.05 mm); Oscillator: Self-Made Manual Light Source Culture Box: 2×500 W Iodine Tungsten Light Source: SYY1-1 Model Salinity Meter; Ph-3B Model PH Meter; Electrothermal Steam Sterilizer (YXQ602 Model) DMP, DEP and DBP are A.R.; ocean algae (*Plaeodectylum tricornutum*, Bull; *Platymonas* sp; *Isochrysis galbana*; *Skeletonema costatum*) are cultured from standard culture media.

### 1.2 Experimental conditions

Temperature: 22 ℃±2 ℃; Illumination: 3000-4000 Lux.

### 1.3 Pretreatment

(1) With 0.45 μm filter paper, suction filtering 100mL ocean water filtrated by sands.

(2) Sterilize several 250 mL Erlenmeyer flasks, kept 45 minutes at 120 ℃ and about 0.157 mPa.

(3) Sterilize ocean water under the same conditions.

(4) Prepare nutrient solution.

### 1.4 Algae culture

Control the salinity of sterilized ocean water at about 27; After the addition of nutrient solution, add some algae seeds, culturing for one week at room temperature. Concentration of alga cells is $5\times10^5$ cell/mL.

### 1.5 Experiment methods

Adopt the method of periodically measuring biology quantities, *i.e.* chla method. The light absorbance is different for solutions with different concentrations. And there exists a corresponding relation between them. So this method can be used to measure light absorbance to observe the variation of biomass. 50 % lethal concentration and lethal concentration also could be gotten through the graphical method.

## 2 Results and Discussion

### 2.1 Normal growth curves of algae (see Fig. 1)

It could be seen that, under normal growing conditions, 4 algae grow well; biomasses of the 4 algae are gradually enlarged with time; the growing speed is pretty fast within 48 -120 h, a bit slowly at the beginning and the end; value of $E_{48c50}$ is between 300 and 400, value of $E_{96c50}$ is between 120 and 200, consistent with theoretical and real situations.

### 2.2 Effect curve of organic substances on algae (See Figs. 2, 3, 4)

It could be obviously observed in Fig. 2 that DBP has severe restraining effect on the growth of the three kinds of algae, especially *Platymonas* sp and *Plaeodectylum tricornutum*. With the increase of concentration of DBP in the nutrient solution, its relative growing rate decreases. Toxic effects of DBP for *Platymonas* sp and *Plaeodectylum tricornutum* are larger than that for *Isochrysis galbana*. From the point of view of biomass, its quantities are reduced continually, and the reducing degree of 48 h is faster

than that of 96 h.

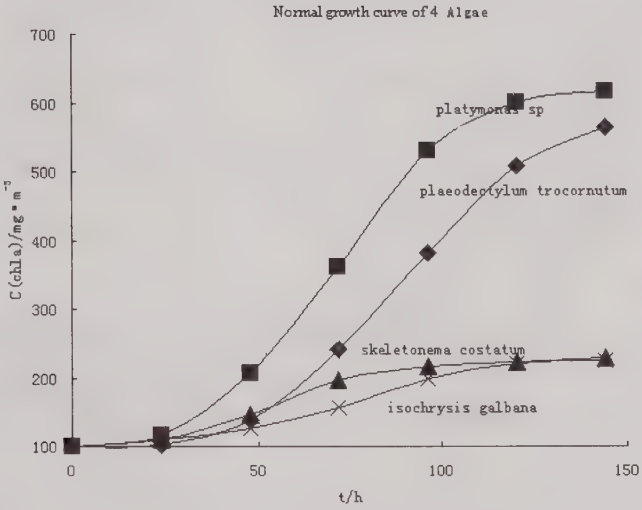


**Fig. 1 Growth curves of four kinds of algae**

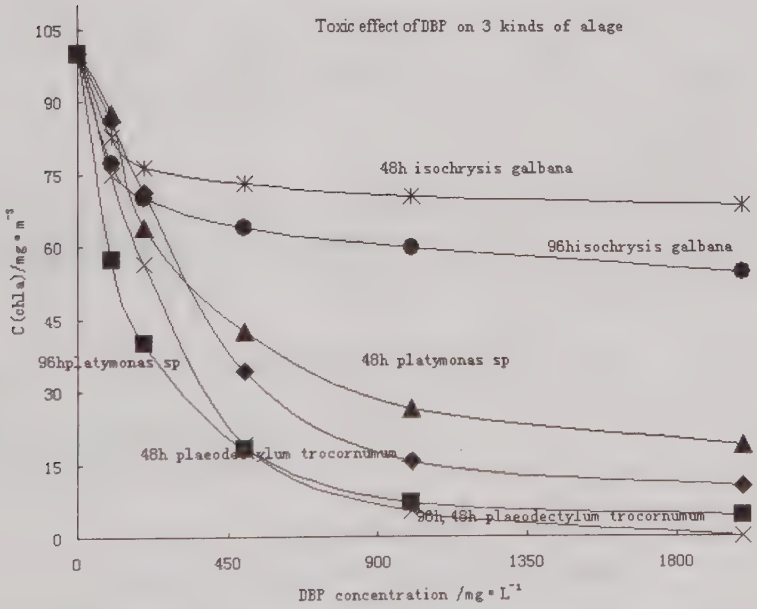


**Fig. 2 Toxic effects of DBP on three kinds of algae**

It could be seen in Fig. 3 that DEP also has severe restraining effect on the growth of the three kinds of algae. With the increase of concentration of DEP in the nutrient solution, its relative growing rate decreases obviously too. Toxic effects of DBP for *Platymonas* sp, P*laeodectylum tricornutum* and *Isochrysis galbana* are all pretty large. From the point of view of biomass, its quantities are reduced continually, and the reducing degree of 48 h is faster than that of 96 h too.

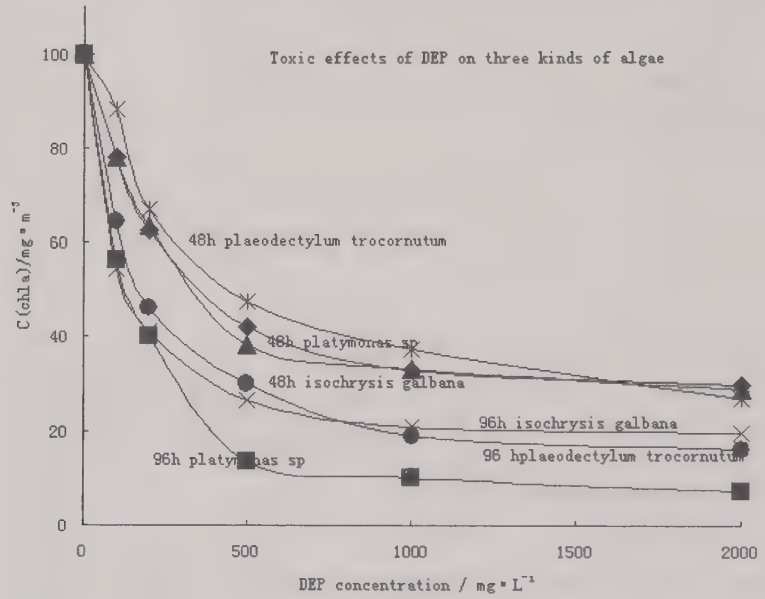


**Fig. 3 Toxic effects of DEP on three kinds of algae**

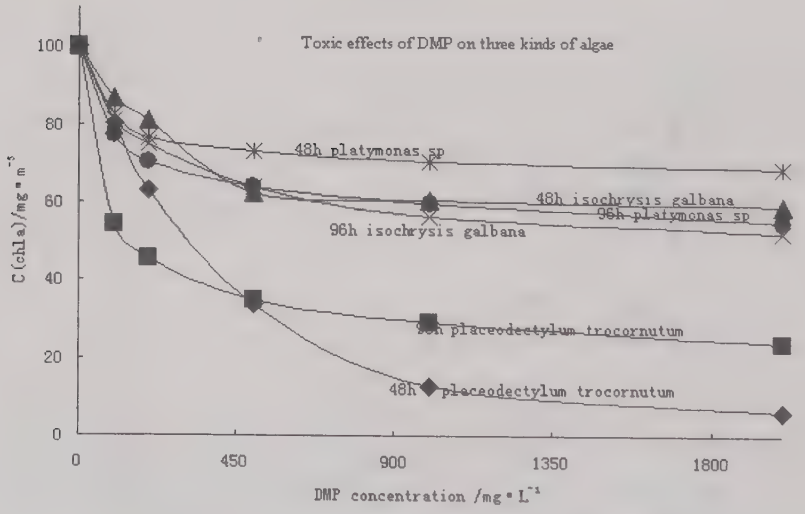


**Fig. 4 Toxic effects of DMP on three kinds of algae**

Fig. 4 shows that DMP has severe restraining effect on the growth of the three kinds of algae, especially *Platymonas* sp and *Isochrysis galbana*. With the increase of concentration of DMP in the nutrient solution, its relative growing rate also decreases. Toxic effects of DBP for *Plaeodectylum tricornutum* are larger than that for *Platymonas* sp and *Isochrysis galbana*. Biomasses are also reduced continually, and the reducing degree of 48 h is faster than that of 96 h.

It can be seen from the results that the toxic effects of DMP, DEP and DBP on ocean algae are

reduced obviously with the existence of suspended substances. This shows that suspended substances have some adsorption function for DMP, DEP and DBP, which influences the toxic effects of the three toxic substances algae directly or indirectly. It also shows that in the natural water environment, the relation of influence of toxic substances to ocean primary productivity and concentration of toxic substances is not linear. The toxic effects are related not only to the concentration of toxic substances, but also closely to the ocean environment, especially the existence of suspended substances.

### 2.3 50 % lethal concentration $E_{50}$ and safe concentration of toxic effects of four kinds of algae (see Tabs. 1, 2)

It could be seen from Tab.1 that 50 % lethal concentration of 48 h is larger than that of 96 h for each experiment, consistent with theoretical and real situations. But all of them are larger than the standard for aquatic organisms. It shows that the three toxic organic substances have severe restrain effects on the 4 kinds of algae.

**Tab. 1 $E_{50}$ of toxic effects of four kinds of algae in different solvents**

| Items Measured value Organic substances | 48 h $E_{50}$/ mg • $L^{-1}$ | | | | 96 h $E_{50}$/ mg • $L^{-1}$ | | | |
|---|---|---|---|---|---|---|---|---|
| Algae | *Plaeodectylum tricornutum* | *Platymonas* sp | *Isochrysis galbana* | *Skeletonema costatum* | *Plaeodectylum tricornutum* | *Platymonas* sp | *Isochrysis galbana* | *Skeletonema costatum* |
| DMP | 362.3 | 389.2 | 352.3 | 195.3 | 133.8 | 195.3 | 166.2 | 176.6 |
| DEP | 447.2 | 391.3 | 347.4 | 184.8 | 177.6 | 129.6 | 128.6 | 148.6 |
| DBP | 331.6 | 396.2 | 370.2 | 180.6 | 173.6 | 247.6 | 156.4 | 139.4 |

Safe concentration of three toxic organic substances in Tab 2 is calculated by the formula $0.1 \times E_{96c50}$.

**Tab. 2 The main table of the safe concentration**

| Algae Safe concentration Organic substances | Plaeodectylum tricornutum | Platymonas sp | Isochrysis galbana | Skeletonema costatum |
|---|---|---|---|---|
| DMP | 13.3 | 19.5 | 16.6 | 17.7 |
| DEP | 17.7 | 12.9 | 12.8 | 14.8 |
| DBP | 17.3 | 24.7 | 15.6 | 14.0 |

## 3 Conclusions

Results of toxic effects of DMP, DEP and DBP for 4 kinds of algae show that:

(1) $E_{48c50}$ and $E_{96c50}$ of each organic substance are far beyond the standard for aquatic organisms. So, it could be considered that the above-mentioned 4 kinds of algae have low sensitivity to DMP, DEP

and DBP. In the natural water environment, DMP, DEP and DBP are nontoxic for algae.

( 2 ) Considering the sensitivity of 4 kinds of algae to organic substances, *Isochrysis galbana* is the least sensitive to DMP and DBP. With the concentration increase of nutrient solution, its relative growth has a pretty large decrease trend.

( 3 ) If suspended grains are added into the above experimental vessels, the degradation function of organic substances will be made to speed indirectly by the carrier function of microflora due to the thickening function for organic substances in water.

## Acknowledgments

The paper was supported by the National Natural Science Foundation of Fujian (B0310001).

## References

[1] Zhao Zhenhua. Research on pollution of phenolphthalein for China environment. *Serial Books of Environmental Science,* 1986, 7(5): 50-56.

[2] Jin Xiangcan. *Pollution Chemistry of Organic Compound.* Tsing-Hua Press. 1990, 14-23.

[3] Defoe DL. Solubility and Toxicity of Eight phthalate Esters to four Aquatic organisms. Environmental Toxicity and chemistry, 1990, 9: 623-636.

[4] Thuren A. Effects of phthalate Esters on the Locomotors Activity of the Fresh Water Amphipod Gommarus Pulox. *Bull Environ Contam. Toxico.* 1991, 146: 159-166.

[5] Odum E P (Translated by Sun Ruyong). *Basic of Ecology.* Beijing: the People's Education Press, 103-105.

[6] Min Hai, Lei Zhifang, Ye Changming. Dynamic research on degradation effects of Scenedesmus on dimethyl (o-) phthalate. *Acta Scientiae Circumstantiae,* 1998, 18(2): 210-220.

# Marine Science Bulletin

**Marine Science Bulletin** publishes papers on marine science and technology including physical oceanography, chemical oceanography, marine biology, marine geology, environmental oceanography, estuarine & coastal sciences, marine technology, digital ocean, coastal zone management, ocean engineering, marine economics, etc., and aims to promote international academic exchange.

**Editor-in-Chief:** LIN Shaohua (林绍花)
**Deputy Editor-in-Chief:** HE Guangshun (何广顺) YANG Ying (杨 鹰)
**Executive Editor:** LIN Baofa (林宝法) HE Xuewu (何学武) ZHANG Deshan (张德山)
ZHANG Xiaoxian (张潇娴) WANG Zhankun (王占坤)
**Computer typist:** CHENG Xiuchun (程秀春)

**Marine Science Bulletin** (Vol. 7 No. 2 Oct. 2005)

**Responsible Institution:**
State Oceanic Administration of China
**Edited and Published Semi-annually by:**
National Marine Data and Information Service
**Address:** 93 Liuwei Road, Hedong District, Tianjin 300171, China
**E-mail:** msb@mail.nmdis.gov.cn

ISSN1000-9620
CN12-1271/N